Washington University in St. Louis

Washington University Open Scholarship

5-24-2011

Analysis of Zinc Transporters in C. elegans

Hyun Cheol Roh
Washington University in St. Louis

Follow this and additional works at: https://openscholarship.wustl.edu/etd

WASHINGTON UNIVERSITY

Division of Biology and Biomedical Sciences

Program in Molecular Cell Biology

Dissertation Examination Committee:
S. Kerry Kornfeld, Chair
Peter T. Chivers
Stuart A. Kornfeld
Jason C. Mills
Jeanne M. Nerbonne
Tim B. Scheidl

ANALYSIS OF ZINC TRANSPORTERS IN *C. ELEGANS*

by

Hyun Cheol Roh

A dissertation presented to the
Graduate School of Arts and Sciences
of Washington University in
partial fulfillment of the
requirements for the degree
of Doctor of Philosophy

August 2011

Saint Louis, Missouri

ABSTRACT OF THE DISSERTATION

Analysis of Zinc Transporters in *C. elegans*

By

Hyun Cheol Roh

Doctor of Philosophy in Biology and Biomedical Sciences

(Molecular Cell Biology)

Washington University in Saint Louis, 2011

Professor S. Kerry Kornfeld, Chairperson

Zinc is a trace element essential for organisms, and organisms have homeostatic mechanisms to control zinc metabolism. Zinc metabolism is mediated by numerous proteins including zinc transporters, zinc-responsive transcription factors and zinc-binding proteins. Of these proteins, zinc transporters, composed of CDF and ZIP families, play a major role and are implicated in a variety of human diseases. However, the mechanisms by which zinc transporters coordinate to regulate zinc homeostasis in whole animals and by which they are related to human diseases are not well understood.

To address these questions, we used *C. elegans* as a model system. While three *C. elegans cdf* genes have been characterized previously, the majority of zinc transporters remain to be studied. Here, we characterized *cdf-2* and *ttm-1* and conducted initial studies of other zinc transporters. We demonstrated that lysosome-related organelles in intestinal cells, termed gut granules, function as a major site of zinc storage. Gut granules were important for detoxification of excess zinc as well as mobilization of zinc in response to low-zinc environments, and CDF-2 was necessary for these processes. In

high zinc conditions, gut granules displayed morphological changes characterized by a bilobed morphology with asymmetric distributions of molecules. These findings suggest novel mechanisms of zinc storage, detoxification and mobilization in *C. elegans*.

ttm-1 encodes two isoforms, *ttm-1a* and *ttm-1b,* by using different transcription start sites. TTM-1 plays a role in the excretion of zinc and is involved in zinc detoxification via the action of TTM-1B which localizes to the apical membrane of intestinal cells. These functions of TTM-1 are critical specifically in the absence of CDF-2, suggesting that TTM-1coordinates with CDF-2 to regulate zinc homeostasis of whole animals. Studies of other zinc transporters including expression pattern analysis suggested novel functions of zinc transporters in biological processes. These results suggest that further studies of *C. elegans* zinc transporters may contribute to understanding of sophisticated networks of zinc transporters in zinc metabolism and elucidate physiological functions of zinc transporters.

ACKNOWLEDGEMENTS

TABLE OF CONTENTS

LIST OF TABLES AND FIGURES

CHAPTER 1

Introduction:

Overview of Zinc Metabolism

Metal ions are trace elements essential for all living organisms. Among the many metal ions present in biological systems, zinc is the most widely used and is involved a broad range of biological processes (Vallee and Falchuk, 1993). Zinc plays an important role in the function of numerous proteins by acting as a catalytic and/or structural cofactor. Zinc is required for more than 300 metalloproteins in all six major enzyme classes, and it is a critical structural component of thousands of proteins including zinc-finger transcription factors (Vallee and Falchuk, 1993). In humans, it has been estimated that about 10% of the proteome are zinc-binding proteins (Andreini et al., 2006). Furthermore, zinc functions in signal transduction during development, neurotransmission and immune responses by acting as a signaling molecule (Murakami and Hirano, 2008).

The wide use of zinc in biological system is likely to be attributed to its unique chemical properties. First, zinc is a nontransition metal which lacks redox activity in contrast to other biological metals such as iron and copper (Berg and Shi, 1996). This property renders zinc stable and less damaging in physiological conditions where the redox state fluctuates. Second, zinc has high coordination flexibility; it can accommodate multiple coordination geometries ranging from two to eight coordinate complexes (Vallee and Falchuk, 1993). This property enables zinc to make complexes with varying ligand types in a broad range of proteins.

The biological significance of zinc is illustrated by the broad range of defects resulting from zinc deficiency. Zinc deficiency results in defects in cell growth and proliferation in all organisms (Beyersmann and Haase, 2001). In humans, zinc deficiency leads to functional impairment of multiple tissues including of epidermal, gastrointestinal,

skeletal, reproductive, nervous, and immune systems (Hambidge, 2000). In addition to zinc deficiency, excess zinc is toxic (Fosmire, 1990). Although the mechanism of zinc toxicity is not understood, it is thought that excess zinc may interfere with the function of other metal ions by competing for their protein binding sites. Therefore, organisms have evolved precise homeostatic mechanisms for the regulation of zinc levels and distribution at cellular and organismal levels. Over the past several decades, extensive studies of zinc metabolism have identified many proteins that are involved in zinc homeostasis including zinc transporters, zinc-responsive transcription factors and zinc-binding proteins. Many of the genes have been implicated in human diseases. However, the mechanism by which the zinc metabolism-related genes contribute to zinc homeostasis of an individual, how multiple proteins interact to achieve zinc homeostasis, and how zinc metabolism is related to human disease are not well understood.

ZINC METABOLISM IN THE YEAST, *S. CEREVISIAE*

Studies with the yeast, *S. cerevisiae*, have made significant contributions to the molecular characterization of genes and proteins that mediate zinc metabolism (Eide, 2006). These studies have uncovered zinc transporters and zinc-responsive transcription factors as important players in cellular zinc homeostasis. Zinc transporters are integral membrane proteins that mediate the movement of zinc ions across membranes. There are six families of zinc transporters from bacteria to mammals (Hantke, 2001). Three of these families function only in prokaryotes, and they will not be discussed here. In eukaryotes, two families of zinc transporters, CDF (cation diffusion facilitator) and ZIP (Zrt-, Irt-like Protein) proteins, are well conserved in bacteria, fungi, plants and

3

mammals (Gaither and Eide, 2001a). CDF proteins decrease cytoplasmic zinc levels by transporting zinc to the outside of the cell or into intracellular organelles(Eide, 2006). Most CDF proteins have six transmembrane (TM) domains and a histidine-rich motif in the loop between TM 4 and 5, which is predicted to be important for zinc binding or zinc transport. Many CDF proteins have been reported to make homo- or heterocomplexes. Regarding their mechanism of transport activity, CDF proteins appear to be secondary active transporters which move zinc using another ion gradient such as H^+ and K^+. For example, the yeast CDF protein Zrc1 is a Zn/H+ antiporter (MacDiarmid et al., 2002). In contrast to CDF proteins, ZIP proteins increase cytoplasmic zinc levels through uptake of zinc from the extracellular space and transporting zinc out of intracellular organelles . ZIP proteins have eight TM domains and a histidine-rich motif in the loop between TM 3 and 4 similar to CDF proteins (Eide, 2006).

Zinc transporters regulate the flow of zinc across the plasma membrane, which is the first step for the control of cellular zinc homeostasis. The yeast ZIP proteins, Zrt1 and Zrt2, are localized on the plasma membrane and mediate the uptake of zinc into the cell (Eide, 2006). While Zrt1 has a high affinity for zinc and is required for growth in low zinc conditions (Zhao and Eide, 1996a), Zrt2 has a lower affinity for zinc and functions during mild zinc deficiency (Zhao and Eide, 1996b). Since yeast CDF proteins on the plasma membrane which mediate efflux of zinc have not been identified, the expression levels of Zrt1 and Zrt2 proteins affect the uptake rate of zinc and thus regulate overall cellular zinc levels. Once taken up into the cytoplasm, zinc is rapidly transported into intracellular organelles by zinc transporters because free zinc is toxic. Zinc transporters on the membranes of intracellular organelles regulate the level of zinc in the organelles

4

and contribute to the control of intracellular zinc distribution. For instance, Msc2/Zrg17 CDF-heteromeric complex mediates the transport of zinc into the lumen of the ER and Golgi complex (Ellis et al., 2005; Li and Kaplan, 2001), which is thought to be important for the supply of zinc to zinc-dependent proteins synthesized in the organelles. The CDF proteins Zrc1 and Cot1, and ZIP protein Zrt3 regulate the zinc level in the vacuolar lumen (MacDiarmid et al., 2000), which functions as an important site for zinc storage and detoxification. In high zinc conditions, Zrc1 and Cot1 move excess zinc into the vacuole to protect the cell from zinc toxicity. In response to low zinc conditions, Zrt3 mobilizes zinc from the vacuole to meet the cellular zinc requirements.

Another major mechanism to maintain zinc homeostasis in response to fluctuating levels of zinc in the environment is transcriptional regulation of the expression of zinc-metabolism-related genes. The yeast Zap1 zinc-responsive transcription factor senses cellular zinc levels through its zinc-finger domain and controls target gene expression by binding to a specific DNA sequence called zinc-responsive element (ZRE) (Zhao and Eide, 1997). When zinc is limiting, Zap1 is activated and induces the expression of Zrt1 and Zrt2 to promote zinc uptake from the environment and Zrt3 to mobilize zinc from the vacuole. Conversely, excess zinc causes the downregulation of Zrt1 expression to decrease zinc influx and the induction of Zrc1 and Cot1 to sequester excess zinc in the vacuole. Thus, cellular zinc metabolism is a sophisticated process that involves the networks of zinc-responsive transcription factors and zinc transporters from multiple intracellular localizations.

ZINC METABOLISM IN ANIMALS

The mechanisms underlying zinc metabolism in yeast are well conserved in higher organisms. However, zinc metabolism in animals is more complicated because it involves many processes in multiple tissues: the absorption and secretion of zinc by the gastrointestinal tract, the excretion of zinc into urine by the kidneys, and the distribution and exchange of zinc between tissues (Krebs, 2000). In addition, a large number of proteins are involved in zinc metabolism in animals and they fall into three major classes; zinc-binding proteins, zinc-responsive transcription factors and zinc transporters. A number of studies have characterized these zinc metabolism-related proteins.

In animals, metallothioneins (MTs) are zinc-binding proteins that have been widely studied and implicated in zinc metabolism. MTs are small intracellular cysteine-rich proteins that bind metal ions including zinc and cadmium (Coyle et al., 2002). In mice, there are four MT genes. MT-1 and MT-2 are ubiquitously expressed, while MT-3 is mainly expressed in the brain, and MT-4 is found in squamous epithelia and the maternal decidua. Although many studies have suggested that MTs function in the response to a variety of chemical and physical insults, the function of MTs has yet to be clearly defined. One of the most feasible functions of MTs is their protective role against metal toxicity. Mice lacking MT-1 and MT-2 displayed relatively normal development and growth, but they were susceptible to metal toxicity. On the other hand, transgenic mice overexpressing MTs displayed higher zinc accumulation and protection against excess zinc and cadmium (Coyle et al., 2002; Klaassen and Liu, 1998). However, the precise function of MTs in zinc homeostasis remains still elusive.

Metal-responsive element-binding transcription factor-1 (MTF-1) is a zinc-responsive transcription factor (Radtke et al., 1993). Similar to yeast Zap1, MTF-1 is a

zinc-finger transcription factor, and its zinc finger domains are critical for sensing cellular zinc levels. When zinc is abundant, MTF-1 is activated, translocates to the nucleus, binds a metal-responsive element (MRE) in the promoter of its target genes and induces expression (Smirnova et al., 2000). The targets of MTF-1 include many zinc metabolism-related genes such as MTs and zinc transporters, suggesting it plays an important role in zinc metabolism. Homozygous deletion of MTF-1 in mice results in embryonic lethality due to degeneration of hepatocytes, suggesting that MTF-1 is essential for liver development (Gunes et al., 1998).

In mammals, there are 10 members in the CDF (also called ZnT or SLC30) family and 14 members in the ZIP (also called SLC39) family (Lichten and Cousins, 2009). Extensive studies using mammalian cell lines and mouse models have been characterized each member of the zinc transporter families. ZnT-1, which is the first zinc transporter identified in mammals, displays ubiquitous tissue expressions and is localized to the plasma membrane (Liuzzi et al., 2001; Palmiter and Findley, 1995). ZnT-1 expression is regulated by dietary zinc levels via MTF-1 (Langmade et al., 2000). As ZnT-1 is highly expressed in the intestine and localized to basolateral membrane of enterocytes, it is thought to function in the transport of zinc from enterocytes into the bloodstream (McMahon and Cousins, 1998). ZnT-1 deficient mice display early embryonic lethality suggesting an essential role in embryonic development. ZnT-2 is expressed in the small intestine, liver, kidney and mammary gland, and its expression is upregulated by MTF-1 in response to high levels of zinc in the diet (Lichten and Cousins, 2009; Liuzzi et al., 2001). In contrast to ZnT-1, ZnT-2 is localized to the membrane of intracellular vesicles (Palmiter et al., 1996a). ZnT-2 is involved in the transport of zinc

into milk in the mammary gland, and a mutation in human ZnT-2 causes the production of zinc deficient milk (Chowanadisai et al., 2006). ZnT-3 is expressed in the brain, especially in the hippocampus and is required for the transport of zinc into synaptic vesicles (Cole et al., 1999; Palmiter et al., 1996b). Synaptic zinc is not required for normal brain function, as demonstrated by the ZnT-3 knockout mouse, but ZnT-3 is likely to be involved in age-related learning and memory (Adlard et al., 2010; Sindreu et al., 2011). ZnT-4 was identified by the search for a gene that causes lethal milk (*lm*) syndrome (Huang and Gitschier, 1997). While ZnT-4 localizes to intracellular vesicles and is involved in transporting zinc into milk in the mammary gland similar to ZnT-2, its expression is independent of dietary zinc levels (Lichten and Cousins, 2009). ZnT-5 is ubiquitously expressed but abundant in pancreatic β-cells (Kambe et al., 2002), and it functions in the transport of zinc into secretory vesicles in heterooligomeric complexes with ZnT-6 (Ellis et al., 2005). ZnT-5 knockout mice display growth defects, abnormal bone development and male-specific cardiac arrhythmias, suggesting that ZnT-5 has important roles in growth and development (Jackson et al., 2007). ZnT-7 is expressed mainly in the lung and small intestine and localized to the Golgi apparatus (Kirschke and Huang, 2003). ZnT-7 knockout mice displayed zinc deficiency, poor growth and reduced fat content (Huang et al., 2007), suggesting ZnT-7 may function in fat metabolism in addition to growth control. ZnT-8 is highly expressed in pancreatic β-cells and localized to the membrane of insulin granules where zinc forms a complex with insulin (Chimienti et al., 2004). Recent studies using mouse models and human genomic analyses suggest that ZnT-8 is involved in pancreatic β-cell function and is implicated in the development of diabetes (Rutter, 2010). ZnT-9 and ZnT-10 have been identified but not yet

8

functionally characterized.

Mammalian ZIP proteins were identified based on the homology with ZIP proteins from the yeast and plants. ZIP-1 is expressed a wide range of human tissues and involved in zinc uptake (Gaither and Eide, 2001b). ZIP-1 is located on the plasma membrane or in intracellular vesicles depending on the type of cell (Lichten and Cousins, 2009), and its localization is regulated by levels of zinc (Wang et al., 2004). Similar to ZIP-1, ZIP-2 and ZIP-3 promote zinc uptake in cells, but their tissue distribution is limited compared to ZIP-1 (Dufner-Beattie et al., 2003). Homozygous deletion of ZIP-1, ZIP-2, or ZIP-3 in mice resulted in normal development and viability but increased embryonic lethality when zinc is limited (Dufner-Beattie et al., 2006; Peters et al., 2007). Even triple knockout of ZIP-1, 2 and 3 resulted in no phenotype while mice were fed a normal zinc diet and they exhibited hypersensitivity to zinc deficiency (Kambe et al., 2008). ZIP-4 is the best characterized protein in the ZIP family because mutations in ZIP-4 gene cause the genetic disorder acrodermatitis enteropathica which is characterized by zinc deficiency (Kury et al., 2002; Wang et al., 2002). ZIP-4 is highly expressed in tissues mediating zinc absorption including the intestine. Acting on the apical membrane of enterocytes, ZIP-4 mediates the uptake of zinc from the intestinal lumen (Wang et al., 2002). ZIP-4 expression is regulated by zinc levels—ZIP-4 expression is induced by zinc deficiency, zinc excess downregulates ZIP-4 expression. Regulation of ZIP-4 expression occurs at multiple levels including transcription, mRNA stability, protein localization and stability (Lichten and Cousins, 2009). ZIP-5 displays similar tissue distribution as ZIP-4, but it is localized to the basolateral membrane of the cells (Dufner-Beattie et al., 2004), suggesting that ZIP-5 may function in the removal of

zinc from the blood antagonistically to ZIP-4. ZIP-6 was identified as a novel gene whose expression is regulated by estrogen in breast cancer cells (Manning et al., 1988). ZIP-6 has a role in the epithelial-mesenchymal transition and the immune response in dendritic cells (Kitamura et al., 2006; Yamashita et al., 2004). ZIP-7 is ubiquitously expressed and localized to the Golgi apparatus in cells, and it is implicated in breast cancer progression (Taylor et al., 2007; Taylor et al., 2008). ZIP-8 is detected in a wide range of tissues including lung, kidney, liver, brain and intestine, and it is functionally involved in immune activation in human monocytes (Begum et al., 2002). ZIP-10 was the first ZIP protein found to be regulated by MTF-1. While other MTF-1-regulated genes such as ZnT-1 are activated by MTF-1, ZIP-10 expression is suppressed by MTF-1 (Wimmer et al., 2005). ZIP-13 has been implicated in the development of connective tissues, bone and teeth (Fukada et al., 2008), and ZIP-14 is involved in the response to inflammation (Liuzzi et al., 2005). Although many zinc metabolism-related genes in animals have been characterized as described above, understanding of the molecular mechanisms of their actions and their networks for zinc homeostasis control is still limited.

ZINC METABOLISM IN HUMAN HEALTH AND DISEASE

Zinc metabolism is closely associated with human health and a variety of human diseases. First, as zinc is an essential micronutrient, failure to take adequate amounts of zinc from the diet leads to zinc deficiency which is a significant problem in underdeveloped countries (Hambidge and Krebs, 2007). Zinc deficiency can also be caused by inherited genetic mutations. The autosomal recessive disease acrodermatitis

enteropathica was identified by the symptoms of zinc deficiency in infants (Moynahan, 1974). Patients with the disease have a loss-of-function mutation in ZIP-4, which plays a major role in the uptake of zinc from the diet in the intestine (Kury et al., 2002; Wang et al., 2002). Since the mutations in ZIP-4 result in inefficient uptake of zinc, oral zinc supplementation has been a successful treatment to the patient. Studies of infants with the symptoms of zinc deficiency have identified loss-of-function mutations in another zinc transporter, ZnT-2 (Chowanadisai et al., 2006). ZnT-2 is highly expressed in the mammary gland and functions in the supply of zinc into secretory vesicles. Mutations in ZnT-2 lead to generation of low zinc breast milk and subsequently cause zinc deficiency in breastfed infants.

Abnormal zinc metabolism is implicated in several types of cancers. Studies of prostate cancer demonstrated that there is an association between cellular zinc levels and cell proliferation (Costello and Franklin, 2006). While normal prostate cells have higher levels of zinc compared to other cell types, prostate cancer cells display significantly reduced zinc levels. Treatment with supplemental zinc was shown to suppress cell proliferation in prostate cancer cell lines (Liang et al., 1999), suggesting that high levels of zinc may have inhibitory effects on cell growth and cancer progression. Zinc metabolism is also implicated inbreast cancer progression. In contrast to prostate cancer cells which accumulate less zinc, breast cancer cells display higher levels of zinc compared to normal cells (Geraki et al., 2002). Studies with breast tissue biopsies indicated that there is a correlation between the levels of zinc and the onset of breast cancer (Cui et al., 2007b). Molecular studies have demonstrated that ZIP-6 and/or ZIP-7 are associated with breast cancer; Increased ZIP-6 expression is one of the markers of

11

estrogen-receptor positive cancer (Schneider et al., 2006), and ZIP-7 is required for increasing cellular zinc levels in breast cancer cell lines (Taylor et al., 2008).

Neurodegenerative diseases are associated with imbalance in zinc metabolism. The brain contains a large amount of zinc, and zinc is concentrated in the presynaptic vesicles in glutamatergic neurons (Frederickson et al., 2005). Upon excitation, zinc is released from the neurons along with neurotransmitters, like glutamate, into the synapse and then rapidly taken up by cells. During this process, zinc interacts with various ion channels and transporters and thereby regulates synaptic activity and plasticity. However, excessive release of zinc from synaptic vesicles is toxic and is involved in neuronal and glial cell death. For instance, zinc released from dying cells during seizures or ischemia contributes to cell death and thereby brain damage (Frederickson et al., 2004). Excess zinc is also associated with the pathogenesis of Alzheimer's disease. Zinc promotes the aggregation of amyloid β-peptide, and zinc chelation inhibits the formation of amyloid β-plaques in Alzheimer's disease mouse models (Frederickson et al., 2005)

Diabetes is another disease related to zinc metabolism. The pancreas plays a critical role in glucose homeostasis and contains high levels of zinc. Zinc is concentrated in insulin-granules of pancreatic β-cells where zinc forms stable complexes with insulin. Although the function of zinc stored in insulin granules is not well defined, zinc status may be linked to the progression of diabetes. Type 1 diabetes patients display lower serum zinc levels compared to the healthy individuals (Terres-Martos et al., 1998). Zinc deficiency appears to contribute to pancreatic β-cell function failure (Chausmer, 1998), while dietary supplemental zinc has a protective effect in diabetic mouse models (Ho et al., 2001).. ZnT-8 has been implicated in the pathology of both of type 1 and 2 diabetes.

12

ZnT-8 is as a major autoantigen in 60~80% of new onset of type 1 diabetes (Wenzlau et al., 2007). Recent genome-wide association studies identified genetic variations in ZnT-8 that are significantly associated with type 2 diabetes (Sladek et al., 2007). Although the mechanisms by which the genetic variations affect pancreatic β-cell function are unknown, ZnT-8 knockout mice recently have been generated and exhibited glucose intolerance in response to a high fat diet (Lemaire et al., 2009), suggesting that ZnT-8 may play a critical role in pancreatic β-cell function during stress conditions such as obesity.

Recently, Ehlers-Danlos syndrome (EDS) type IV has been associated with abnormal zinc metabolism. EDS is characterized by progressive kyphoscoliosis, hypermobility of joints, hyperelasticity of skin and severe hypotonia of skeletal muscles, caused by abnormal connective tissue development (Beighton et al., 1998). Analysis of the genomes of EDS patients identified loss-of-function mutations in ZIP-13 (Giunta et al., 2008). ZIP-13 knockout mice displayed phenotypes that are similar to the symptoms observed in EDS patients such as defects in the maturation of osteoblasts, chondrocytes, odontoblasts and fibroblasts (Fukada et al., 2008), suggesting that zinc metabolism is involved in bone and connective tissue development. Despite the implication of zinc metabolism in these various diseases, the molecular mechanisms by which zinc metabolism affect the diseases are not well understood and remain to be addressed as one of the most important topics in zinc pathophysiology.

ZINC METABOLISM IN *C. ELEGANS*

The nematode *C. elegans* is an important model system that has been used to

elucidate fundamental, evolutionarily conserved biological processes, such as apoptosis and RNA interference (Fire et al., 1998; Sulston and Horvitz, 1977), and to develop innovative experimental techniques, such as *in vivo* expression of green fluorescent protein (GFP) (Chalfie et al., 1994). *C. elegans* has been a relevant model organism for the study of metal biology, including iron and heme metabolism, and metal toxicity (Gourley et al., 2003; Liao and Freedman, 1998; Rajagopal et al., 2008).

Mechanisms of zinc metabolism are well conserved between *C. elegans* and other species. Analysis of the *C. elegans* genome revealed that *C. elegans* has 2 metallothionein genes (*mtl-1* and *mtl-2*), 14 putative *cdf* genes and 14 *zip* genes (Kambe et al., 2006). Intriguingly, there is no protein identified that has sequence similarity to the known zinc-responsive transcription factors, the yeast Zap1 or mammalian MTF-1, suggesting that *C. elegans* may have unique gene expression regulatory mechanisms for zinc metabolism. *C. elegans* has several advantages to study zinc metabolism compared to other model organisms such as the yeast and mouse. While it is a multicellular animal that is complex enough to study the networks of zinc metabolism in the whole animal, it has a simpler anatomy than mammals which facilitates the analysis of the system. *C. elegans* is genetically tractable, allowing forward genetics, reverse genetics and the analysis of genetic interactions among multiple genes. Furthermore, culture methods that permit precise control over dietary zinc have been established (Bruinsma et al., 2008; Davis et al., 2009; Szewczyk et al., 2003).

C. elegans has provided novel insights into zinc metabolism. The *C. elegans cdf* genes *cdf-1* and *sur-7* were identified in a forward genetic screen for suppressors of Ras-mediated signaling during vulva development (Bruinsma et al., 2002; Yoder et al., 2004).

These studies demonstrated not only the functional role of CDF-1 and SUR-7 in the control of zinc metabolism of the animal but also the novel biological function of zinc ions as signaling molecules that modulate developmental processes. Studies using forward genetic screens also identified multiple mutations that confer resistance to zinc toxicity and subsequently characterized a novel gene that mediates zinc resistance, *haly-1* (Bruinsma et al., 2008; Murphy et al., 2011). These studies revealed a novel mechanism of zinc metabolism in which histidine can act as a zinc buffering system to control zinc toxicity. We recently developed various analytic methods to measure zinc metabolism, such as maturation rate, population growth rate and total zinc content, and we applied these methods to identify and characterize another *cdf* gene, *cdf-2* (Davis et al., 2009).

ANALYSIS OF ZINC TRANSPOTERS IN *C. ELEGANS*

The analysis of *C. elegans* zinc transporters is important to understand the function of these proteins in zinc metabolism and other biological processes. Furthermore, the discoveries made by the analysis of *C. elegans* zinc transporters will contribute to the understanding of the complicated processes of zinc metabolism and how they are related to human disease.

In this study, I describe the function of zinc transporters in the regulation of zinc metabolism in *C. elegans* and their roles in other biological processes. In Chapter 2, I demonstrate that zinc is stored in lysosome-related organelles called gut granules in *C. elegans* intestinal cells . Labile zinc was stored in gut granules by the action of the CDF-2 zinc transporter, and zinc storage was important for zinc detoxification and mobilization in response to fluctuating levels of zinc. Gut granules displayed novel

morphological changes, the formation of asymmetric bilobed vesicles, in response to high levels of zinc. These results suggest that zinc is stored in *C. elegans* gut granules by active mechanisms that involve zinc transporters and vesicular transformation.

In Chapter 3, I describe the function of a novel *cdf* gene, *ttm-1* (toxin-regulated target of p38MAPK). *ttm-1* encodes two isoforms, *ttm-1a* and *ttm-1b*, by using different transcription start sites. Genetic analysis demonstrated that TTM-1 is important for zinc excretion and involved in zinc detoxification, and TTM-1B plays a key role in these processes by acting on the apical membrane of intestinal cells. TTM-1 interacts with CDF-2 in regulating zinc metabolism. These studies suggest that TTM-1 is another important player in the zinc metabolism of *C. elegans*.

In Chapter 4, I discuss the implication of these studies and the future studies to further extend our knowledge of zinc metabolism.

In Appendix A, we report new methods to monitor zinc metabolism in *C. elegans* and the initial studies of *cdf-2*. CDF-2 was expressed in the intestine and localized to the membrane of intracellular vesicles, and a loss-of-function mutation in *cdf-2* caused reduced total zinc content. These findings led to the hypothesis that CDF-2 plays a role in zinc storage in *C. elegans*. In Appendix B, I describe the initial analyses of uncharacterized *C. elegans* zinc transporters with the focus on ZIP family proteins. Expression pattern studies identified the tissue distributions and intracellular localization of many ZIP proteins. Genetic analysis using loss-of-function mutations suggested several zinc transporters are involved in specific biological processes.

CHAPTER 2

Lysosome-Related Organelles in Intestinal Cells Function as a Zinc Storage Site in *C. elegans*

ABSTRACT

Zinc is an essential trace element involved in many biological processes and human diseases. Animals require homeostatic mechanisms to store and mobilize zinc in response to dietary fluctuations, but these mechanisms are not well defined. Here we demonstrate that lysosome-related organelles called gut granules present in intestinal cells of *C. elegans* function as the major site of zinc storage. Zinc storage in gut granules promotes detoxification and subsequent mobilization, since mutant animals lacking gut granules were defective in both processes. The cation diffusion facilitator protein CDF-2 plays a critical role in this process by transporting zinc into gut granules. In response to high dietary zinc, gut granules displayed structural changes characterized by a bilobed morphology with asymmetric distributions of molecular markers. Glo genes were required for this structural change of gut granules. These findings elucidate novel mechanisms of zinc storage, detoxification and mobilization in *C. elegans* and may be relevant to other animals.

INTRODUCTION

Zinc is a trace nutrient that is essential for all life. Zinc has roles in many biological processes; protein-bound zinc contributes to enzymatic activity and protein structure, and labile zinc functions in signal transduction (Murakami and Hirano, 2008; Vallee and Falchuk, 1993). Zinc is important for human health, since zinc deficiency causes a broad range of defects in multiple organ systems including skin, immune, skeletal and reproductive (Hambidge, 2000). Zinc deficiency caused by inadequate dietary intake is a major world-wide problem. Zinc deficiency is also associated with genetic diseases caused by mutations of zinc transporters, such as acrodermatitis enteropathica. Excess zinc is also deleterious, since it may displace other trace metals or bind low affinity sites, leading to protein dysfunction (Fosmire, 1990). Therefore, organisms require mechanisms for zinc metabolism and homeostasis to control the levels and distribution of this essential metal.

Zinc metabolism in animals involves many processes: the absorption and secretion of zinc by gastrointestinal tracts, the excretion of zinc into urine by kidney, and the distribution and exchange of zinc between tissues (Cummings and Kovacic, 2009; Krebs, 2000). Within cells, zinc is partitioned between the cytosol and the lumen of intracellular organelles, and it can be labile or protein bound. Two families of zinc transporters play critical roles in eukaryotic organisms: cation diffusion facilitator (CDF/SLC30) and Zrt-, Irt-like protein (ZIP/SLC39) (Cragg et al., 2005; Eide, 2006; Feeney et al., 2005). CDF proteins decrease cytoplasmic levels by transporting zinc across the plasma membrane or into intracellular organelles, whereas ZIP proteins

19

increase cytoplasmic levels by transporting zinc in the opposite direction. Mammals contain 10 CDF and 14 ZIP proteins that have specific tissue distributions and intracellular localizations (Lichten and Cousins, 2009). Thus, a network of zinc transporters is likely to regulate zinc metabolism in animals.

Organisms have evolved to deal with variable nutrient availabilities by having mechanisms to regulate uptake and excretion. Furthermore, when nutrients are replete, excess nutrients are stored so that they can be mobilized under nutrient deficient conditions. In natural environments, the availability of metal is variable, so it is likely that organisms have mechanisms for metal storage and mobilization. For example, iron is essential in mammals for erythropoietic function and oxidative metabolism, and iron is stored in the liver in the forms of ferritin or hemosiderin (Munoz et al., 2009). Mechanisms of zinc storage have been characterized in the yeast *Saccharomyces cerevisiae*. When zinc is abundant, the CDF proteins Cot1 and Zrc1 transport zinc into the vacuole, which functions to store excess zinc and protect from zinc toxicity. When yeast are challenged with zinc deficient conditions, the ZIP protein Zrt3 mobilizes stored zinc by transporting it out of the vacuole (Eide, 2006).

In mammals, it has been demonstrated that high levels of zinc are detected in several tissues and intracellular organelles. Synaptic vesicles in neuronal cells (Palmiter et al., 1996b), insulin granules in pancreatic β-cells (Chimienti et al., 2004) and secretory vesicles in mammary cells display high levels of zinc (Kelleher and Lonnerdal, 2003). Studies using zinc-specific fluorescent dyes have demonstrated that zinc is detected in punctate vesicles in a variety of cell types, which are putatively termed as zincosomes and may be endosomal or lysosomal compartments (Eide, 2006). However, the role of

these zinc-containing organelles in zinc storage and mobilization in response to fluctuating dietary zinc at organism levels has not been well characterized.

The nematode *C. elegans* has been a relevant model organism for the study of metal biology, including iron and heme metabolism, metal toxicity, and zinc signaling (Bruinsma et al., 2002; Gourley et al., 2003; Liao and Freedman, 1998; Rajagopal et al., 2008; Vatamaniuk et al., 2001; Yoder et al., 2004). We are using *C. elegans* to study zinc metabolism, because this animal has conserved mechanisms of zinc metabolism, powerful genetics and culture system (Bruinsma et al., 2002; Bruinsma et al., 2008; Davis et al., 2009). We demonstrated that *C. elegans* exposed to a high zinc diet accumulate substantial amounts of zinc, indicating that these animals store excess zinc. (Davis et al., 2009). In this study, we sought to identify the site of zinc storage by developing methods to visualize zinc in *C. elegans* using a zinc-specific fluorescent dye, FluoZin-3. Labile zinc was detected in gut granules in intestinal cells. Gut granules have been classified as lysosome-related organelles based on the presence of lysosomal proteins and staining with lysosome-specific fluorescent dyes such as LysoTracker (Clokey and Jacobson, 1986; Hermann et al., 2005; Kostich et al., 2000). To assess the function of gut granules, we analyzed gut-granule-loss (Glo) mutant animals. These animals displayed zinc storage defects and zinc hypersensitivity, indicating that gut granules are critical for zinc storage and detoxification. The cation diffusion facilitator protein CDF-2 plays a critical role in the mechanism of zinc storage. CDF-2 localized to the membrane of gut granules, and *cdf-2* loss-of-function mutant animals were defective in zinc storage and hypersensitive to high levels of dietary zinc. We demonstrated that zinc stored in gut granules can be mobilized in zinc deficient conditions. Finally, we

21

characterized a novel morphology of gut granules, asymmetric bilobed vesicles, in response to high dietary zinc, and *glo* genes are necessary for the morphological change. These findings identify the site of zinc storage in an animal and demonstrate a key role for a CDF protein during zinc storage.

RESULTS

Gut Granules Contain Labile Zinc

By using inductively coupled plasma-mass spectrometry (ICP-MS) to measure total zinc content in worm extracts, we previously demonstrated that culturing *C. elegans* with high dietary zinc results in elevated levels of total zinc, suggesting that excess zinc is stored (Davis et al., 2009). To elucidate the spatial distribution of zinc and identify the site of zinc storage, we used zinc-specific fluorescent dyes to visualize zinc. We conducted pilot studies with several dyes and selected FluoZin-3 based on its high zinc-sensitivity and specificity (Gee et al., 2002). Hermaphrodites were cultured on noble agar minimal medium (NAMM) dishes (Bruinsma et al., 2008) containing FluoZin-3, and live animals were analyzed by fluorescence microscopy. Wild-type animals cultured without supplemental zinc displayed green fluorescence in vesicles in the intestinal cells (Figure 2.1A). To test if the FluoZin-3 fluorescence is due to zinc binding, we manipulated dietary zinc using supplemental zinc and the zinc chelator, N,N,N′,N′-Tetrakis (2-pyridylmethyl) ethylenediamine (TPEN). FluoZin-3 fluorescence intensity displayed significant, dose-dependent enhancement and diminishment in worms cultured with

supplemental zinc and TPEN, respectively (Figures 2.1A and 2.1B). These results

indicate that FluoZin-3 fluorescence monitors labile zinc in live worms, and zinc is

concentrated in vesicles of intestinal cells.

To investigate the relationship between FluoZin-3 fluorescent vesicles and

intestinal gut granules, we performed costaining experiments using LysoTracker

(Hermann et al., 2005). With no supplemental zinc, the patterns of FluoZin-3 and

LysoTracker fluorescence were highly overlapping in intestinal cells (Figure 2.1C and

Supplemental Figure 2.1), indicating that zinc detected by FluoZin-3 is stored in gut

granules. Because gut granules contain birefringent and autofluorescent materials, we

determined how autofluorescence compares to FluoZin-3 fluorescence by comparing

animals cultured with FluoZin-3 to control animals cultured with no dye. Animals

cultured with FluoZin-3 displayed 2.6, 3.5 and 4.3-fold higher signal than control

animals when cultured with 0μM, 100μM and 200μM supplemental zinc, respectively

(Supplemental Figure 2.2). These results indicate that the signal is primarily due to

FluoZin-3 binding zinc with a minor contribution from autofluorescence.

Gut Granules are the Major Site of Zinc Storage

To characterize the function of gut granules in zinc storage, we analyzed Glo

mutant animals that have reduced numbers of gut granules due to defects in lysosome

biogenesis (Hermann et al., 2005). We analyzed three genes, *pgp-2, glo-1* and *glo-3,*

because well characterized loss-of-function mutations in these genes cause Glo

phenotypes of different severities; wild-type animals contain hundreds of gut granules,

whereas *pgp-2(kx49)* animals contain 10~100 gut granules, and *glo-1(zu391)* and *glo-*

3(zu446) animals contain less than 10 gut granules (Hermann et al., 2005; Rabbitts et al., 2008; Schroeder et al., 2007). *pgp-2* encodes an ABC transporter that is localized to the membrane of gut granules, *glo-1* encodes a predicted Rab GTPase that localizes to gut granules, and *glo-3* has not been molecularly identified. All of the Glo animals displayed reduced FluoZin-3 fluorescence compared to wild-type animals at 0μM and 100μM supplemental zinc (Figure 2.2A). Consistent with the severity of Glo phenotype, *pgp-2* mutant animals contained a small number of FluoZin-3 positive granules, and *glo-1* and *glo-3* mutant animals displayed very few granules stained with FluoZin-3. These results support the conclusion that gut granules are the site of labile zinc detected by FluoZin-3.

To quantify zinc storage defects in Glo animals, we used ICP-MS as an independent method to measure total zinc content. In culture conditions with 0μM and 200μM supplemental zinc, *pgp-2* mutants displayed a moderate reduction of total zinc content, and *glo-1* mutants displayed a severe reduction of total zinc content compared to wild-type animals (Figure 2.2B). The total zinc content of the Glo animals was well correlated with the severity of the Glo phenotype. With 200μM supplemental zinc, *glo-1* mutants contained approximately 50% of the total zinc content of wild-type animals. These results indicate that gut granules are the major site of zinc storage in *C. elegans* that contains about half of the total zinc in the body.

To determine whether gut granules are also used to store additional metals, we analyzed the total metal content of four additional physiological metals from Glo animals using ICP-MS. Glo animals did not exhibit a consistent change in total levels of magnesium, iron, manganese or copper compared to wild-type animals (Supplemental Figure 2.3). These results indicate that gut granules are specifically involved in zinc

storage.

High Dietary Zinc Induces CDF-2 Expression, and CDF-2 Promotes Zinc Storage in Gut Granules

cdf-2 mRNA levels are increased by high dietary zinc, and CDF-2 is expressed specifically in intestinal cells and localized to autofluorescent vesicles (Davis et al., 2009). To analyze the regulation of CDF-2 protein expression by dietary zinc, we used transgenic animals expressing CDF-2::GFP. The level of CDF-2::GFP was induced in a concentration-dependent manner by approximately 3-fold and 4-fold at 100 and 200μM supplemental zinc, respectively, compared to 0μM supplemental zinc (Figures 2.3A and 2.3B). These results suggest that high levels of CDF-2 play an important role in the response to high dietary zinc. To elucidate the relationship between CDF-2 and zinc storage, we cultured transgenic animals expressing CDF-2::mCherry on NAMM dishes containing FluoZin-3. In animals cultured with no supplemental zinc, FluoZin-3 and CDF-2::mCherry fluorescence overlapped almost completely (Supplemental Figure 2.4, left), indicating that CDF-2 is localized to the gut granules that concentrate zinc.

To determine the function of CDF-2 in zinc storage in gut granules, we analyzed animals with reduced or increased levels of CDF-2 activity. Activity was reduced by the *cdf-2(tm788)* deletion mutation that causes a strong loss-of-function, whereas activity was increased by generating transgenic animals that contain multicopy, extrachromosomal arrays expressing CDF-2::mCherry in the *cdf-2(tm788)* background. *cdf-2(tm788)* mutant animals displayed significantly lower FluoZin-3 fluorescence at both 0μM and 100μM supplemental zinc compared to wild-type animals (Figures 2.3C

25

and 2.3D). ICP-MS analysis revealed that *cdf-2(tm788)* mutant animals had a severe

reduction of total zinc content, similar to *glo-1* mutant animals (Figure 2.2B), consistent

with our previous studies (Davis et al., 2009). These results indicate that CDF-2 is

necessary to concentrate zinc into gut granules. Since *cdf-2(tm788)* mutant animals

displayed slightly increased FluoZin-3 fluorescence at 100μM compared to 0μM

supplemental zinc, a CDF-2 independent mechanism might concentrate zinc in gut

granules. One possibility is that an alternative zinc transporter is induced in *cdf-2* mutant

animals, and differences were observed in mRNA levels of other *cdf* genes in *cdf-2*

mutants animals compared to wild-type animals (data not shown). Transgenic animals

that overexpress CDF-2::mCherry displayed higher FluoZin-3 fluorescence at 0μM and

100μM supplemental zinc compared to *cdf-2* mutants and wild-type animals (Figures

2.3C and 2.3D). Thus, overexpression of CDF-2 was sufficient to concentrate zinc into

gut granules.

Transgenic animals containing extrachromosomal arrays display mosaic

expression of transgenes spontaneously and at a low frequency. To determine whether

CDF-2 functions cell-autonomously, we analyzed mosaic animals that lack transgene

expression in specific intestinal cells. Because these animals contain the *cdf-2(tm788)*

mutation, an intestinal cell that lacks transgene expression lacks all CDF-2 function. The

intestinal cells lacking CDF-2::mCherry expression displayed lower FluoZin-3

fluorescence compared to the flanking cells that express CDF-2::mCherry (Figure 2.3E).

These results indicate that CDF-2 functions cell-autonomously in intestinal cells to

promote zinc concentration in gut granules.

High Dietary Zinc Alters Gut Granule Morphology

To characterize how the intracellular localization of CDF-2 responds to high dietary zinc, we examined the colocalization of CDF-2 and LysoTracker. In the absence of supplemental zinc, CDF-2::GFP colocalized completely with LysoTracker (Figure 2.4A, left). This observation demonstrates directly that CDF-2 localizes to the membrane of gut granules. In the presence of 200μM supplemental zinc, CDF-2::GFP expression remained restricted to gut granules, but gut granules displayed altered morphology. Many vesicles had a bilobed appearance, and the two lobes displayed distinct staining patterns; one side was positive for both CDF-2 and LysoTracker, whereas the other side was positive for CDF-2 and negative for LysoTracker (Figure 2.4A, right). Since LysoTracker labels acidic organelles, these results indicate that one lobe may lack the determinants that concentrate the LysoTracker or the LysoTracker dye may be present but not fluorescent due to high pH. To examine a possible pH difference, we used LysoSensor Green DND-153, which is highly fluorescent in neutral compartments (Zhang et al., 2010). Colocalization analysis with CDF-2::mCherry demonstrated that LysoSensor Green strain only one side of the bilobed gut granules (Supplemental Figure 2.5), similar to LysoTracker staining. These results suggest that asymmetric staining of bilobed vesicles may reflect an asymmetric distribution of the molecules that bind these fluorescent probes.

To characterize additional differences between the two dies of bilobed gut granules, we first investigated the distribution of zinc. Zinc was visualized with FluoZin-3, and gut granules were visualized with LysoTracker. With 100μM supplemental zinc, FluoZin-3 and LysoTracker fluorescence displayed asymmetric staining in the bilobed

27

gut granules. The LysoTracker-positive side displayed relatively weak FluoZin-3 staining, whereas the LysoTracker-negative side displayed relatively strong FluoZin-3 staining (Figure 2.1C, right). To examine the relationship between zinc levels and CDF-2 protein in the bilobed gut granules, we visualized zinc using FluoZin-3 and CDF-2::mCherry. Whereas FluoZin-3 fluorescence was asymmetric and strong in only one side of bilobed granules, CDF-2::mCherry was localized to both sides (Supplemental Figure 2.4, right). These results indicate that while the distribution of labile zinc may be asymmetric in bilobed gut granules, CDF-2 protein may be symmetric.

C. elegans has been used to identify and characterize genes that are localized to specific endosomal and lysosomal compartments. To define the molecular properties of bilobed gut granules, we examined the localization of several of these marker proteins. The GTPase Rab-5 is localized to early endosomes in mammalian cells (Zerial and McBride, 2001), and *C. elegans* RAB-5 expressed in intestinal cells localizes to small punctate structures that appear to be early endosomes (Chen et al., 2006; Hermann et al., 2005). RAB-5 did not colocalize with LysoTracker or CDF-2 (data not shown), indicating that CDF-2 does not accumulate in early endosomes. *C. elegans* RAB-7::GFP appears to stain early endosomes and late endosomes, similar to the localization patterns in other systems (Chen et al., 2006; Zerial and McBride, 2001). Lysosome associated membrane proteins (LAMPs) are localized predominantly in lysosomes in vertebrates, and *C. elegans* LMP-1 localizes to specific gut granules of intestinal cells (Kostich et al., 2000). A subset of LMP-1 and RAB-7 colocalized with LysoTracker in gut granules (Figure 2.4B and Supplemental Figure 2.6A). In high zinc, LMP-1 and RAB-7 were localized on only one side of the bilobed vesicles that were visualized using CDF-

2::mCherry (Figure 2.4C and Supplemental Figure 2.6B). These results indicate that the gut granules that contain CDF-2 also contain the late endosomal/lysosomal proteins RAB-7 and LMP-1. The bilobed granules displayed an asymmetric distribution of RAB-7 and LMP-1, indicating that one lobe has typical lysosomal characteristics whereas the other lobe lacks lysosomal proteins.

C. elegans PGP-2 is an ABC transporter that localizes specifically to the gut granule membrane (Schroeder et al., 2007). With no supplemental zinc, CDF-2::mCherry and PGP-2::GFP colocalized completely in gut granules; these gut granules also displayed autofluorescence (Supplemental Figure 2.7, left). In the presence of 100μM supplemental zinc, CDF-2 and PGP-2 fully colocalized on both sides of the bilobed gut granules. Autofluorescence displayed an asymmetric pattern and was only prominent on one side, similar to the LysoTracker staining pattern (Supplemental Figure 2.7, right). These results indicate that bilobed gut granules contain proteins that are symmetrically distributed on both lobes, such as PGP-2 and CDF-2, and proteins that are asymmetrically localized, such as RAB-7 and LMP-1.

Glo Genes are Required for the Formation of Bilobed Gut Granules

To identify mechanisms that are important for the formation of bilobed gut granules, we examined the gut granule morphology in mutant animals by colocalization experiments of PGP-2::GFP, LysoTracker and FluoZin-3. *cdf-2* mutant animals displayed bilobed vesicles that contain PGP-2::GFP symmetrically on both lobes and LysoTracker asymmetrically on one lobe (Supplemental Figure 2.8A). As expected, bilobed gut granules did not stain with FluoZin-3 in *cdf-2* mutant animals (Supplemental Figure

2.8B). These results indicate that the formation of bilobed vesicles does not require *cdf-2* activity, but acculumation of zinc in these vesicles does require *cdf-2*.

To dissect the molecular process involved in the bilobed gut granule formation, we blocked lysosome biogenesis and endocytosis pathways by RNAi knockdown of *rab-7* and *rme-8, respectively,* and examined its effect on gut granule morphology. Bilobed vesicles were detected in *rab-7* and *rme-8* RNAi fed animals (Figure 2.5), indicating that neither lysosome biogenesis nor endocytosis is required for the formation of bilobed gut granule. Since only gut granule-specific proteins were found on both sides of bilobed vesicles, we hypothesized that bilobed vesicle formation may be also regulated by gut granule-specific processes. To test the hypothesis, we knockdowned *glo* genes, *pgp-2* and *glo-3*. In *pgp-2* and *glo-3* RNAi fed animals, bilobed morpholgy was not detected, and there were separate compartments which display CDF-2:GFP but not LysoTracker (Figure 2.5). These results indicate that *Glo* genes that function in gut granule formation are required for the formation of bilobed morphology in response to high zinc.

Gut Granules are Necessary for Zinc Detoxification

To investigate whether storage in gut granules is a protective mechanism that promotes zinc detoxification, we analyzed the growth rate of animals in response to increasing levels of dietary zinc. Animals were synchronized at the first larval (L1) stage, cultured on NAMM dishes supplemented with zinc for a specific time period, and analyzed individually to measure length as an indicator of growth. Wild-type animals displayed a dose-dependent decrease in growth rate, indicating that high dietary zinc inhibits growth (Figure 2.6A). *pgp-2, glo-1* and *glo-3* mutant animals displayed

significantly lower growth rates than wild-type animals with all supplemental zinc (Figure 2.6A). The severity of the zinc sensitivity phenotype correlated with the severity of Glo phenotype; *pgp-2* mutants were moderately zinc sensitive whereas *glo-1* and *glo-3* mutants were strongly zinc sensitive. These results indicate that gut granules play an important protective role in response to zinc toxicity. To determine the role of CDF-2 in this mechanism of zinc detoxification, we examined a *cdf-2* loss-of-function mutant that is defective in zinc storage. Similar to Glo animals, *cdf-2* mutants were hypersensitive to dietary zinc compared to wild-type animals (Figure 2.6B). Since *cdf-2* mutants have normal formation of gut granules shown by LysoTracker staining (Supplemental Figure 2.8B), these findings indicate that CDF-2 mediated zinc transport into gut granules is a critical mechanism for zinc detoxification.

To investigate whether gut granules have a general role in metal detoxification, we examined the sensitivity of Glo animals to the toxic effects of additional metals. Glo animals were similar to wild-type animals in sensitivity to dietary cadmium (Figure 2.6C) and copper (data not shown), indicating that gut granules are not necessary to detoxify these metals. The growth of *cdf-2(tm788)* mutant animals was also similar to wild-type animals in the presence of supplemental cadmium (Figure 2.6D) and copper (data not shown). These results indicate that CDF-2 function is specific to zinc and support the conclusion that gut granules are not a general site of metal storage and may be specific for zinc storage.

Gut Granules Provide a Source of Zinc that Can Be Mobilized in Response to Deficiency.

One possible function of storing zinc in gut granules is to provide a supply of zinc that can be mobilized in response to zinc deficient conditions. To test this model, we monitored the levels of zinc in gut granules using FluoZin-3 in the shift from high zinc to different zinc conditions. Wild-type animals were first cultured with 200μM supplemental zinc. There was approximately 2.5-fold increase in FluoZin-3 fluorescence compared to the control animals cultured with no supplemental zinc, indicating that zinc is stored in gut granules during the preculture with high zinc (Figures 2.7A and 2.7B). Animals were then shifted to high (200μM supplemental zinc), normal (0μM supplemental zinc) or low zinc (100μM TPEN) conditions, and analyzed to measure FluoZin-3 fluorescence. When animals were continuously cultured with 200μM supplemental zinc, FluoZin-3 fluorescence further increased (Figures 2.7A and 2.7B). When animals were shifted to the normal zinc condition, FluoZin-3 fluorescence increased by ~1.7-fold after 24h of the shift and then after 48h it slightly decreased. When animals were shifted to the low zinc, FluoZin-3 fluorescence increased by ~1.4-fold after 24h, but after 48h FluoZin-3 fluorescence dramatically decreased below the initial fluorescence. These results indicate that zinc stored in gut granules can be mobilized in response to low zinc conditions.

To independently investigate zinc mobilization, we analyzed the growth of animals that were precultured with either normal or high zinc conditions and subsequently cultured in low zinc conditions. Wild-type animals precultured with 50μM supplemental zinc displayed a significantly increased growth rate in the presence of TPEN compared to animals precultured with 0μM supplemental zinc (Figure 2.7C). These results indicate that wild-type animals store zinc that can be used later to cope

32

with zinc deficiency. *cdf-2* mutant animals precultured with 0μM or 50μM supplemental zinc displayed similar growth rates in the presence of TPEN (Figure 2.7C). These results indicate that CDF-2 is necessary for preculturing with high zinc to promote the resistance to subsequent zinc deficiency, probably because CDF-2 promotes the storage of zinc in gut granules.

To test the model that gut granules are the source of zinc that is mobilized during zinc deficiency, we examined Glo animals. *glo-1, glo-3* and *pgp-2* mutants precultured with 0μM supplemental zinc displayed slower growth rates than wild-type animals when challenged with zinc deficient conditions (Figure 2.7D). Furthermore, whereas wild-type animals displayed a significant increase in growth when preincubated with 50μM supplemental zinc, preincubation with supplemental zinc did not significantly affect the growth of Glo animals (Figure 2.7D). Thus, *glo-1, glo-3, pgp-2* and *cdf-2* were necessary for animals to respond to preincubation with supplemental zinc. These results indicate that gut granules, which are the major site of zinc storage during dietary excess, are the source of zinc mobilized during zinc deficiency.

DISCUSSION

Gut Granules in Intestinal Cells Function as a Zinc Storage Site

Zinc is essential, but zinc availability fluctuates. Thus, mechanisms to store and mobilize zinc are important. We used *C. elegans* to characterize the site of zinc storage in an animal by developing methods to visualize labile zinc using a zinc-specific

fluorescent dye, FluoZin-3. Labile zinc was detected primarily in lysosome-related organelles in intestinal cells called gut granules. The biogenesis of gut granules has been studied using Glo mutant animals that have reduced numbers of gut granules (Hermann et al., 2005; Rabbitts et al., 2008; Schroeder et al., 2007). We used these mutants to demonstrate that Glo animals have reduced levels of labile zinc and total zinc, and the severity of the Glo phenotype correlated with the reduction in zinc levels. Glo animals had wild-type levels of other metals such as copper. Thus, these results support the conclusion that gut granules function specifically in zinc storage, and provide direct evidence for the presence of a zinc-specific storage site in animals.

In the yeast *Saccharomyces cerevisiae*, the vacuole plays a central role in zinc storage (Eide, 2006). In mammals, zinc storage has not been well defined. Kinetic studies using zinc stable isotopes have suggested that exchangeable pools of zinc are limited (Krebs and Hambidge, 2001). However, these studies have limitations because these studies examined a very small fraction of total zinc pools and the range of dietary zinc that can be tested was relatively narrow. Our studies using *C. elegans* with a wider range of dietary zinc allowed the identification of a site of zinc storage. Since *C. elegans* has conserved mechanisms of zinc metabolism, such as zinc transporter proteins and metallothioneins, these results suggest that zinc storage mechanisms may be present in higher animals.

     C. elegans gut granules and yeast vacuoles both have lysosomal properties. This similarity leads us to speculate that lysosome-related organelles may have a role in zinc storage in higher animals. In fact, labile zinc is detected by zinc-responsive fluorescent dyes in intracellular organelles called zincosomes in various types of mammalian cells,

which have lysosomal properties (Eide, 2006). Furthermore, there are specialized lysosome-related organelles that may function in zinc storage, similar to *C. elegans* gut granules. For instance, secretory granules in paneth cells in the intestine contain zinc, and paneth cell number and the granule morphology are affected by dietary zinc conditions (Giblin et al., 2006). Acidocalcisomes are acidic organelles conserved from bacteria to human that contain calcium and polyphosphate, and zinc is found in acidocalcisomes in several species (Docampo et al., 2005). Thus, the roles of these lysosome-related organelles in zinc storage and zinc homeostasis of animals will be intriguing future topics to be studied.

The cation diffusion facilitator protein CDF-2 plays a critical role in zinc storage. Colocalization experiments with gut granule markers demonstrated that CDF-2 is localized to the membrane of gut granules. Reducing the activity of *cdf-2* with a loss-of-function mutation and increasing the activity of *cdf-2* by overexpression demonstrated that *cdf-2* is both necessary and sufficient for zinc storage in gut granules. Consistent with the model that CDF-2 directly transports zinc into gut granules, CDF-2 functions cell-autonomously in intestinal cells to promote zinc accumulation. *C. elegans* CDF-2 is homologous to mammalian ZnT2 which plays a role in the secretion of zinc into breast milk (Chowanadisai et al., 2006). Similar to CDF-2, ZnT2 is localized to intracellular vesicles and upregulated by dietary zinc (Liuzzi et al., 2001), suggesting that ZnT2 may be involved in zinc storage in mammals.

Zinc Storage in Gut Granules Promotes Detoxification and Provides a Source of Zinc that is Mobilized During Deficiency

We characterized two functions of zinc storage in gut granules. The first is detoxification. Glo animals were hypersensitive to zinc toxicity, and the hypersensitivity correlated with the severity of the Glo defect. These findings indicate that gut granules have a critical role in zinc detoxification. c*df-2* loss-of-function mutants which had normal gut granules were hypersensitive to dietary zinc, and CDF-2 was induced by dietary zinc, suggesting that CDF-2 mediated transport of zinc into gut granules is an important mechanism to detoxify high levels of dietary zinc. The yeast vacuole plays a role in zinc detoxification. In multicellular animals, the protective role of zinc-containing organelles in the whole body zinc homeostasis has not been demonstrated. Thus, these studies of *C. elegans* document a novel role of lysosome-related organelles in zinc metabolism in animals. High levels of dietary zinc induce changes in gene expression, such as induction of metallothionein genes, and these alterations in gene expression may play a role in detoxification (Lichtlen and Schaffner, 2001). An important direction for future research will be to determine how zinc sequestration in lysosome-related organelles relates to other mechanisms of zinc tolerance such as expression of zinc-binding proteins.

The second function of zinc storage in gut granules is to provide a source of zinc that can be utilized during dietary deficiency. To test this process, we examined the zinc level in gut granule using FluoZin-3 in the shift from high zinc to low zinc conditions. For the first 24h after the shift, FluoZin-3 fluorescence slightly increased, but after 48h, it significantly decreased. These results indicate that zinc stored in gut granules during preculture in high zinc can be mobilized in the shift to low zinc conditions, and zinc mobilization appeared to occur between 24h and 48h after the shift conditions. It is possible that, within the 24h, gut granules keep taking up remaining excess zinc in the

animal. Between 24h and 48h after the shift, animals perhaps experience zinc deficiency and begin to mobilize zinc from gut granules.

As an independent approach, we also examined the growth of animals in the shift from high zinc to low zinc conditions. Wild-type animals with a high level of zinc storage grew better in zinc deficient conditions than animals with a low level of zinc storage, indicating that stored zinc can be mobilized during zinc deficiency. An alternative explanation for this observation is that exposure to high dietary zinc results in another change, such as altered gene expression, that promoted growth in zinc deficient conditions. The analysis of Glo animals and *cdf-2* mutants suggests this is unlikely, since gut granules and CDF-2 mediated zinc transport were necessary for effective storage and mobilization. Therefore, we propose that zinc stored in gut granules during periods of dietary excess can be mobilized to support growth during periods of zinc deficiency. This process requires Glo genes that mediate biogenesis of gut granules and CDF-2 that transports zinc into gut granules.

Mobilization of stored zinc has been analyzed in yeast. The ZIP protein Zrt3 is localized to the vacuole and transports zinc into the cytoplasm in response to zinc deficiency (MacDiarmid et al., 2000). In multicellular animals, although the loss of zinc from zinc-containing organelles has been observed in the process of signal transduction (Aydemir et al., 2009), zinc mobilization from a site of zinc storage in response to dietary deficiency has been not demonstrated. The characterization of gut granules described here is the first documentation of a specific site of zinc storage that is mobilized during dietary deficiency. Mobilization is likely to require a transporter that shuttles zinc from the lumen of gut granules to the cytoplasm, and future studies will focus on the

37

identification of this transporter.

Gut Granules Change Morphology in High Dietary Zinc

Gut granules displayed novel morphological changes in response to high dietary zinc. In standard culture conditions, gut granules were typically round in shape, autofluorescent, stained with LysoTracker, LysoSensors, and FluoZin-3, and the membrane contained CDF-2, RAB-7, LMP-1 and PGP-2 (Supplemental Figure 2.9). In high dietary zinc, gut granules were frequently bilobed in shape. The bilobed vesicles displayed asymmetric distribution of molecules; one side displayed almost the identical molecular properties to normal state gut granules, whereas the other side contained only gut granule-specific proteins, PGP-2 and CDF-2, and displayed strong FluoZin-3 staining (Supplemental Figure 2.9). These results suggest that one side that has a high concentration of zinc may have unique molecular properties and specialized functions in zinc metabolism.

We speculate that bilobed vesicles may have two functions. First, this structural change may be a mechanism to promote zinc storage. Generating additional adjacent vesicles which are devoted to storing zinc can improve the capacity of storage and facilitate rapid sequestration. Second, bilobed vesicles may function in the secretion of excess zinc beyond the gut granule capacity. When zinc is accumulated over the capacity of gut granules in high zinc conditions, gut granules may undergo the structural changes to make specialized secretory vesicles full of excess zinc. Thus, gut granules may play a role in the balance between storage and excretion of zinc. Studies of the fate of bilobed vesicles will be future research to understand the function of the structure.

To study the process of bilobed gut granule formation, we tested the role of

38

CDF-2. Interestingly, *cdf-2* mutants displayed bilobed vesicles containing PGP-2, but these vesicles did not show strong FluoZin-3 fluorescence, indicating that there may be other processes that sense zinc levels and induce this morphological changes independently of CDF-2. To investigate this process, we tested lysosome biogenesis and endocytosis process by RNAi of *rab-7* and *rme-8*. RNAi of these genes did not block the formation of bilobed morphology, indicating the general lysosome biogenesis or endocytic pathways are not likely to be required for the process. On the other hand, RNAi of *glo* genes, *pgp-2* and *glo-3* blocked the formation of bilobed morphology. These results indicate that gut granule specific trafficking pathway is critical for the generation of bilobed vesicles. The discovery of this novel structure raises important new questions concerning the relationship between intracellular trafficking and zinc metabolism.

EXPERIMENTAL PROCEDURES

General Methods and Strains

C. elegans strains were cultured at 20℃ on nematode growth medium (NGM) seeded with *E. coli* OP50 unless otherwise noted (Brenner, 1974). The wild-type *C. elegans* and parent of all mutant strains was Bristol N2. The following mutations and transgenes were used: *pgp-2(kx48) I* (Schroeder et al., 2007), *unc-119(ed3) III* (Praitis et al., 2001), *cdf-1(n2527) X* (Bruinsma et al., 2002), *cdf-2(tm788) X* (Davis et al., 2009), *glo-1(zu391) X* (Hermann et al., 2005), *glo-3(zu446) X* (Rabbitts et al., 2008), *amIs4(cdf-2::GFP::unc-119(+))* (Davis et al., 2009), *pwIs50 (lmp-1:GFP)* (Treusch et al., 2004), *pwIs72 (Pvha-*

6::GFP::rab-5) (Hermann et al., 2005)*, pwIs170 (Pvha-6::GFP::rab-7)* (Chen et al., 2006)*,* and *kxEx98(pgp-2::GFP;rol-6^D)* (Schroeder et al., 2007). *amEx132(cdf-2::mCherry;rol-6^D)*, and *amEx142(cdf-2::mCherry::unc-119(+))* are described here. Double mutant animals were generated by standard methods, and genotypes were confirmed by PCR or DNA sequencing.

Transgenic Strain Construction

We previously described *amIs4*, an integrated transgene generated by bombardment transformation that expresses CDF-2::GFP from the *cdf-2* promoter (Davis et al., 2009). *cdf-2(tm788);amIs4* animals were generated by standard methods and used to analyze CDF-2::GFP expression. We generated pSC6 by inserting the coding sequence for mCherry from pCJF104 (a gift from M. Nonet), the *unc-54* 3'UTR from pPD95.77 (a gift from A. Fire), and the *cdf-2* promoter region and coding sequences into pBluescript SK+ (Stratagene). pSC6 and the marker pRF4 were microinjected into *cdf-2(tm788)* animals (Mello et al., 1991). Two independently derived strains containing extrachromosomal arrays were isolated, *amEx129* and *amEx132*. We made pSC23 by inserting CDF-2::mCherry coding sequences from pSC6 into plasmid pMM016 (a gift from J. Austin) that contains *unc-119(+)* (Praitis et al., 2001). pSC23 was transformed into *unc-119(ed3)* animals by bombardment to generate *amEx142*. For colocalization analysis, *amEx142* animals were crossed with animals containing *pwIs72, pwIs170, pwIs50* or *kxEx98*.

Metal Sensitivity Assays

Gravid adult hermaphrodites were treated with NaOH and bleach, and eggs were incubated in M9 solution overnight to allow hatching and synchronized arrest at the L1 stage. L1 animals were transferred to NAMM dishes supplemented with zinc sulfate (ZnSO$_4$), cadmium chloride (CdCl$_2$) or copper sulfate (CuSO$_4$), and seeded with concentrated OP50. After 3 days, animals were washed twice in M9 containing 0.01% Tween-20, paralyzed with 10mM sodium azide (NaN$_3$) in M9, and mounted on a 2% agarose pad on a microscope slide. Nomarski images were captured with a Zeiss Axioplan 2 microscope equipped with a Zeiss AxioCam MRm digital camera. Length of animals was measured using ImageJ software (NIH) by drawing a line from the nose to the tail tip.

Quantitative Analysis of CDF-2::GFP Expression by Fluorescence Microscopy

cdf-2(tm788);amIs4 animals were synchronized at L1 stage and cultured on NGM dishes. L4 stage hermaphrodites were then cultured for 24h on NAMM dishes supplemented with ZnSO$_4$ and seeded with concentrated OP50. Animals were paralyzed with 0.1% tricaine and 0.01% tetramisole in M9, mounted on 2% agarose pads on microscope slides, and imaged with a Zeiss Axioplan 2 microscope equipped with a Zeiss AxioCam MRm digital camera using identical settings and exposure times. GFP fluorescence intensity was quantified using ImageJ software (NIH). Briefly, the Spot Enhancing Filter 2D plugin was used to amplify signals from gut granules, and then threshold settings were used to specifically select the fluorescent regions of gut granules. The selected regions were overlaid on the original images and analyzed for mean fluorescence intensity of the area.

Staining with FluoZin-3, LysoTracker and LysoSensors

FluoZin-3 acetoxymethyl (AM) ester (Molecular Probes F24195) was reconstituted in

dimethylsulfoxide (DMSO) to generate a 1mM stock solution, diluted in M9 and

dispensed on NAMM dishes to yield a final concentration of 3μM. L4 stage

hermaphrodites were cultured on these dishes for 12-24 h in the dark, transferred to

NGM dishes without FluoZin-3 for 30 min to reduce FluoZin-3 in the intestinal lumen,

and analyzed by fluorescence microscopy as described above. The intestine on the

anterior half of each animal was analyzed because this structure was typically observed

in the same focal plane. Residual fluorescence from the intestinal lumen was manually

removed and excluded from the analysis.

LysoTracker RED DND-99 (1mM, Invitrogen L7528), or LysoSensor Green

DND-153 (1mM, invitrogen L7534) were diluted in M9 and dispensed on NAMM dishes

to yield a final concentration of 2μM. L4 stage hermaphrodites were cultured for 12-24 h

in the dark, transferred to NGM dishes without dye for 30 min to reduce the dyes in the

intestinal lumen, and imaged as described above. Confocal microscopy was performed

using an Olympus FV500 confocal microscope system equipped with multi-line argon

(458/488/515nm) and krypton (568nm) lasers.

Metal Content Analysis by Inductively Coupled Plasma-Mass Spectrometry (ICP-MS)

To obtain a large population of animals, we cultured hermaphrodites on multiple 100mm

NGM dishes, washed the animals three times in M9 containing 0.01% Tween-20,

resuspended the animals in concentrated OP50 in M9, and cultured the animals on multiple 100mm NAMM dishes supplemented with $ZnSO_4$. After 24 h, animals were washed three times in magnesium-free (Mg-free) M9 containing 0.01% Tween-20, incubated in 1mM serotonin in Mg-free M9 for 30 min to remove bacteria from the intestinal lumen, washed twice in Mg-free M9, and transferred to preweighed tubes and frozen at -80℃. The metal content was determined as described by Davis et al. (2009). Briefly, samples were freeze-dried, reweighed to obtain the dry pellet weight, and digested by incubation in a hot block digester at 90℃ for 1.5h with concentrated nitric acid (HNO_3) and hydrogen peroxide (H_2O_2) solution. The solution was diluted to a volume of approximately 10mL with deionized water, and internal standards were added to correct for matrix effects. Instrument calibration standards were prepared from multi-element stock solutions (High-Purity Standards) to generate a linear calibration curve, and samples were analyzed using a VG Axiom high-resolution ICP-MS (Thermo Fisher Scientific). The content of zinc, iron, copper, magnesium and manganese was determined as a value in parts-per-million (ppm) by dividing metal weight by dry pellet weight (μg/g).

Zinc Shift Assay

L4 stage animals were cultured for 12-16h on NAMM dishes with FluoZin-3 containing 0 or 200μM $ZnSO_4$, and then analyzed by fluorescence microscopy. Animals from the NAMM dishes with 200μM $ZnSO_4$ were washed, transferred to NAMM dishes with FluoZin-3 containing 0 or 200μM ZnSO4 or 100μM TPEN with FluoZin-3, and analyzed for fluorescence microscopy after 24h and 48h.

To analyze growth assay, we cultured synchronized L1 stage animals on NAMM dishes supplemented with 0 or 50μM ZnSO$_4$ for 12h. We chose 50μM supplemental zinc because it caused relatively mild toxicity as measured by subsequent growth, whereas 100 and 200μM supplemental zinc caused substantial toxicity (data not shown). Animals were washed three times, incubated in M9 containing 0.01% Tween-20 for 30 min to minimize residual bacteria, and washed one time in M9 containing 0.01% Tween-20. Animals were cultured for 3 days on NGM dishes supplemented with TPEN and seeded with concentrated OP50, and the length of each animal was determined.

RNA interference

RNAi feeding experiments were performed as described by Kamath et al. (2001) with minor modifications using the Ahringer RNAi library (Geneservice). Briefly, bacteria containing an RNAi clone were cultured in LB containing carbenicillin (50μg/ml) overnight. The bacterial culture was diluted into LB containing carbenicillin and cultured for ~6h, and the bacteria were seeded on NGM containing carbenicillin and IPTG (1mM) and dried overnight. RNAi of *rab-7* and *rme-8* causes embryonic lethality (Kamath et al., 2003) , and RNAi of *pgp-2* and *glo-3* causes the Glo phenotype (Rabbitts et al., 2008; Schroeder et al., 2007). To avoid affecting embryonic development, we cultured *cdf-2(tm788);amIs4* animals at the L1 stage on NGM dishes seeded with RNAi bacteria. L4 stage animals were stained with LysoTracker and analyzed by fluorescence microscopy as described above.

Statistics

All data were analyzed by two-tailed unpaired Student's t-test, and $p < 0.05$ was considered statistically significant.

FIGURE LEGENDS

Figure 2.1. Zinc is stored in gut granules (A) Wild-type hermaphrodites cultured with FluoZin-3 and the indicated levels of supplemental zinc and TPEN. Fluorescence images of live animals were captured with identical settings and exposure times. Each panel displays the anterior half of the intestine of a single animal with pharynx to the left and tail to the right. Scale bar: 50μm. (B) Quantification of fluorescence images like those shown in panel A using ImageJ software. The fluorescence intensity (shown in arbitrary units, A.U.) was normalized by setting the value at 0μM supplemental Zn equal to 1.0. Bars indicate mean values ± SEM (n=15) (** $p<0.001$; *** $p<0.0001$). (C) Fluorescence images of live wild-type animals costained with FluoZin-3 (green) and LysoTracker (red). Boxed regions are magnified in the right panels. Animals cultured with 100μM supplemental zinc displayed bilobed gut granules with asymmetric staining; one side was strongly positive for FluoZin-3 (arrow), and the other side was strongly positive for LysoTracker (arrowhead). Scale bars: 10μm and 2μm (boxed regions) (see also Supplemental Figure 2.1 and 2.2).

Figure 2.2. Gut granules are the major site of zinc storage (A) Fluorescence microscope images of live wild-type, *pgp-2(kx48), glo-1(zu391)* and *glo-3(zu446)* animals cultured with FluoZin-3 and the indicated levels of supplemental zinc. Images show the intestine with pharynx to the left and tail to the right. All images had identical exposure times and settings. Scale bar: 50μm. (B) Total zinc content of wild-type, *pgp-2(kx48)*, *glo-1(zu391)* and *cdf-2(tm788)* animals. Populations of animals consisting of a

46

mixture of developmental stages were cultured on NAMM dishes with the indicated

levels of supplemental zinc, and total zinc content was determined by ICP-MS and

calculated in parts-per-million (ppm). Bars indicate mean values ± SEM of two

independent experiments (see also Supplemental Figure 2.3).

Figure 2.3. CDF-2 functions cell autonomously to promote zinc storage in gut

granules (A) Fluorescence microscope images of live transgenic animals containing an

integrated array, *amIs4*, expressing CDF-2::GFP, and the *cdf-2(tm788)* mutation. L4

stage hermaphrodites were cultured with the indicated levels of supplemental zinc, and

images were captured with the identical settings and exposure times. Each panel displays

one representative animal oriented with pharynx to the left and tail to the right. Scale bar:

100μm. (B) Quantification of fluorescence images like those shown in panel A. The

fluorescence intensity (shown in arbitrary units, A.U.) was normalized by setting the

value at 0μM supplemental zinc equal to 1.0. Bars indicate mean values ± SEM (n=15)

(*** $p < 0.0001$). (C) Fluorescence microscope images of wild-type, *cdf-2(tm788)*, and

transgenic *cdf-2(tm788)* animals containing a multicopy extrachromosomal array,

amEx132, expressing CDF-2::mCherry. Images show the intestine (pharynx to the left,

tail to the right) of live animals cultured with FluoZin-3 and the indicated levels of

supplemental zinc. Scale bar: 50μm. (D) Quantification of fluorescence images like those

shown in panel A. The fluorescence intensity (shown in arbitrary units, A.U.) was

normalized by setting the value of wild-type animals at 0μM supplemental Zn equal to

1.0. Bars indicate mean values ± SEM (n=15) (* $p < 0.01$; ** $p < 0.001$; *** $p < 0.0001$). (E)

Images of a live *cdf-2(tm788);amEx132* animal that displayed mosaic expression of the

CDF-2::mCherry. The animal was cultured with FluoZin-3 and no supplemental zinc, and the intestine was imaged by fluorescence microscopy (pharynx to the left, tail to the right). The intestinal cell lacking CDF-2::mCherry expression is marked with a star (*). Scale bar: 50μm (see also Supplemental Figure 2.4).

Figure 2.4. High zinc induces the formation of asymmetric bilobed gut granules (A) Fluorescence images of live transgenic animals expressing CDF-2::GFP cultured with LysoTracker and the indicated levels of supplemental zinc. The differential interference contrast (DIC) image shows the intestinal lumen (triangle) and adjacent intestinal cells with pharynx to the left and tail to the right. Boxed regions are magnified in the right panels. With 200μM supplemental zinc, many gut granules appear to be bilobed and asymmetric; one side is positive for CDF-2::GFP and LysoTracker (arrowhead), whereas the other side is positive for CDF-2::GFP and negative for LysoTracker (arrow). Scale bars: 10μm and 2μm (boxed regions) (see also Supplemental Figure 2.5). (B) Confocal microscope images of live transgenic animals expressing LMP-1::GFP cultured with LysoTracker and the indicated levels of supplemental zinc. Images show intestinal cells with pharynx to the left and tail to the right. Scale bar: 10μm and 2μm (insets). (C) Confocal microscope images of live transgenic animals expressing LMP-1::GFP and CDF-2::mCherry cultured with 200μM supplemental zinc. Images show intestinal cells with pharynx to the left and tail to the right. Insets are magnified images of the boxed regions. Scale bar: 10μm and 2μm (insets) (see also Supplemental Figures 2.6 and 2.7).

Figure 2.5. Bilobed gut granule formation is dependent on *Glo* genes. Fluorescence

microscope images of live transgenic animals expressing CDF-2::GFP transgenic

animals stained with LysoTracker. L1 stage animals were fed RNAi bacteria to reduce

expression of the indicated genes, L4 stage animals were cultured with LysoTracker and

200μM supplemental zinc for ~16h and visualized. Images shows intestinal cells with

pharynx to the left and tail to the right, Boxed regions are magnified in the bottom panels.

Scale bar: 10μm and 2μm (bottom) (see also Supplemental Figure 2.8).

Figure 2.6. Zinc storage in gut granules promotes detoxification. Wild-type, *pgp-2(kx48), glo-1(zu391), glo-3(zu446)* and *cdf-2(tm788)* hermaphrodites were synchronized

at the L1 stage and cultured on NAMM dishes for 3 days with the indicated levels of

supplemental zinc (A, B) or supplemental cadmium (C, D). The length of individual

animals was measured using microscopy and ImageJ software. To compare strains that

have different growth rates under optimal conditions, we normalized the length of worms

by setting the value at 0μM supplemental zinc equal to 1.0 for each strain. Each point

indicates mean values ± SD (n=10 for Zn, and n=20 for Cd).

Figure 2.7. Zinc in gut granules can be mobilized in response to zinc deficiency (A)

FluoZin-3 staining of animals in the shift from high zinc to different zinc conditions.

Wild-type L4 stage hermaphrodites were first cultured on NAMM dishes containing

FluoZin-3 with 0 or 200μM supplemental zinc. Next, animals from 200μM supplemental

zinc were transferred to NAMM dishes containing the indicated levels of zinc or TPEN.

After 24h and 48h of subsequent culture, FluoZin-3 fluorescence was analyzed by

fluorescence microscopy. (B) Quantification of fluorescence images like those shown in

panel A. The fluorescence intensity (shown in arbitrary units, A.U.) was normalized by setting the value at 0μM supplemental Zn before the shift equal to 1.0. Each point indicates mean values ± SEM (n=10). (C) Wild-type and *cdf-2(tm788)* L1 stage hermaphrodites were precultured for 12h on NAMM dishes containing 0 or 50μM supplemental zinc, cultured for 3 days on NGM dishes with the indicated levels of TPEN, and analyzed individually for length. Each point indicates mean value ± SD (n=20). (D) Wild-type, *glo-1(zu391), glo-3(zu446)* and *pgp-2(kx48)* animals were analyzed as described in panel C. The results with 100μM TPEN are presented, because this concentration was the most informative with wild-type animals. The length of individual worms at 100μM TPEN was divided by the average length at 0μM TPEN. Bars indicate mean values ± SD (n=20). This ratio compares the growth of worms in deficient and normal zinc conditions - lower values indicate more severely reduced growth in response to zinc deficiency. Animals were precultured with 0 (black) or 50μM (white) supplemental zinc. For each strain, the white bar was compared to the black bar (*** $p < 0.0001$). All the mutant strain black and white bar values were significantly different than the wild-type black and white bar values, respectively.

Supplemental Figure 2.1. FluoZin-3 and LysoTracker colocalize in gut granules of intestinal cells Wild-type L4 stage hermaphrodites were cultured with the indicated levels of supplemental zinc and costained with FluoZin-3 and LysoTracker. Images show an entire live hermaphrodite from pharynx (upper left) to tail (bottom right): bright field shows morphology, green displays FluoZin-3 fluorescence, red displays LysoTracker fluorescence, and the merge shows green and red. FluoZin-3 fluorescence was captured

with the identical settings and exposure times. Scale bar: 100μm.

Supplemental Figure 2.2. FluoZin-3 detects zinc in gut granules (A) Fluorescence microscope images of live wild-type animals cultured with or without FluoZin-3. L4 stage hermaphrodites were cultured with the indicated levels of supplemental zinc. Images were captured with the identical settings and exposure times. Images of animals cultured with FluoZin-3 are identical to Figure 1A. Fluorescence of gut granules of animals cultured with FluoZin-3, which is a combination of FluoZin-3 and autofluorescence, was much brighter than fluorescence of gut granules of control animals, which is entirely autofluorescence. (B) Quantification of fluorescence images like those shown in panel A. The fluorescence intensity (shown in arbitrary units, A.U.) was normalized by setting the value of animals cultured without FluoZin-3 at 0μM supplemental Zn equal to 1.0. Bars indicate mean values ± SEM (n=15) (*** $p < 0.0001$, compared to no dye control at the same concentration of supplemental zinc).

Supplemental Figure 2.3. Gut granules are not a general site of metal storage Total magnesium (Mg), iron (Fe), manganese (Mn) and copper (Cu) content of wild-type, *pgp-2(kx48)*, *glo-1(zu391)* and *cdf-2(tm788)* animals. Populations of animals consisting of a mixture of developmental stages were cultured on NAMM dishes with the indicated levels of supplemental zinc, and total metal content was determined by ICP-MS and calculated in parts-per-million (ppm). Bars indicate mean values ± SEM of two independent experiments. The same samples were used to measure total zinc content in Figure 2B.

Supplemental Figure 2.4. Colocalization of CDF-2 and zinc in gut granules

Fluorescence microscope images of intestinal cells of live transgenic animals expressing CDF-2::mCherry cultured with FluoZin-3 and the indicated levels of supplemental zinc. Green displays FluoZin-3 and red displays CDF-2::mCherry protein. Boxed regions are magnified in the right panels. Animals cultured with 100μM supplemental zinc displayed bilobed gut granules. CDF-2::mCherry localized symmetrically to the membrane of both sides, whereas FluoZin-3 staining was asymmetric, with one side staining strongly (arrow) and the other side staining weakly (arrowhead). The scale bars represent 10μm and 2μm (boxed region).

Supplemental Figure 2.5. Neutral lysosomal pH indicators display similar staining patterns to LysoTracker Confocal microscope images of live transgenic animals expressing CDF-2::mCherry cultured with the indicated levels of supplemental zinc and LysoSensor Green DND-153. Images show intestinal cells with pharynx to the left and tail to the right, red displays CDF-2::mCherry, green displays LysoSensor Greens, and the merge shows green and red. Insets are magnified images of the boxed regions. The scale bars represent 10μm and 2μm (boxed region).

Supplemental Figure 2.6. Asymmetric distribution of molecules in bilobed gut granules (A) Confocal microscope images of live transgenic animals expressing GFP::RAB-7 cultured with LysoTracker and the indicated levels of supplemental zinc. Images shows intestinal cells with pharynx to the left and tail to the right, green displays

52

GFP::RAB-7, red displays LysoTracker, and the merge shows green and red. The scale bar represents 10μm. (B) Confocal microscope images of live transgenic animals expressing GFP::RAB-7 and CDF-2::mCherry cultured with 200μM supplemental zinc. Images shows intestinal cells with pharynx to the left and tail to the right, green displays GFP::RAB-7, red displays CDF-2::mCherry, and the merge shows green and red. The scale bar represents 10μm.

Supplemental Figure 2.7. CDF-2 and PGP-2 colocalize on the membrane of gut granules Fluorescence microscope images of live transgenic animals expressing CDF-2::mCherry and PGP-2::GFP cultured with the indicated levels of supplemental zinc. Red displays CDF-2::mCherry, green displays PGP-2::GFP, and blue displays autofluorescence. Images show a lateral view of intestinal cells, and boxed regions are magnified in the right panels. In the presence of 100μM supplemental zinc, gut granules appear to be bilobed and asymmetric. CDF-2::mCherry and PGP-2::GFP proteins fully colocalized on the membrane of gut granules at both 0μM and 100μM supplemental zinc (arrow). Autofluorescence fully colocalized with CDF-2::mCherry and PGP-2::GFP with 0μM supplemental zinc (triangle), but autofluorescence was detected only on one side of bilobed granules with 100μM supplemental zinc (arrowhead). The scale bars represent 10μm and 2μm (boxed regions).

Supplemental Figure 2.8. Bilobed gut granules formation is independent of CDF-2 activity (A) Fluorescence microscope images of live transgenic animals expressing PGP-2::GFP in the background of the *cdf-2(tm788)* mutation cultured with 200μM

supplemental zinc. Images show a lateral view of intestinal cells, green displays PGP-2::GFP, red displays LysoTracker, and merge displays green and red. The scale bar represents 10μm. (B) Fluorescence microscope images of wild-type and *cdf-2(tm788)* mutant animals costained with FluoZin-3 and LysoTracker and cultured with the indicated levels of supplemental zinc. Images show intestinal cells, green displays FluoZin-3, red displays LysoTracker, and merge displays green and red. While wild-type animals display bilobed morphology of gut granules with an asymmetric staining of FluoZin-3 and LysoTracker, *cdf-2* mutants display single round shape of gut granules. The scale bar represents 10μm.

Supplemental Figure 2.9. Molecular properties of gut granules in normal and high zinc conditions In normal zinc conditions, gut granules are round vesicles that are autofluorescent and stained by LysoTracker, LysoSensors, and FluoZin-3 staining. Gut granule membrane contains late endosomal or lysosomal proteins, RAB-7 and LMP-1, and gut granule-specific proteins, CDF-2 and PGP-2, not an early endosomal protein, RAB-5. In high zinc conditions, gut granules are bilobed in shape, and the bilobed granules display different distribution of molecules. One side displays autofluorescence, staining of LysoTracker, LysoSensors, and FluoZin-3, and the localization of RAB-7, LMP-1, CDF-2 and PGP2 proteins, identical to regular state gut granules. The other side contains PGP-2 and CDF-2 and displays strong FluoZin-3 staining. The plus (+) and minus (-) signs indicate the presence and absence of the molecules, respectively. The low and high indicate the relative levels of the molecule.

Figure 2.1
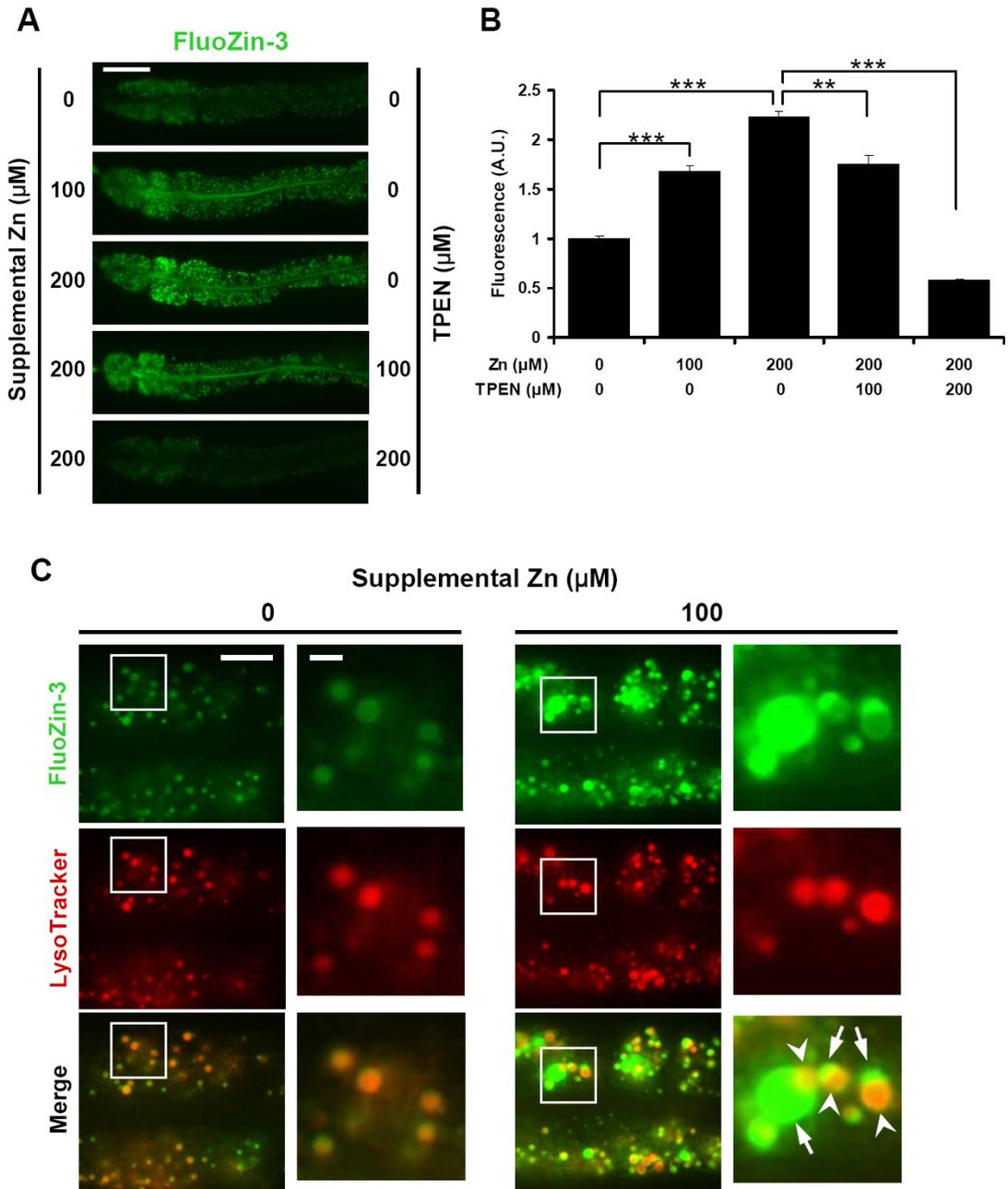
Figure 2.2
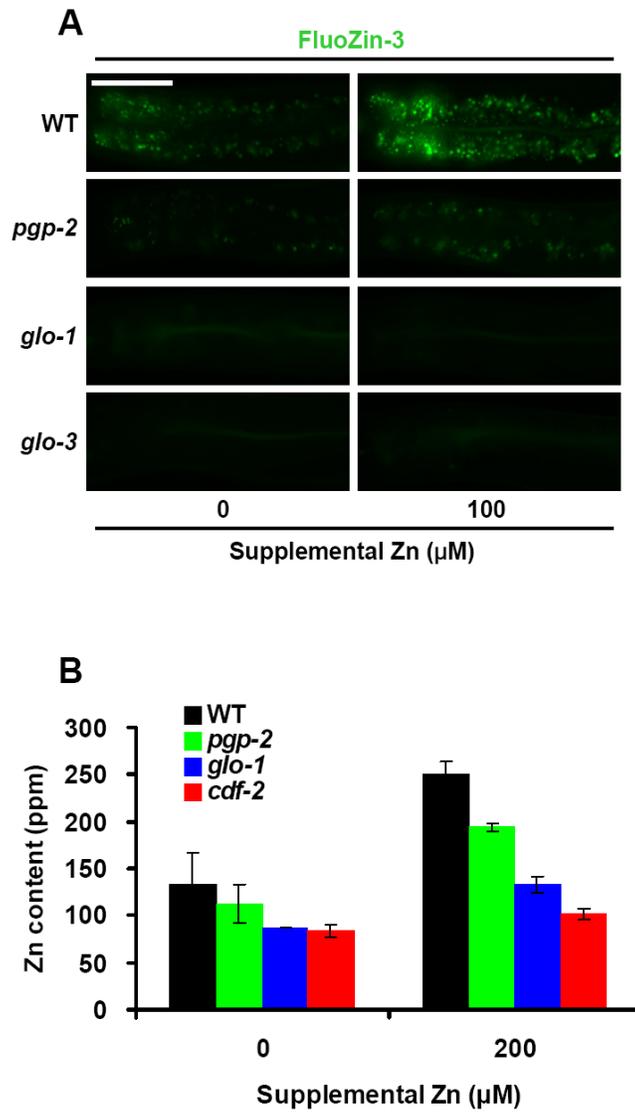
Figure 2.3
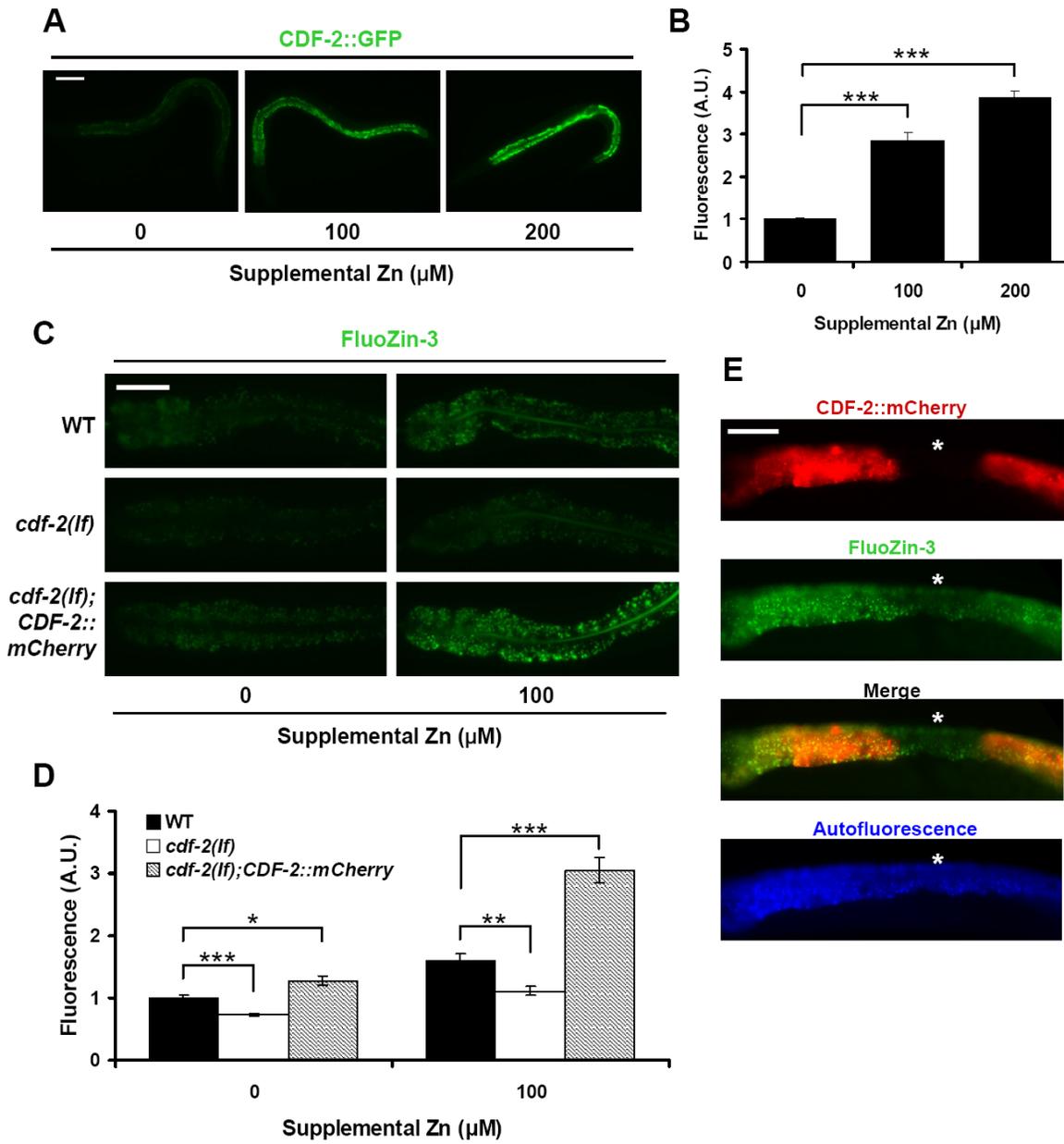
Figure 2.4
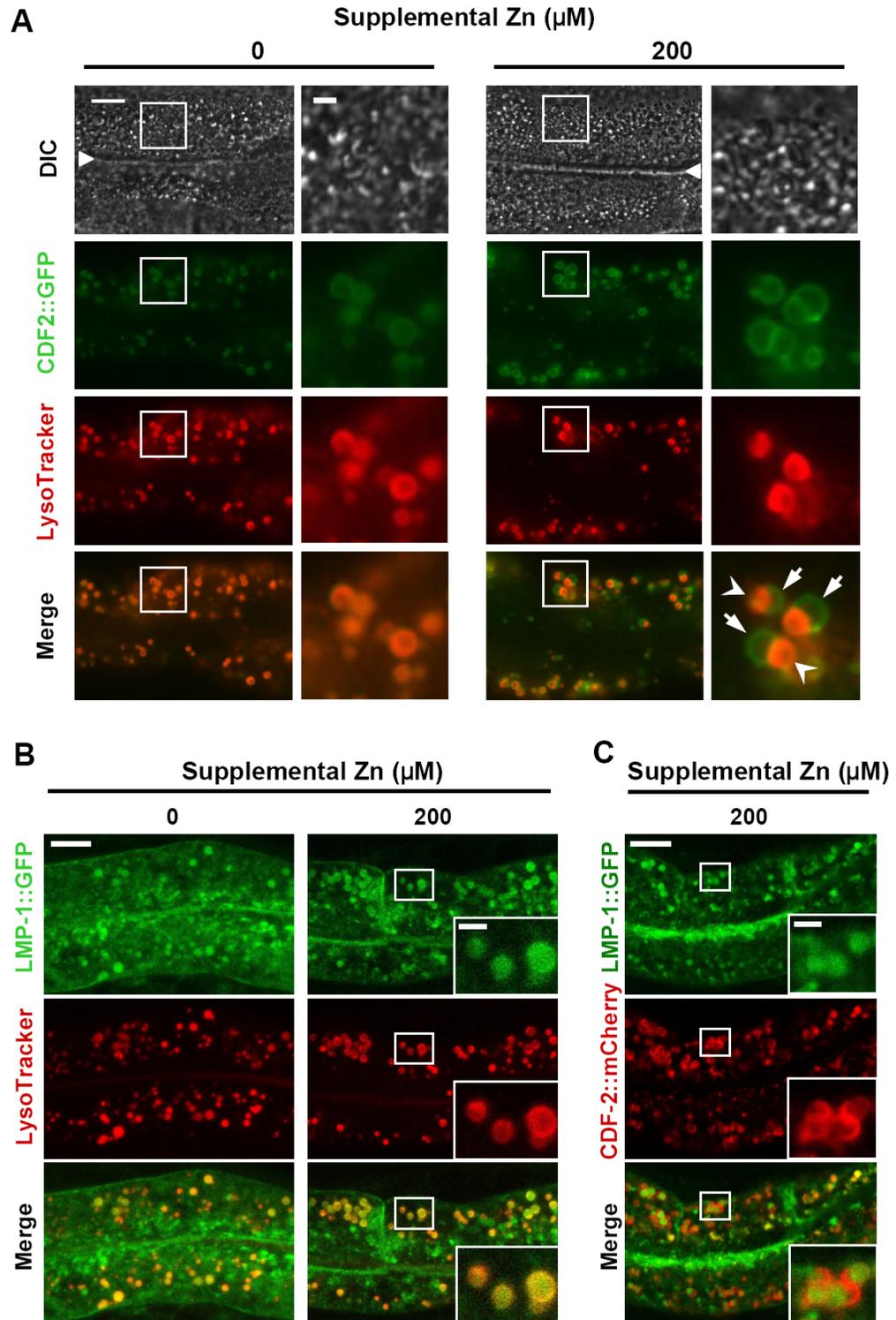
Figure 2.5
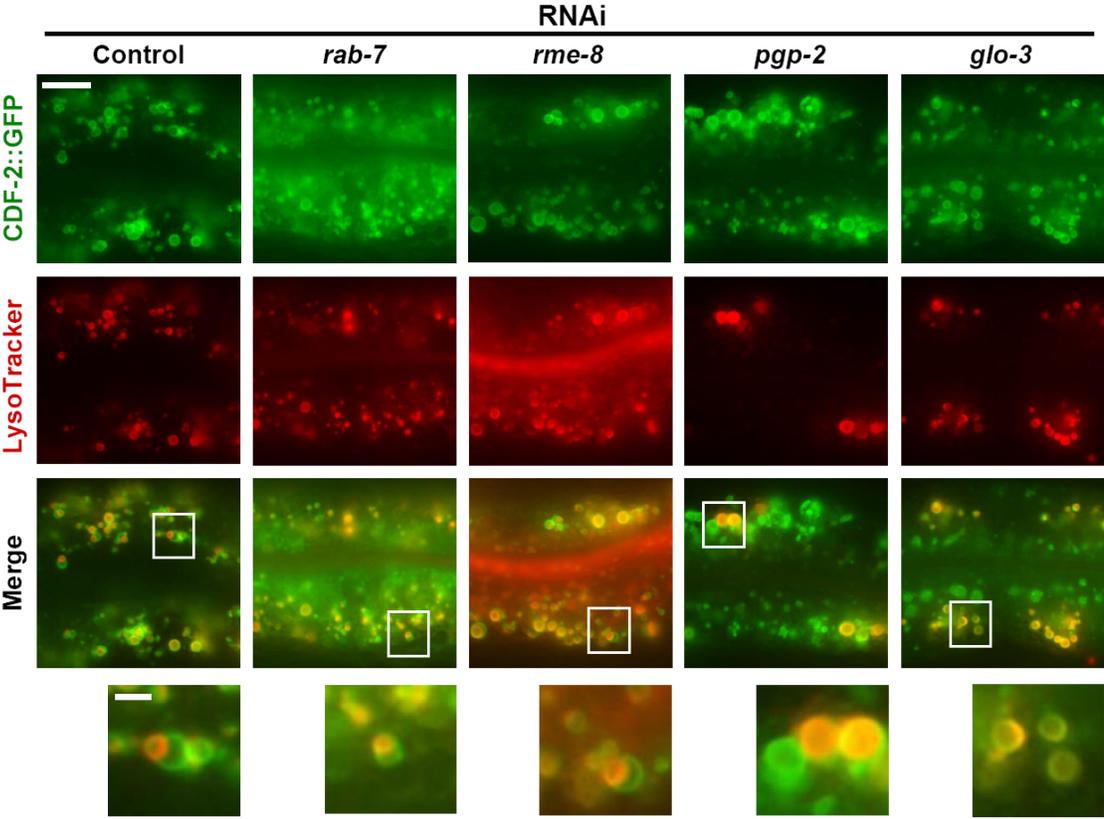
Figure 2.6
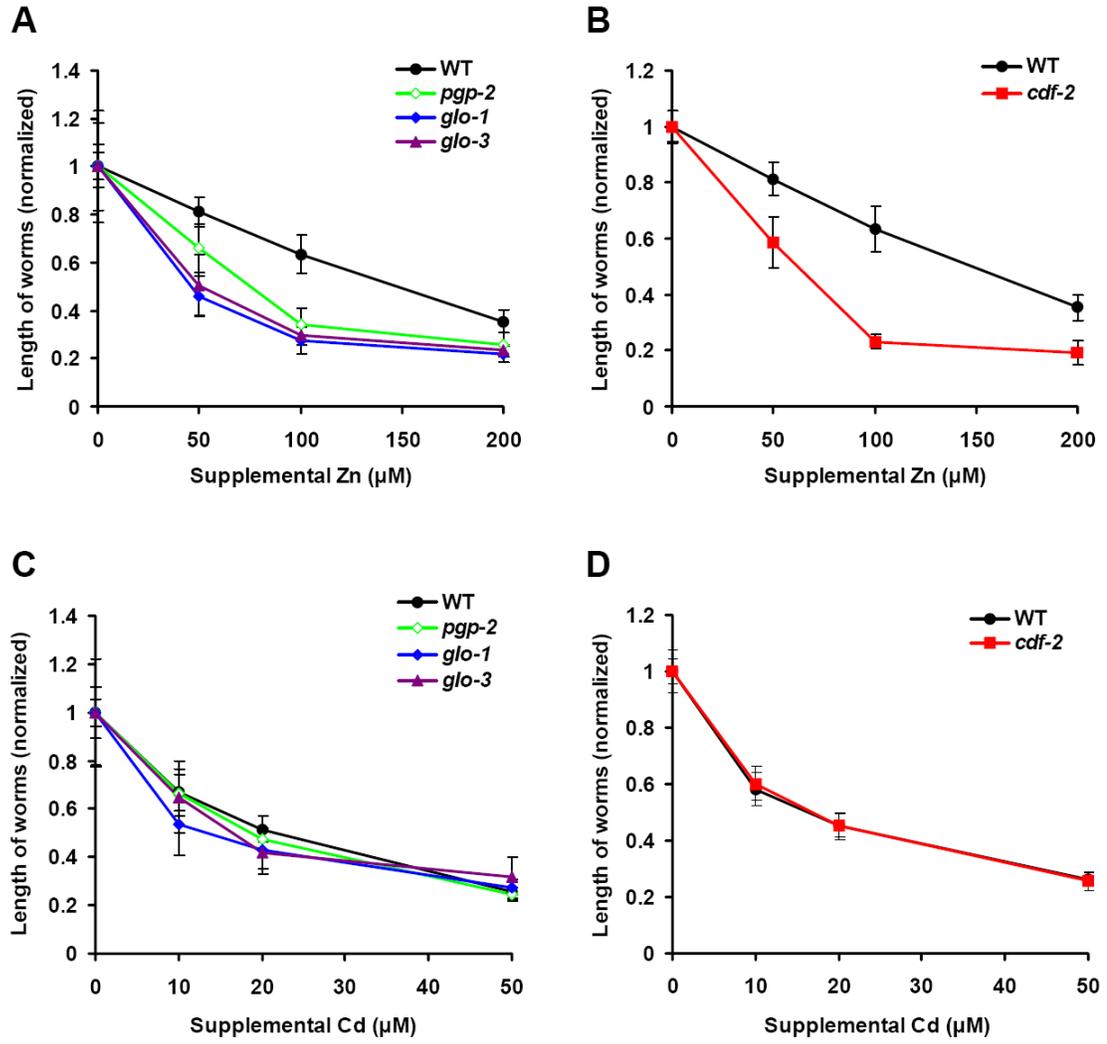
Figure 2.7
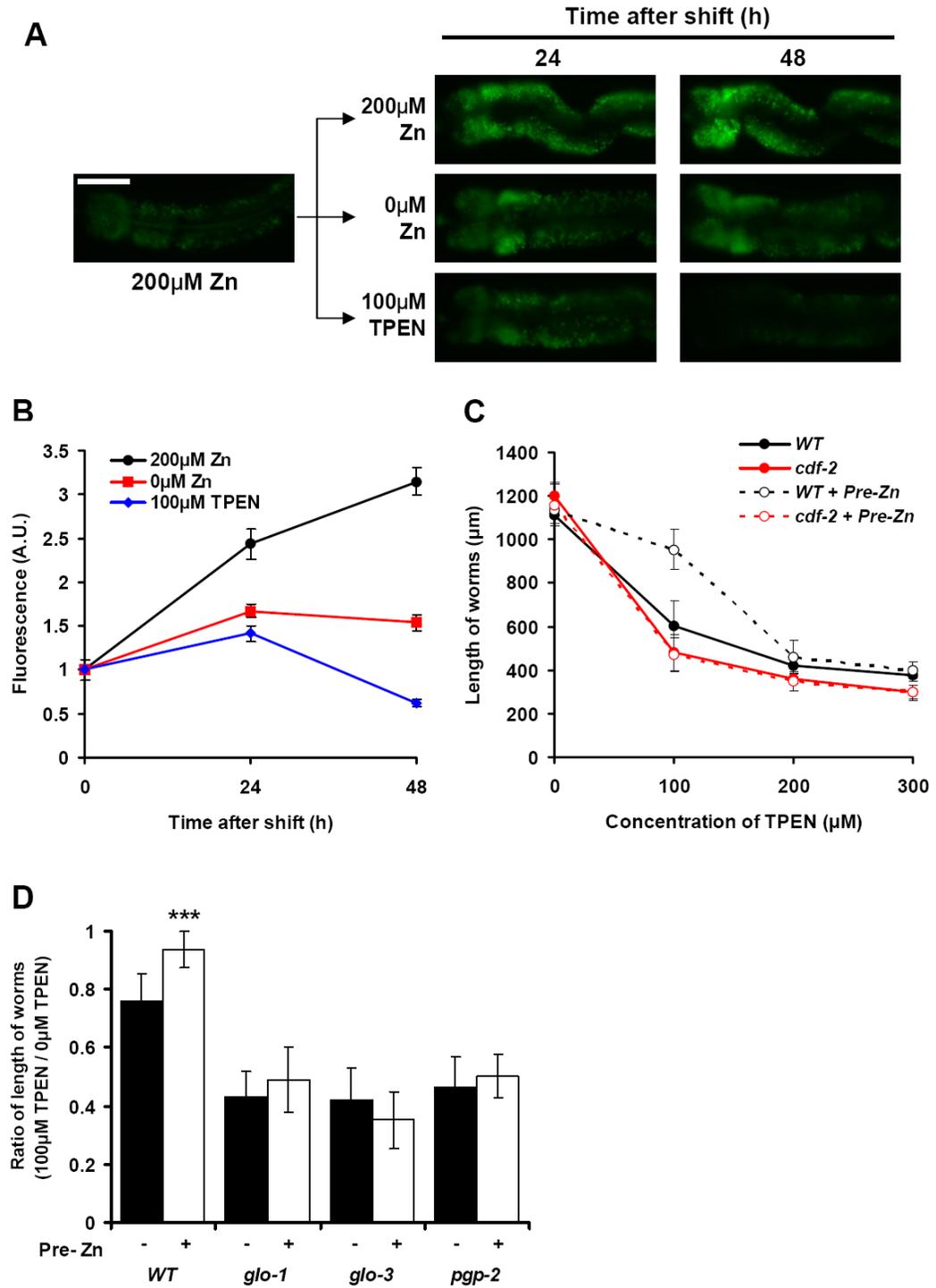
Supplemental Figure 2.1
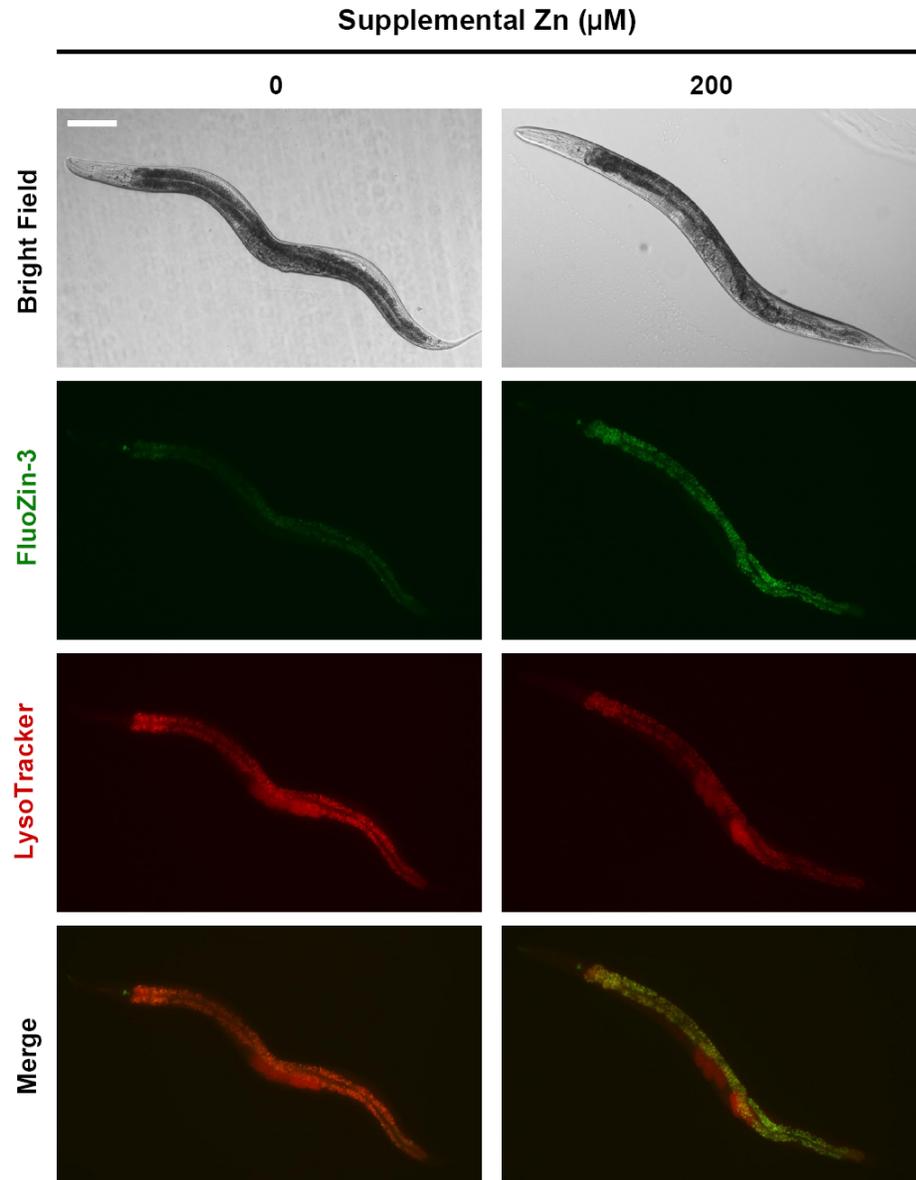
Supplemental Figure 2.2
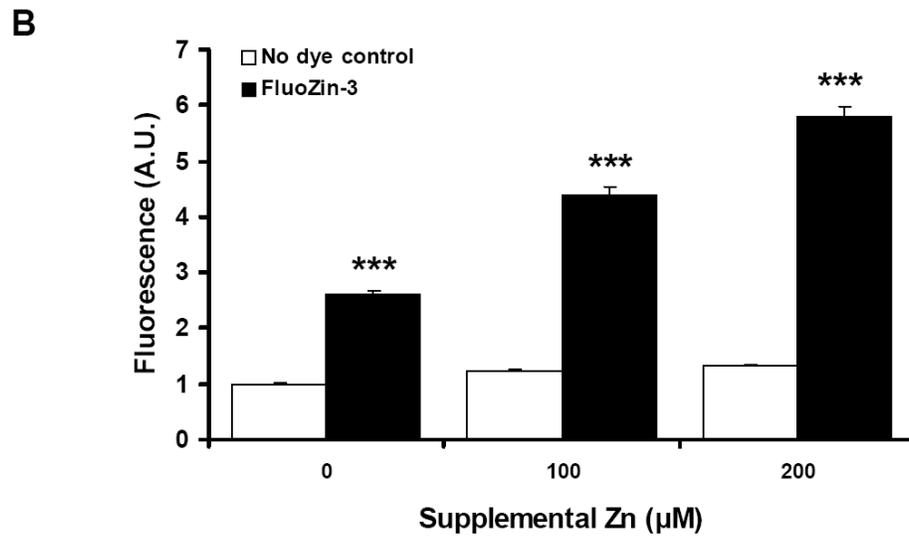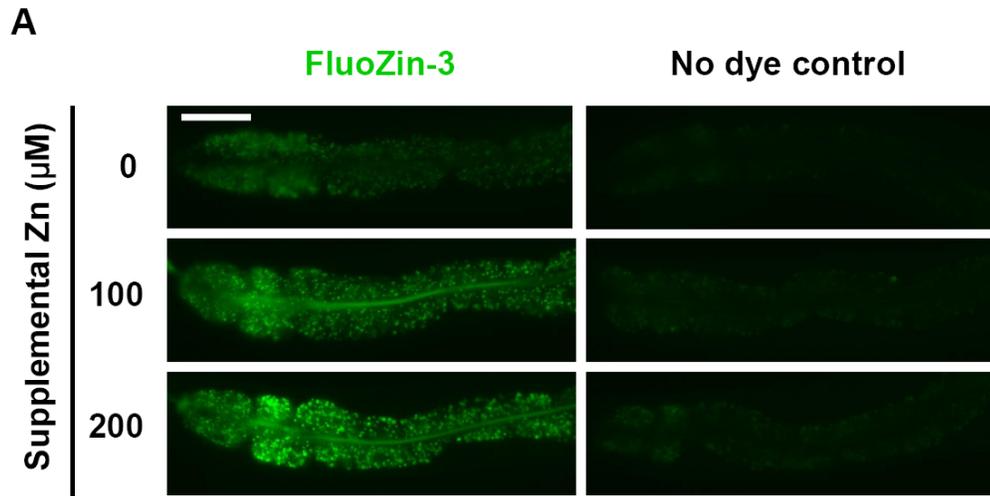
Supplemental Figure 2.3
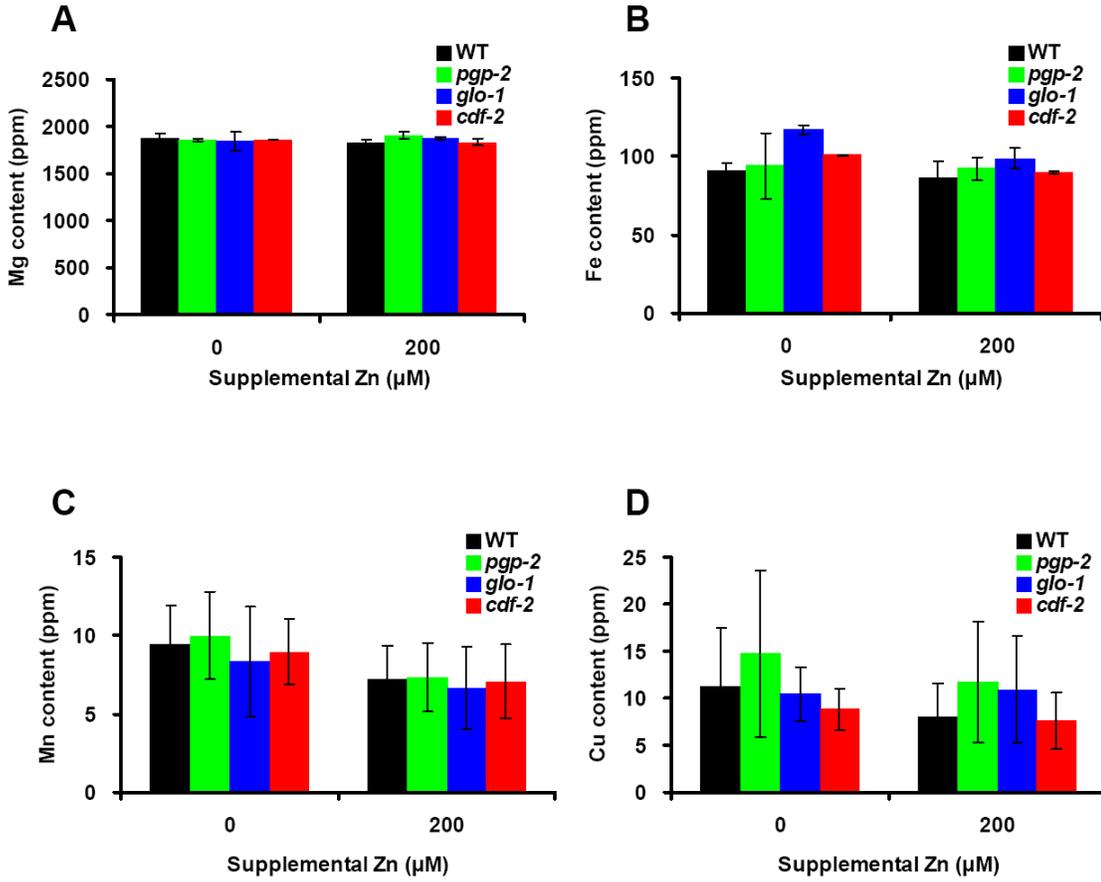
Supplemental Figure 2.4
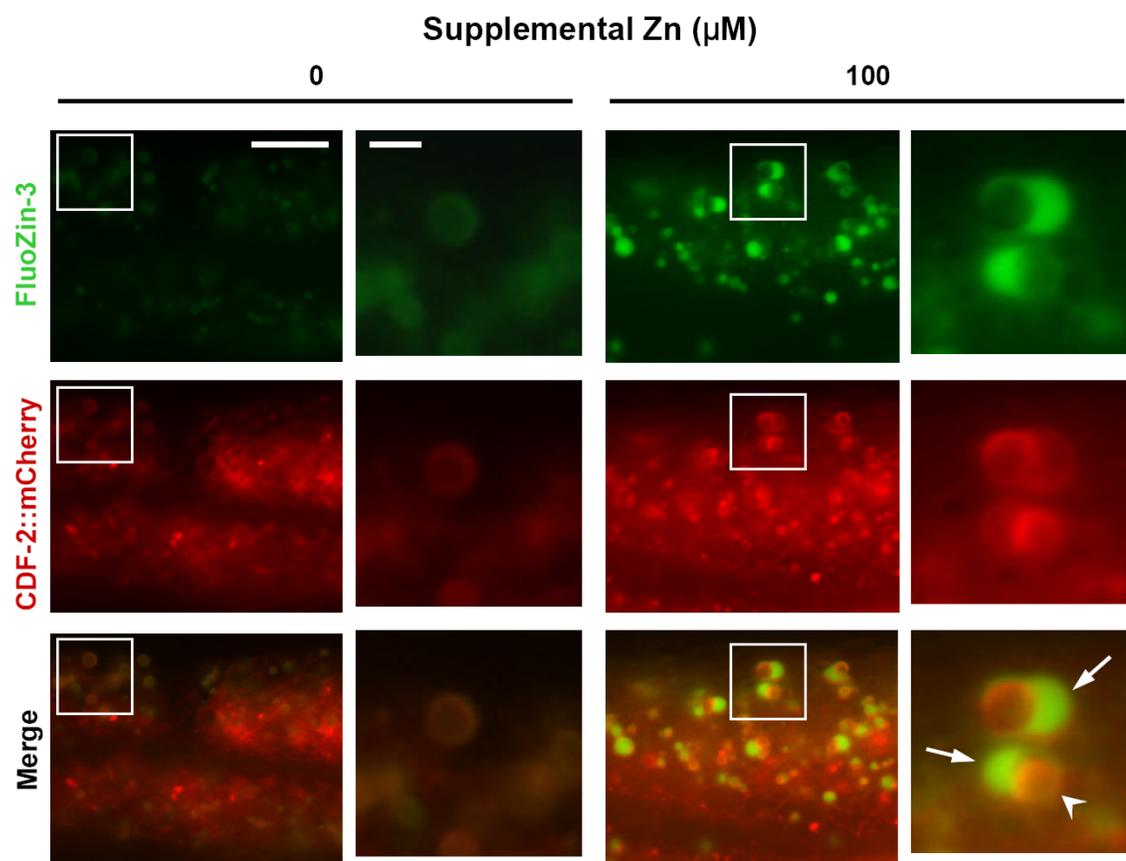
Supplemental Figure 2.5
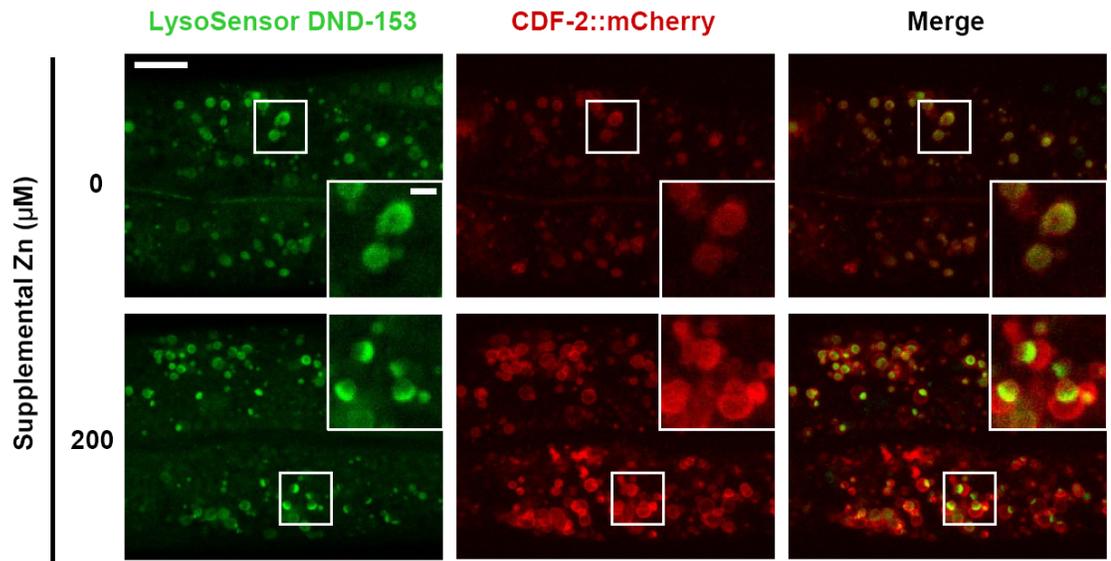
Supplemental Figure 2.6

Supplemental Zn (μM)

0   100
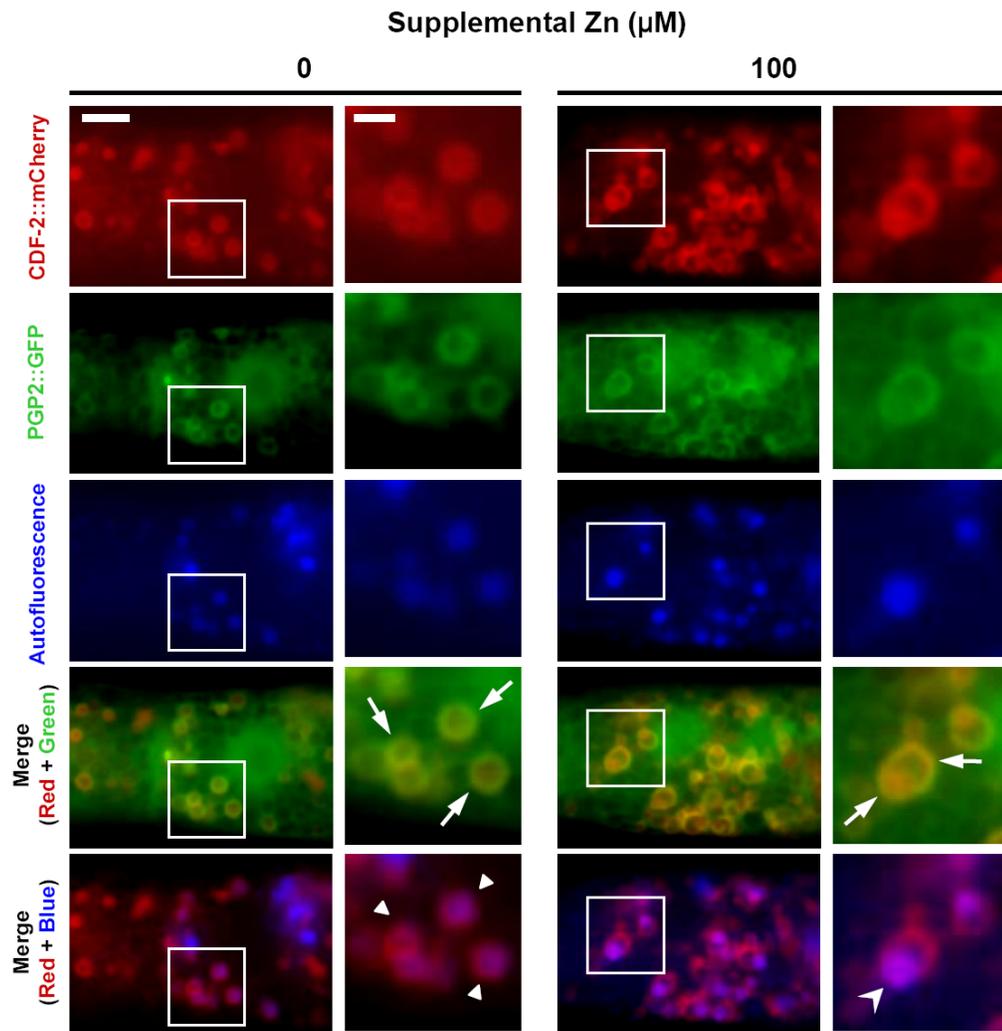
Supplemental Figure 2.8
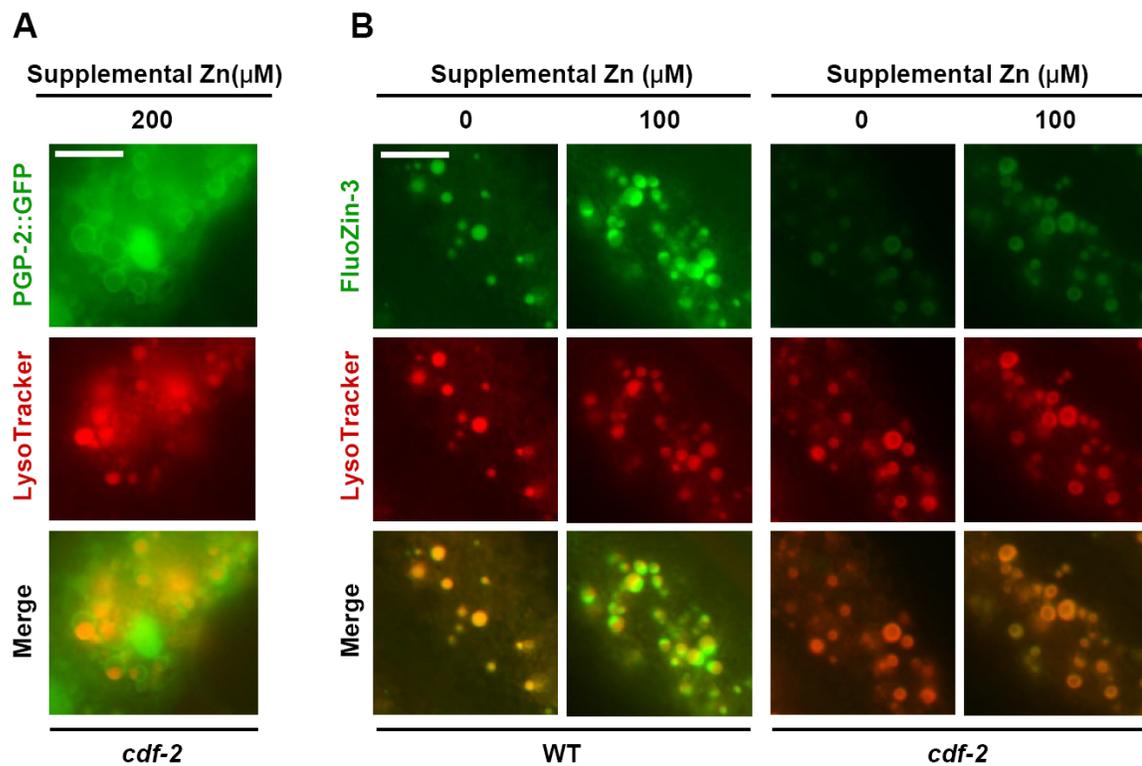
Supplemental Figure 2.9
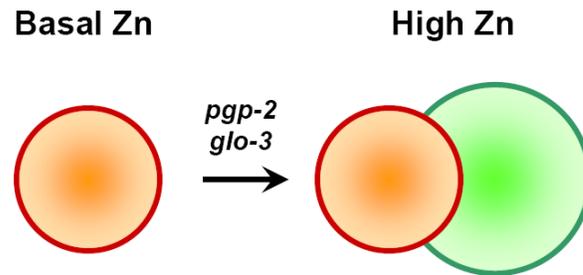
	Basal Zn		High Zn	
Autofluorescence	+		+	-
LysoTracker	+		+	-
Acidic LysoSensor	+		+	-
Neutral LysoSensor	+		+	-
CDF-2	+		+	+
PGP-2	+		+	+
RAB-7	+		+	-
LMP-1	+		+	-
RAB-5	-		-	-
FluoZin-3 (Zinc)	+ (Low)		+ (Low)	+ (High)

CHAPTER 3

The Cation Diffusion Facillitator TTM-1 Functions in Zinc Excretion in *C. elegans*

[The work in Chapter 3 is in preparation for submission with the following authors: Hyun Cheol Roh, Sara Collier, James Guthrie, J. David Robertson, and Kerry Kornfeld.

H.C.R designed and performed all experiments and analyses except: S.C. performed quantitative RT-PCR (Figures 3.2, 3.5B, 3.5C), and J.G. and J.D.R. performed the ICP-MS (Figure 3.5A).]

ABSTRACT

Zinc is the most widely used essential trace metal element. Organisms have evolved precise mechanisms to maintain zinc homeostasis, and zinc transporters play an important role in this process. Although many zinc transporters have been studied, how multiple zinc transporters act in a coordinated manner is not well defined. Here we characterize a *C. elegans cdf* gene, *ttm-1*, and its two isoforms, *ttm-1a* and *ttm-1b*. TTM-1A localized to intracellular compartments of the intestine and hypodermis, and expression was not induced by dietary zinc. TTM-1B localized to the apical membrane of intestinal cells, and expression was induced by dietary zinc. Analyses of loss-function mutations demonstrated that TTM-1 is involved in zinc excretion and is important for zinc detoxification in the absence of CDF-2. These findings indicate that TTM-1 plays a role in zinc detoxification and excretion in concert with CDF-2 in *C. elegans*.

INTRODUCTION

Zinc is an essential trace element that is required for a wide range of biological processes and implicated in a variety of human diseases (Vallee and Falchuk, 1993). Since zinc deficiency and excess zinc are deleterious (Fosmire, 1990; Hambidge, 2000), organisms have evolved mechanisms to achieve zinc homeostasis. As positively charged zinc ions cannot move across the membrane of lipid bilayers, transmembrane zinc transporter proteins are necessary for the movement of zinc in the cell (Eide, 2006).

Zinc transporters are divided into two major families, cation diffusion facilitator (CDF/ZnT/SLC30) and Zrt-, Irt-like protein (ZIP/SLC39) (Kambe et al., 2006). CDF proteins have six conserved transmembrane motifs, and they transport cytoplasmic zinc out of the cell or into intracellular organelles, resulting in the decrease in the cytoplasmic zinc concentrations. In contrast, ZIP proteins have eight conserved transmembrane motifs, and they move zinc either from the outside of the cells or from intracellular compartments into the cytoplasm. In mammals, there are 10 members in the CDF family and 14 members in the ZIP family. Each zinc transporter displays different tissue distributions and intracellular localizations (Lichten and Cousins, 2009), and the cooperation of zinc transporters at multiple locations contributes to the regulation of zinc homeostasis in the cell and in the whole organism. For example, in intestinal epithelial cells, ZIP-4 localizes to the apical membrane while ZnT-1 localizes to the basolateral membrane. These proteins function antagonistically to modulate intracellular zinc levels, and the interaction between these zinc transporters is critical for the uptake of zinc from the diet and the distribution of zinc to other tissues of the body. However, although

previous studies have identified many zinc transporters, our understanding of the networks of zinc transporters in an entire individual is limited.

C. elegans is an excellent system to study zinc metabolism (Bruinsma et al., 2008; Davis et al., 2009; Murphy et al., 2011). Unlike the yeast, *C. elegans* contains multiple tissues such as an intestine, musculature, nervous system, reproductive tracts and epithelia, which allows the study of networks of zinc transporters at multiple locations. The powerful genetic techniques in *C. elegans* biology facilitate the analysis of functional interaction between zinc transporters, which have been difficult in mammalian system. In addition, culture conditions have been developed that allow precise control over dietary zinc(Bruinsma et al., 2008; Davis et al., 2009).

Previous studies of *C. elegans* characterized three *C. elegans* CDF proteins which function in the control of zinc metabolism in the intestine. CDF-1 is localized to the plasma membrane of intestinal cells, probably on the basolateral side, and transport zinc from the intestine to the body cavity similar to mammalian ZnT-1. Zinc transported by CDF-1 is excreted from the body perhaps via the excretory cell (Bruinsma et al., 2002). CDF-2 localizes to the membrane of lysosome-related organelles, termed gut granules, which store excess zinc during high zinc conditions (Davis et al., 2009). SUR-7 is present in the ER/Golgi complex and appears to be involved in the excretion of zinc by transporting it into secretory vesicles (Yoder et al., 2004). Therefore, the intestine is a critical tissue for maintaining zinc homeostasis in *C. elegans* and multiple CDF proteins contribute to this process.

Here, we characterize the *C. elegans cdf* gene, *ttm-1* (toxin-regulated target of p38MAPK). *ttm-1* was identified as a downstream transcriptional target of p38 kinase in

74

response to bacterial toxins (Huffman et al., 2004). TTM-1 is also involved in the response to environmental cadmium (Cui et al., 2007a). We demonstrate that *ttm-1* is composed of two isoforms, *ttm-1a* and *ttm-1b*, that are specified by different transcription start sites. Expression of *ttm-1a* was not responsive to dietary zinc and TTM-1A localized to intracellular compartments. In contrast, *ttm-1b* was strongly induced by dietary zinc and TTM-1B localized to the apical membrane of intestinal cells. Genetic analysis demonstrated that TTM-1B is involved in zinc excretion and is important for zinc detoxification in combination with CDF-2. These results advance our understanding of networks of zinc transporters for the regulation of zinc homeostasis in animals.

RESULTS

Gene Structure of *ttm-1*

Based on the computational algorithm Gene Finder and the analysis of expression sequence tags (ESTs), it was predicted that *ttm-1* contained five exons and encoded two variants, *ttm-1a* and *ttm-1b* (Figure 3.1A). To determine the molecular mechanism that is responsible for the generation of the two isoforms, we performed 5' rapid amplification of cDNA ends (5' RACE). Using a primer specific to both predicted isoforms of *ttm-1*, we detected two different mRNA products fused to the SL1 trans-spliced leader sequence at the 5' end. While SL1 of *ttm-1a* mRNA is 3 bp apart from the start codon, SL1 of *ttm-1b* mRNA is 4 bp apart from the start codon (data not shown).

75

These results suggest that *ttm-1* generates at least two isoforms using different transcription start sites (Figure 3.1A).

BLAST searches indicated that TTM-1A/B are closely related to *C. elegans* CDF-2 and human ZnT-2, but they are also similar to human ZnT-3, 4, and 8 (Figure 3.1B). TTM-1A and TTM-1B contain distinct N-terminal sequences (Figure 3.1B). Most CDF proteins contain a conserved histidine motif, $(HX)_n$ in the loop between the fourth and fifth transmembrane motifs, and this motif is presumed to regulate zinc transporter activity (Gaither and Eide, 2001a; Kawachi et al., 2008).TTM-1B has a unique histidine- and glycine-rich motif at its N-terminus which is similar to the $(HX)_n$ motif in the loop between the fourth and fifth transmembrane motifs (Figures 3.1B and C). This N- terminal $(HX)_n$ motif is unique to *C. elegans* TTM-1B and may be an important regulatory or functional domain.

Regulation of *ttm-1b* by Dietary Zinc

The expression of genes involved in zinc metabolism, such as *mtl-1, mtl-2* and *cdf-2,* are regulated by the level of dietary zinc (Davis et al., 2009; Freedman et al., 1993). To determine whether *ttm-1* expression is affected by dietary zinc levels, we performed quantitative RT-PCR on animals grown with different levels of zinc. *ttm-1a* mRNA levels were constant across all zinc concentrations. In contrast, *ttm-1b* mRNA was strongly induced by 200μM supplemental zinc compared to 0μM supplemental zinc (Figure 3.2). These results suggest that only *ttm-1b* is responsive to excess dietary zinc and may be more important than *ttm-1a* for the response to high zinc conditions.

Tissue Distribution of *ttm-1*

To determine the cell types expressing *ttm-1a* and *ttm-1b*, we generated transgenic animals that express GFP under the control of the predicted *ttm-1a* and *ttm-1b* promoters. For *ttm-1a*, the region between the *ttm-1a* start codon and the 3' end of the adjacent upstream gene was used to drive GFP expression (Figure 3.1A). *Pttm-1a::GFP* transgenic animals displayed GFP expression in the hypodermis and the intestine (Figure 3.3A). For *ttm-1b*, because its transcription starts upstream of exon 3, intro 2 is likely to function as a promoter region. The large size of intron 2 (~10kbp) suggests that it may contain important promoter elements that drive *ttm-1b* expression. We built a construct containing ~6kb upstream of the *ttm-1b* start codon (*Pttm-1b(-6kb)::GFP*) (Figure 3.1A). Transgenic animals containing this construct displayed GFP expression in multiple tissues including the intestine, head neurons, seam cells, hypodermis and the vulva (Figure 3.3B). These results suggest that each *ttm-1* isoform has the unique tissue distribution.

To determine if the expression patterns observed in transgenic animals reflects the endogenous *ttm-1b* expression pattern, we tested whether GFP expression was induced in *Pttm-1b(-6kb)::GFP* transgnic animals (Figure 3.2). When incubated with 200μM supplemental zinc, these animals displayed a significant increase in intestinal GFP expression (Figure 3.3C, a-b). This induction of GFP was restricted to the intestine. GFP expression in head neurons, for example, was not affected by zinc (Figure 3.3C, c-d). These results suggest that the 6kb fragment immediately upstream of the TTM-1B start codon contains elements important for tissue specific and zinc-responsive expression.

To determine the location of the key promoter elements responsible for *ttm-1b*

expression, we built a truncated construct that contains ~2.4kb upstream of the *ttm-1b*

start codon (*Pttm-1b(-2.4kb)::GFP*) (Figure 3.1A). In *Pttm-1b(-2.4kb)::GFP* transgenic

animals, GFP expression was absent from intestinal cells but detected in the other tissues

where *Pttm-1b(-6kb)::GFP* was expressed (Supplemental Figure 3.1A). In addition, GFP

was not induced in response to high zinc levels in *Pttm-1b(-2.4kb)::GFP* transgenic

animals (Supplemental Figure 3.1B). These results suggest that the region between ~6kb

and ~2.4kb upstream of the *ttm-1b* start codon contains elements required for intestinal

and zinc-responsive expression of *ttm-1b*.

Intracellular Localization of TTM-1

To determine the intracellular localization of TTM-1A and TTM-1B proteins, we

generated transgenic animals that express TTM-1A or TTM-1B protein fused to GFP

under the control of each respective promoter (Figure 3.1A). In the head and body

hypodermis, TTM-1A::GFP localized to intricate intracellular networks (Figures 3.4A

and 3.4B). To identify the compartments containing TTM-1A::GFP, we performed

colocalization experiments using MitoTracker and autofluorescence from gut granules.

TTM-1A::GFP was not colocalized with MitoTracker (data not shown) or

autofluorescence from gut granules in the intestine (Figure 3.4C) These data suggest that

TTM-1A is not present in mitochondria or gut granules. We are currently testing

additional molecular markers to identify the TTM-1A intracellular localization.

In intestinal cells, TTM-1B::GFP localized to the apical plasma membrane,

whereas it localized to intracellular structures in other tissues such as hypodermis and

neurons (Figure 3.4D), suggesting that the intracellular localization of TTM-1B may be different depending on the type of tissues. To determine if TTM-1B levels are induced by dietary zinc, we analyzed TTM-1::GFP expression in response to supplemental zinc. Consistent with the induction of *ttm-1b* mRNA expression, TTM-1B::GFP on the apical membrane of intestinal cells was increased in the presence of 100μM supplemental zinc (Figure 3.4E), suggesting that high levels of TTM-1B proteins on the apical membrane of intestinal cells may play an important role in the response to high levels of zinc. In the other tissues such as neurons and hypodermis, TTM-1::GFP expression was not changed (data not shown), consistent with the observation from *Pttm-1b(-6kb)::GFP* transgenic animals. These results suggest that TTM-1B may have two distinct functions. In the tissues including neurons and hypodermis, TTM-1B may be involved in the flow of zinc into intracellular compartments. In the intestine, it may play a role in the excretion of zinc by transporting it directly into the intestinal lumen in response to high levels of zinc.

Role of TTM-1 in Excretion of Zinc

To study the function of TTM-1 in zinc metabolism, we examined the mutant allele *ttm-1(ok3503)* which was generated by the *C. elegans* Gene Knockout Consortium. We analyzed the genomic sequence of the *ttm-1* locus of the *ok3503* strain and found that the *ok3503* allele is a deletion of 877 bp from exon 4 to intron 4 (Figure 3.1A). This deletion is predicted to remove transmembrane motifs II through VI and may cause an early translation termination due to a splicing site disruption and subsequent frame shift (Figure 3.1B). Because of the loss of a large portion of the transmembrane region, we predict *ttm-1(ok3503)* is a loss-of-function allele. Since the deleted region is common to

79

both of *ttm-1a* and *ttm-1b* isoforms, the *ttm-1(ok3503)* is predicted to inactivate both isoforms.

Based on the localization of TTM-1B, we hypothesized that one of the functions of *ttm-1* is to excrete zinc in high zinc conditions. To test the hypothesis, we measured the total zinc content of *ttm-1(ok3503)* animals by using inductively coupled plasma-mass spectrometry (ICP-MS). In normal conditions without supplemental zinc, the zinc content of *ttm-1(ok3503)* animals was similar to wild-type animals. However, in the presence of 200μM supplemental zinc, *ttm-1(ok3503)* animals displayed approximately 40% higher total zinc than wild-type animals, indicating more zinc had accumulated in the mutant animals (Figure 3.5A). These results suggest that TTM-1 promotes the excretion of zinc during high zinc conditions.

To examine the excretory role of TTM-1 by an independent approach, we measured mRNA levels of metallothionein genes. Metallothionein gene expression is upregulated by increased levels of cytoplasmic zinc (Davis and Cousins, 2000). In normal conditions without supplemental zinc, *ttm-1(ok3503)* animals displayed approximately 3-fold higher levels of *mtl-1* compared to wild-type animals. In the presence of 100μM and 200μM supplemental zinc, there was also approximately 2-fold increase in *mtl-1* mRNA levels in *ttm-1(ok3503)* animals compared to wild-type animals (Figure 3.5B). Similar results were observed for *mtl-2* mRNA expression (Figure 3.5C). These results suggest that *ttm-1* mutant animals contain higher levels of cytoplasmic zinc both in normal and high zinc conditions. Furthermore, *mtl-1/2* expression may be a more sensitive measure of cytoplasmic zinc levels than ICP-MS.

Role of *ttm-1* in Zinc Detoxification

To determine the role of TTM-1 in zinc detoxification, we examined zinc sensitivity by measuring growth rate in the presence of different concentrations of supplemental zinc as described in Chapter 2. *ttm-1(ok3503)* animals grew similarly to wild-type animals in under all zinc conditions (Figure 3.6A), suggesting that TTM-1 may not be required for zinc detoxification. CDF-2 is the zinc transporter that is most similar to TTM-1 in *C. elegans*. To determine if these proteins have overlapping functions, we examined zinc sensitivity of *ttm-1(ok3503);cdf-2(tm788)* animals. *ttm-1(ok3503);cdf-2(tm788)* animals displayed a reduced growth rate in normal zinc conditions and an enhanced sensitivity to high levels of zinc compared to *cdf-2(tm788)* animals (Figure 3.6A). These data indicate that TTM-1 may play a role in zinc detoxification in the absence of CDF-2.

To further explore the relationship between TTM-1 and CDF-2, we measured mRNA levels of *mtl-1/2* in *ttm-1(ok3503);cdf-2(tm788)* animals. Without supplemental zinc, *ttm-1* and *cdf-2* single mutant animals displayed approximately 3-fold and 1.5-fold increase in *mtl-1* expression, while *ttm-1(ok3503);cdf-2(tm788)* animals displayed an approximately 18-fold increase (Figure 3.5B). In the presence of 100μM supplemental zinc, *ttm-1(ok3503);cdf-2(tm788)* animals also displayed a synergistic increase of *mtl-1* expression. *mtl-2* mRNA levels displayed similar patterns to *mtl-1* mRNA (Figure 3.5C). These results suggest that TTM-1 and CDF-2 function in parallel to detoxify cytoplasmic zinc.

To test whether TTM-1 cooperates with other known CDF members, we examined alleles of *cdf-1* and *sur-7*. Animals carrying *cdf-1(n2527)* or *sur-7(ku119)* were

hypersensitive to zinc (Bruinsma et al., 2002; Yoder et al., 2004) (Figure 3.6B and Supplemental Figure 3.2). Both *ttm-1(ok3503);cdf-1(n2527)* and *ttm-1(ok3503);sur-7(ku119)* animals were indistinguishable from *cdf-1(n2527)* and *sur-7(ku119)* animals, respectively, in the growth-rate assay (Figure 3.6B and Supplemental Figure 3.2). These results suggest that neither CDF-1 nor SUR-7 functionally interact with TTM-1.

Role of TTM-1B in Zinc Detoxification

To determine which isoform of TTM-1 is important for zinc excretion and detoxification, we performed a rescue experiment by expressing each isoform. We generated transgenic animals expressing either TTM-1A::GFP or TTM-1B::GFP in the *ttm-1(ok3503);cdf-2(tm788)* animals, and measured zinc sensitivity. TTM-1A::GFP did not rescue the zinc hypersensitivity of *ttm-1(ok3503);cdf-2(tm788)* animals, TTM-1B:GFP expression displayed a partial rescue of the phenotype (Figure 3.6C). These results suggest that TTM-1B, but not TTM-1A, plays a critical role in zinc detoxification by promoting excretion of zinc from the intestine.

DISCUSSION

ttm-1 was originally identified as one of the downstream targets of p38 kinase (Huffman et al., 2004). *ttm-1* expression is increased in response to pore-forming bacterial toxins via the p38 MAPK signaling pathway, and RNAi of *ttm-1* causes hypersensitivity to the same toxins. *ttm-1* expression is also induced by cadmium

exposure, and it is important for cadmium tolerance (Cui et al., 2007a). However, the function of *ttm-1* has not been determined.

We demonstrate that TTM-1 plays a role in zinc excretion and is important for zinc detoxification in response to high levels of dietary zinc. Loss of *ttm-1* results in elevated zinc contents and *mtl-1/2* mRNA levels. These data suggest that zinc accumulates in *ttm-1(ok3503)* animals and TTM-1 functions in excretion of zinc in response to high zinc. To study the action of TTM-1, we characterized the tissue distribution and intracellular localization of TTM-1A/B. TTM-1A is localized to intracellular compartments in intestinal and hypodermal cells. TTM-1B displayed two different localizations; while TTM-1B is on the apical plasma membrane of intestinal cells, it is localized to intracellular compartments in other tissues such as hypodermis and neurons. These results suggest that TTM-1A/B has multiple functions depending on the type of cells.

One function of TTM-1 may be to supply zinc to intracellular compartments via the action of TTM-1A. Since *ttm-1a* expression is constant regardless of zinc status, TTM-1A may mediate the flow of zinc into zinc-requiring intracellular compartments. We demonstrated that the intracellular compartments containing TTM-1A are neither mitochondria nor gut granules, and further experiments are required to determine the localization of this protein. Additionally, we are conducting assays to determine the function of TTM-1A.

Given that *ttm-1* mutant animals displayed a zinc accumulation phenotype, the major function of TTM-1 appears to be the excretion of zinc via the action of TTM-1B. *ttm-1b* was most strongly expressed in the intestine which is a metabolically active tissue

83

in *C. elegans*. TTM-1B was localized on the apical plasma membrane of intestinal cells, and its expression was strongly induced by high levels of dietary zinc. Additionally, TTM-1B::GFP rescued the zinc hypersensitivity phenotype of *ttm-1(ok3503);cdf-2(tm788)* animals. Taken together, these results suggest that TTM-1B promotes excretion of zinc from intestinal cells into the lumen during high zinc conditions. To further define the role of TTM-1B, we will use tissue-specific promoters to determine the site of TTM-1B action.

TTM-1 functions with CDF-2 in zinc detoxification. Although TTM-1 plays a role in zinc excretion, it was not required for efficient zinc detoxification. TTM-1 was, however, critical for zinc detoxification in the absence of CDF-2. These results raise two possibilities. First, zinc excretion by TTM-1 plays a minor role in zinc detoxification, and its role is detectable only in sensitized strains that are hypersensitive to zinc. Second, TTM-1 communicates with CDF-2 to control the flow of intracellular zinc. To test these possibilities, we tested the role of TTM-1 in other zinc hypersensitive strains including *cdf-1* and *sur-7* mutant animals. In contrast to *ttm-1;cdf-2* double mutant animals, neither *ttm-1;cdf-1* nor *ttm-1;sur-7* double mutant animals displayed additive phenotypes, suggesting a specific functional interaction between TTM-1 and CDF-2.

As TTM-1 was important in the absence of CDF-2, it is likely that CDF-2 is sufficient for zinc detoxification, and only when CDF-2 is not functional does the role of TTM-1 become critical. Zinc is a valuable nutrient to animals. When exposed to zinc abundant environments, animals store excess zinc rather than excrete it. Therefore, it is natural that zinc storage by CDF-2 in gut granules has the priority for zinc detoxification over zinc excretion by TTM-1 in high zinc conditions. This study demonstrates that

84

functional interaction between zinc transporters is an important mechanism to control

zinc metabolism in an efficient manner. For the molecular mechanism by which CDF-2

has priority over TTM-1, it is possible that CDF-2 has higher affinity for zinc than TTM-

1B so that excess zinc is mainly transported into gut granules. Alternatively, TTM-1B has

a unique histidine-rich motif at its N-terminus, which may receive a signal to attenuate

TTM-1B transporter activity. The interaction between multiple zinc transporters will be

an important future research topic to be addressed in zinc physiology.

MATERIALS AND METHODS

General Methods and Strains

C. elegans strains were cultured at 20℃ on nematode growth medium (NGM) and the *E.*

coli OP50 strain was used for food (Brenner, 1974). The wild-type *C. elegans* and parent

of all mutant strains was Bristol N2. The following mutations were used: *cdf-1(n2527)*

(Bruinsma et al., 2002), *cdf-2(tm788)* (Davis et al., 2009) and *sur-7(ku119)* (Yoder et al.,

2004). *ttm-1(ok3503)* was generated by the *C. elegans* Gene Knockout Consortium and

obtained from the *Caenorhabditis* Genetics Center. *ttm-1(ok3503)* was backcrossed five

times before analysis. The molecular lesion of *ttm-1(ok3503)* was determined by

sequencing of the PCR-amplified *ttm-1* locus using the following primers:

cccgccaaaaattattcaga and accgtaatgggacagacagc. Double mutant animals were generated

by standard methods, and genotypes were confirmed by PCR or DNA sequencing.

5' Rapid Amplification of cDNA Ends (RACE)

To determine the presence of *ttm-1a* and *ttm-1b* isoform transcripts and to study the

mechanism by which those isoforms were encoded by the *ttm-1* genomic locus, we

performed 5' RACE using the 5' RACE System for Rapid Amplification of cDNA Ends

Version 2.0 according to the manufacturer's protocol (Invitrogen, Carlsbad, CA). Briefly,

RNA was purified from wild-type adult animals using TRIzol and reverse-transcribed

using a gene specific primer (GSP1) which hybridizes to exon 4. Next, cDNA was tailed

with oligo(dC) and amplified by PCR using Abridge Anchor Primer and another gene

specific primer (GSP2) which is ~30bp 5' of GSP1. Two different PCR products were

observed after agarose gel electrophoresis and then purified and sequenced. GSP1 is

gtaaccgaatgaaagacgct, and GSP2 gagaattcaagacgtgcacaacgaatcg.

Quantitative real-time PCR

To generate samples of synchronized adult animals, eggs were isolated from gravid adult

hermaphrodites by bleaching, hatched in M9 overnight, and the worms were cultured on

NGM dishes for approximately 2.5 days. Synchronized animals at L4/young adults were

washed off and then cultured on noble agar minimum medium (NAMM) dishes

supplemented with zinc sulfate (ZnSO$_4$) and seeded with concentrated OP50. After 16-

24hr, animals were washed off and collected for RNA purification. RNA analysis was

performed as described by Davis et al. (2009) with modifications. Briefly, RNA was

purified using TRIzol and treated with DNase I, and cDNA was synthesized using the

High-Capacity cDNA Reverse Transcription kit according to the manufacturer's protocol

(Applied Biosystems, Foster City, CA). PCR was performed using a BioRad MyiQ

Single Color Real-Time PCR Detection System thermocycler and iQ SYBR Green

Supermix (BioRad Laboratories, Hercules, CA). Fold change was determined by

comparing the changes in target gene expression between different conditions to the

changes in reference gene expression (*ama-1* and *rps-23*) under the same conditions.

Transgenic Strain Construction & Microscopy

To generate promoter fusion constructs, we inserted the putative promoter region of *ttm-1a* or *ttm-1b*, coding sequence of GFP and the *unc-54* 3'UTR into pBluescript SK+

(Stratagene, Santa Clara, CA). For *ttm-1a*, the region between the *ttm-1a* start codon and

the 3' end of the adjacent upstream gene (~1.2kb) was amplified by PCR using wild-type

genomic DNA and used to make pSC27 *[Pttm-1a::GFP]*. For *ttm-1b*, ~6kb and ~2.4kb

regions upstream of exon 3 were amplified by PCR using wild-type genomic DNA and

used to make pHR6 *[Pttm-1b(-6kb)::GFP]* and pSC28 *[Pttm-1b(-2.4kb)::GFP]*,

respectively. To generate translational fusion constructs, *ttm-1a* cDNA was amplified by

PCR using the EST clone, yk1572h06, which was obtained from the National Institutes

of Genetics in Japan. *ttm-1b* cDNA was generated by combining the exon 4-5 fragment

PCR-amplified from the EST clone, yk1572h06, and the exon 3 fragment PCR-amplified

from wild-type genomic DNA. Next, the promoter, cDNA of *ttm-1a* or *ttm-1b* without

the stop codon, coding sequence of GFP and the *unc-54* 3'UTR were inserted into

pBluescript SK+ to build pSC29 *[TTM-1A::GFP]* and pHR7 *[TTM-1B::GFP]*.

Transgenic animals were generated by coinjecting each plasmid construct and the

coinjection marker pCJF104 [*Pmyo-3::mCherry*].

For fluorescence microscopy, animals were paralyzed in a drop of 10mM

levamisole in M9 on 2% agarose pads on microscope slides. Images were captured using a Zeiss Axioplan 2 microscope equipped with a Zeiss AxioCam MRm digital camera.

Inductively Coupled Plasma-Mass Spectrometry (ICP-MS)

Metal content analysis was performed as described by Davis et al. (2009) with modifications. For the preparation of samples, large populations of animals were generated by culturing on multiple 100mm NGM dishes. Animals were then washed off and cultured on multiple 100mm NAMM dishes supplemented with $ZnSO_4$ and seeded with concentrated OP50. After ~24 h, animals were washed three times in magnesium-free (Mg-free) M9 containing 0.01% Tween-20, incubated in 1mM serotonin in Mg-free M9 for 30 min to remove bacteria from the intestinal lumen, washed twice in Mg-free M9, and transferred to preweighed tubes and frozen at -80°C. For ICP-MS, samples were freeze-dried, reweighed to obtain the dry pellet weight, and digested by incubation in a hot block digester with concentrated nitric acid and hydrogen peroxide solution. The solution was diluted with water, and internal standards were added to correct for matrix effects. Instrument calibration standards were prepared from multi-element stock solutions (High-Purity Standards) to generate a linear calibration curve, and samples were analyzed using a VG Axiom high-resolution ICP-MS (Thermo Fisher Scientific). The content of zinc, iron, copper, magnesium and manganese was determined as a value in parts-per-million (ppm) by dividing metal weight by dry pellet weight (μg/g).

Zinc Sensitivity Assays

Eggs were isolated from gravid adult hermaphrodites by treating with NaOH and bleach

and hatched in M9 overnight. Synchronized L1 animals were then cultured on noble agar

minimum medium (NAMM) dishes supplemented with $ZnSO_4$ and seeded with

concentrated OP50. After about 3 days, animals were washed off, paralyzed with 10mM

sodium azide (NaN_3) in M9, and then mounted on a 2% agarose pad on a microscope

slide. Images were captured as described above. Length of animals was measured using

ImageJ software (NIH) by drawing a line from the nose to the tail tip.

ACKNOWLEDGEMENTS

FIGURE LEGENDS

Figure 3.1. Gene structure and protein sequence of *ttm-1*. (A) *ttm-1* encodes two isoforms, *ttm-1a* and *ttm-1b* using different transcription start sites near exon 1 and exon 3, respectively, as indicated by arrows. Both *ttm-1a* and *ttm-1b* mRNA contain SL1 at their 5' ends. The *ok3503* allele is a deletion of 877bp in the region between exon 4 and intron 4. Transgene constructs used for expression pattern analysis are depicted. (B) TTM-1A/B protein sequence alignment with *C. elegans* CDF-2 and human orthologs. Identical and similar amino acids are displayed in black and gray, respectively. Blue boxes indicate six predicted transmembrane motifs (labeled I-VI) conserved in the CDF family. The pair of red triangles indicates the region deleted by the *ok3503 allele*. The red bar indicates the region containing the unique N-terminal histidine-rich motif of TTM-1B, the green bar indicates the conserved $(HX)_n$ motif of CDF proteins in the loop between the fourth and fifth transmembrane motifs. (C) The unique N-terminal histidine-rich motif (red bar) and the conserved $(HX)_n$ motif in the loop between the fourth and fifth transmembrane motif (green bar) are compared. Histidine residues are displayed in red.

Figure 3.2. Expression of *ttm-1a* and *ttm-1b* mRNA by high dietary zinc. mRNA levels of indicated genes were analyzed by quantitative RT-PCR. The Y-axis represents the fold changes of relative mRNA levels between 0 and 200μM supplemental zinc, and the bars indicate the average ± SEM of two independent experiments. While *ttm-1a* displays the constant mRNA levels, *ttm-1b* displays significant induction of mRNA expression by

200μM supplemental zinc. *ama-1* is a reference gene which is not responsive to zinc, and *cdf-2* is a positive control which is induced by zinc.

Figure 3.3. Fluorescence microscope images of transgenic animals expressing GFP under the control of *ttm-1a* or *ttm-1b* promoter. (A) *ttm-1a* expression in the hypodermis and intestine. (B) *ttm-1b* expression in the head neurons, intestine, hypodermis including seam cells and vulva. (C) (a-b) *ttm-1b* expression is induced in the intestine by 200μM supplemental zinc. The arrows indicate either end of the intestine. (c-d) The head of an animal including the first pair of intestinal cells is displayed (anterior to the right and posterior to the left). While intestinal cells (triangles) display induction of *ttm-1b* by 200μM supplemental zinc, *ttm-1b* expression is not responsive to zinc in the head neurons (arrows).

Figure 3.4. Fluorescence microscope images of transgenic animals expressing TTM-1A or TTM-1B translationally fused to GFP. Localization of TTM-1A::GFP to intracellular compartments in the head hypodermis (A), body hypodermis (B), and intestine (C). In the intestine, green displays TTM-1A::GFP, and blue display autofluorescence from gut granules. TTM-1A::GFP does not colocalize with gut granule autofluorescence. (D) Localization of TTM-1B::GFP on the apical membrane of intestinal cells (top) and to intracellular compartments of the tail hypodermis (bottom). The arrows indicate the lumen of the intestine. (E) Induction of TTM-1B::GFP on the apical membrane of intestinal cells by 100μM supplemental zinc. The arrows indicate the lumen of the intestine.

Figure 3.5. (A) Total zinc contents of wild-type (WT) and *ttm-1(ok3503)* animals measured by ICP-MS. (B-C) mRNA levels of *mtl-1* (B) and *mtl-2* (C) in wild-type (WT), *ttm-1(ok3503), cdf-2(tm788),* and *ttm-1(ok3503);cdf-2(tm788)* animals. mRNA levels were analyzed by quantitative RT-PCR.

Figure 3.6. (A) Zinc sensitivity of wild-type (WT), *ttm-1(ok3503), cdf-2(tm788),* and *ttm-1(ok3503);cdf-2(tm788)* animals. Animals synchronized at the L1 stage were cultured with the indicated levels of supplemental zinc for 3 days. The length of individual animals was measured using microscopy and ImageJ software. The values indicate the average of the length of animals ± SD (n=20). (B) Zinc sensitivity of wild-type (WT), *ttm-1(ok3503), cdf-1(c2527),* and *ttm-1(ok3503);cdf-1(n2527)* animals. (C) Zinc sensitivity of wild-type (WT), *ttm-1(ok3503), cdf-2(tm788), ttm-1(ok3503);cdf-2(tm788),* and transgenic animals expressing TTM-1A::GFP or TTM-1B::GFP in the *ttm-1(ok3503);cdf-2(tm788)* mutation.

Supplemental Figure 3.1. Fluorescence microscope images of transgenic animals expressing GFP under the control of the *short ttm-1b* promoter. (A) GFP is observed in the head neurons, hypodermis and vulva. (B) GFP is not induced by 200μM supplemental zinc.

Supplemental Figure 3.2. Zinc sensitivity of wild-type (WT), *ttm-1(ok3503), sur-7(ku119),* and *ttm-1(ok3503);sur-7(ku119)* animals.

Figure 3.1

Figure 3.2

Figure 3.3

A *Pttm-1a::GFP*
Hypodermis
Intestine
Hypodermis
Intestine

B *Pttm-1b(-6kb)::GFP*
Head neurons
Intestine
Hypodermis
Vulva
Head neurons
Hypodermis

C
Pttm-1b(-6kb)::GFP

Whole animal
a
b

Head
c
d

0   200
Supplemental Zn (µM)

Figure 3.4

A

TTM-1A::GFP

Head hypodermis

B

TTM-1A::GFP

Body hypodermis

C

TTM-1A::GFP

Autofluorescence

Merge

Intestine

D

TTM-1B::GFP   Intestine

TTM-1B::GFP

Tail hypodermis

E

Supplemental Zn (µM)

0   100

TTM-1B::GFP
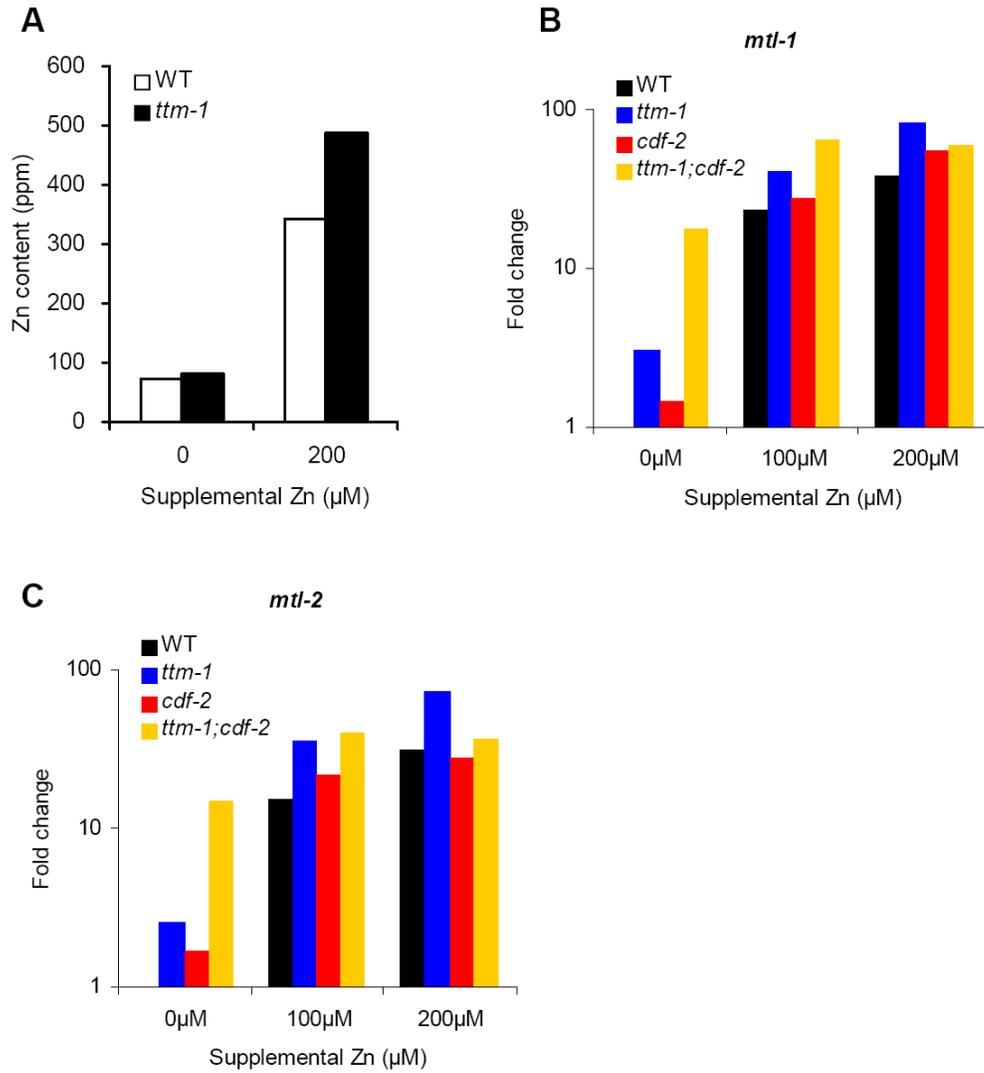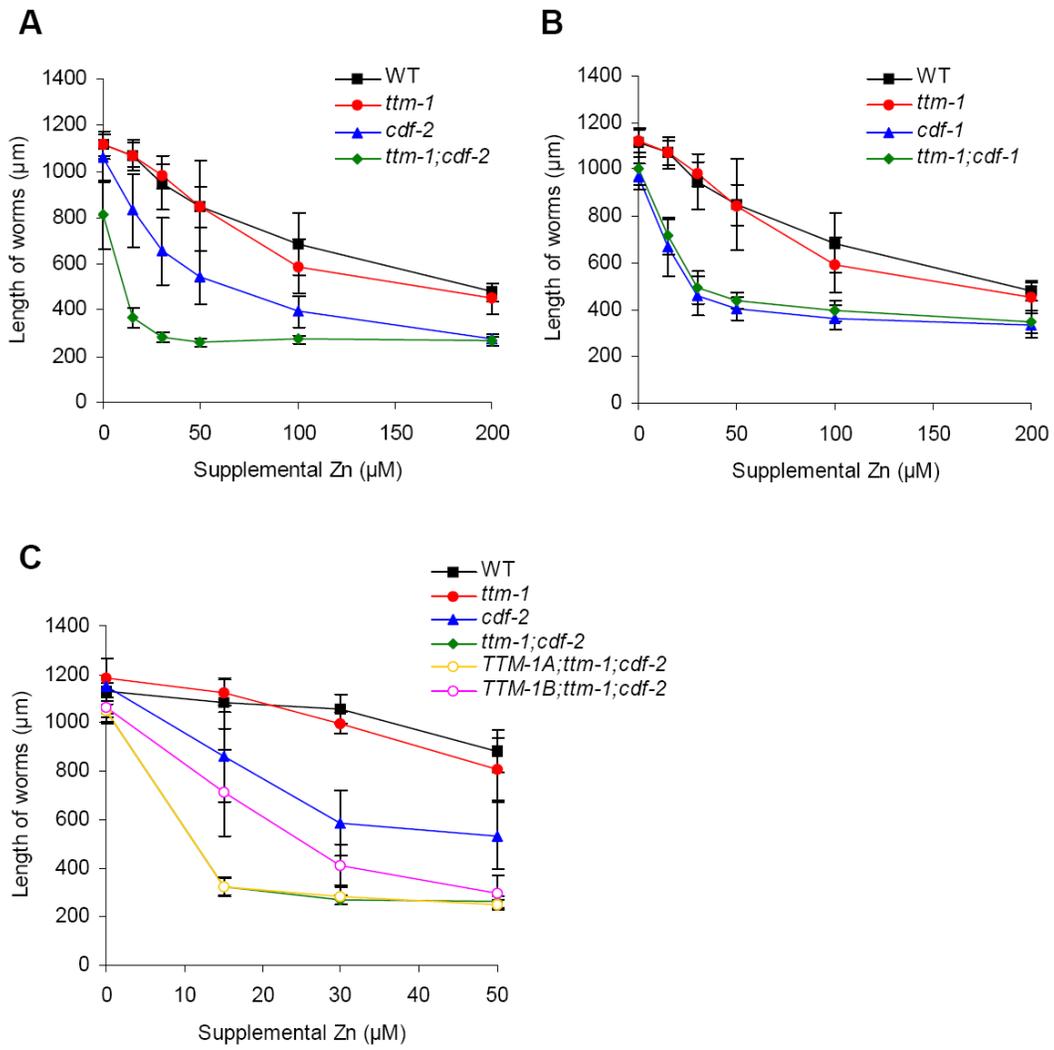
Figure 3.5

Figure 3.6

A

B
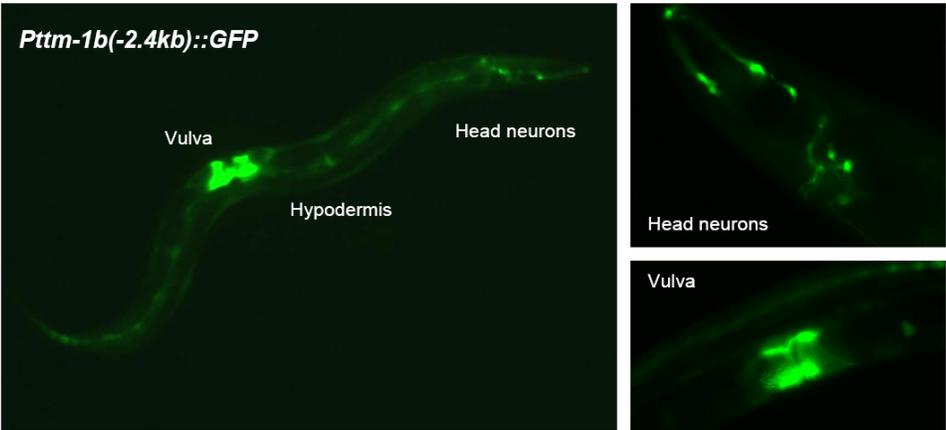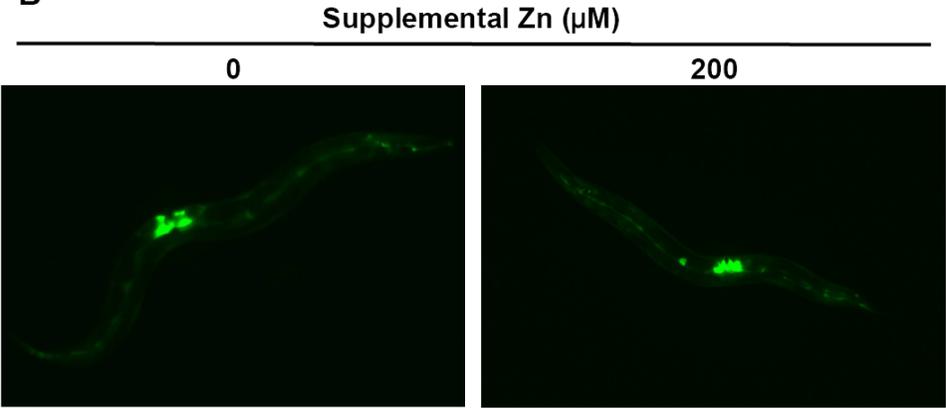
Supplemental Figure 3.2
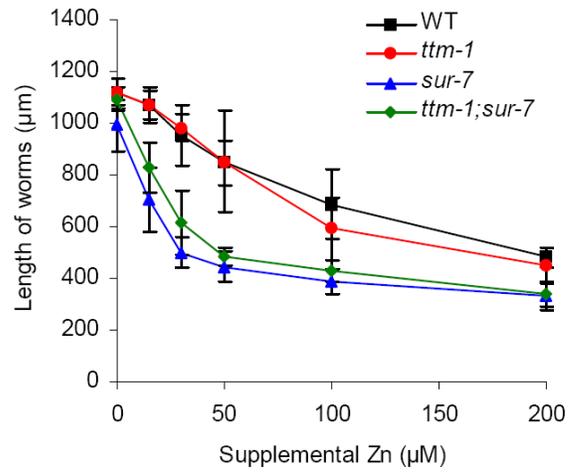
CHAPTER 4

Conclusions, Discussions and Future Directions

Identification of zinc storage site in animals

Organisms have evolved homeostatic mechanisms to regulate uptake, consumption, excretion and storage of nutrients. In these processes, storage of nutrients is critical for survival of organisms in particular in natural environments where nutrient availability fluctuates. When nutrients are replete, excess nutrients are stored so that they can be mobilized under nutrient deficient conditions. For example, carbohydrates and lipids are stored in the forms of glycogen and triacylglycerols in the liver and adipocytes which are specialized tissues for fat storage. In response to nutrient deficiency, the stored nutrients are mobilized to meet the need for energy. In the wild, the availability of metal is also variable, so organisms have mechanisms for metal storage and mobilization. For instance, iron is essential in mammals for erythropoietic function and oxidative metabolism, and iron is stored in the liver in the forms of ferritin or hemosiderin (Munoz et al., 2009).

Mechanisms of zinc storage have been described in the yeast *Saccharomyces cerevisiae*. The vacuole plays a role as a zinc storage site where CDF and ZIP proteins shuttle zinc across the membrane in response to zinc level changes (Eide, 2006). However, zinc storage in multicellular animals has not been well defined. It has been thought that zinc is unlikely to be stored in higher animals, such as mammals, based on kinetic studies using stable zinc isotopes (Krebs and Hambidge, 2001). However, these studies need to be interpreted with caution because they examined a small fraction of the total zinc pools and the range of testable dietary zinc levels was relatively narrow. Our studies of *C. elegans* using a variety of experimental approaches and wider ranges of dietary zinc, described in Chapter 2 and Appendix A, identified a site of zinc storage in

the animal. Lysosome-related organelles in intestinal cells, called gut granules, play a critical role in zinc storage in *C. elegans*, and this discovery suggests a possibility that zinc storage mechanisms may be present in higher animals.

Given that both the yeast vacuole and *C. elegans* gut granules have lysosomal properties, we can hypothesize that lysosome-related organelles may have an evolutionary conserved role in zinc storage. In fact, labile zinc is detected by zinc-specific fluorescent dyes in intracellular organelles which have lysosomal properties and often called zincosomes in various types of mammalian cells (Eide, 2006). There are also specialized lysosome-related organelles in mammals that may be involved in zinc homeostasis. For instance, paneth cells located in the bases of the small intestine contain a large number of secretory granules that have lysosomal proteins and high levels of zinc. The number of paneth cells and their secretory granule morphology are affected by dietary zinc levels (Giblin et al., 2006), suggesting that these cells and the granules might play a role in zinc storage in mammals. Therefore, the investigation of zinc storage in lysosome-related organelles in higher animals will be an important research topic in zinc physiology.

Physiological functions of zinc storage in gut granules

Zinc storage in gut granules has two functional roles in the control of zinc metabolism. One function is zinc detoxification in response to high zinc conditions. When there are defects in gut granule biogenesis or zinc transport into gut granules, animals become hypersensitive to high levels of dietary zinc and suffer severely from zinc toxicity. In yeast, the vacuole functions in zinc detoxification. However, in

multicellular animals, zinc-containing organelles have not been demonstrated to protect organisms from zinc toxicity. Thus, our studies of *C. elegans* document a novel role of lysosome-related organelles in zinc detoxification in animals. Metal detoxification processes are also mediated by many other genes such as metallothionein genes. An important direction for future research can be to study how zinc sequestration in lysosome-related organelles cooperates with other genes such as zinc-binding proteins.

The second function of zinc stored in gut granules is to provide a source of zinc that can be utilized during dietary deficiency. Our studies demonstrated that stored zinc is mobilized from gut granules to meet the need for zinc by visually monitoring gut granule zinc levels and measuring growth rates of animals in the shift from high to low zinc conditions. Mobilization process of stored zinc has been well studied in the yeast, but it has not demonstrated in multicellular animals. Although zinc level changes in organelles of mammalian cells have been detected, it is not a homeostatic process in response to dietary zinc level changes. Our results here provide the first evidence of a site of zinc storage in animals that is mobilized during dietary deficiency. In the yeast, a ZIP protein Zrt3 play a critical role in zinc mobilization by moving zinc out of the vacuole in response to zinc deficiency (MacDiarmid et al., 2000). In *C. elegans* gut granules, mobilization is also likely to require a ZIP protein that shuttles zinc from the lumen of gut granules to the cytoplasm, and future studies will focus on the identification of this zinc transporter.

Function of CDF-2 in zinc storage

The initial study described in Appendix A proposed the role of CDF-2 in zinc

104

storage based on its localization on gut granules and the phenotype of reduced total zinc levels of *cdf-2* mutant animals. Further thorough experiments described in Chapter 2 provide direct evidence of the role of CDF-2 in gut granule zinc storage. Colocalization experiments using markers confirmed that CDF-2 is localized to the membrane of gut granules. CDF-2 expression is induced by high levels of dietary zinc, suggesting its functional importance during high zinc conditions. Most importantly, while zinc storage was reduced by a loss-of-function mutation of *cdf-2*, it was elevated by overexpression of CDF-2 proteins, suggesting that *cdf-2* is necessary and sufficient for zinc storage in gut granules. Consistent with the model that CDF-2 directly transports zinc into gut granules, the action of CDF-2 is cell-autonomous in intestinal cells to promote zinc accumulation. Intriguingly, we observed that a small amount of zinc is likely to be stored even in *cdf-2* mutant animals, suggesting that there may be a CDF-2 independent mechanism that can move zinc into gut granules such as using alternative zinc importer or vesicular trafficking. *C. elegans* CDF-2 is homologous to mammalian ZnT-2. Similar to CDF-2, ZnT-2 is also localized to intracellular vesicles and upregulated by high levels of zinc (Liuzzi et al., 2001). This similarity proposes a possibility that ZnT-2 may be involved in zinc storage in mammals and it can be one way to approach to zinc storage mechanisms of higher animals.

Morphological changes of gut granules in high zinc

In normal conditions, gut granules are single round-shaped vesicles. However, we observed that when exposed to high zinc conditions, gut granules undergo morphological changes and display the shape of bilobed vesicles with asymmetric

distribution of molecules. In particular, lysosomal markers were positive for one side, whereas zinc was highly concentrated in the other side. These findings suggest that high levels of zinc lead to the novel structural changes of gut granules that may have important functions in zinc metabolism. First, it is possible that this structural change is a mechanism to promote zinc storage. Generation of additional adjacent vesicles devoted to storing zinc may improve the capacity of storage and facilitate rapid sequestration. Second, bilobed vesicles may be utilized for the secretion of zinc which exceeds the capacity of gut granule storage. Excess zinc is concentrated in one side of bilobed vesicles, and this side is secreted via certain trafficking pathways to the extracellular space. Thus, the bilobed structure may be imporant for the control of the balance between zinc storage and excretion. These possible functions of the bilobed structure can be studied by monitoring dynamic structures of gut granules in different zinc conditions using time-lapse live imaging.

Genetic analysis to dissect pathways involved in bilobed vesicle formation demonstrated that neither lysosome biogenesis process nor endocytosis is required for this process. Bilobed vesicle formation was also independent of CDF-2 activity. In contrast, *Glo* genes that are required for gut granule biogenesis during development such as *pgp-2* and *glo-3* genes were are also necessary for this morphological change during high zinc conditions. These results suggest that the formation of bilobed vesicles may be mediated by processes specific to gut granules and that intracellular trafficking may play a role in zinc metabolism. The mechanism by which intracellular trafficking regulates zinc metabolism in the aspects of storage or secretion will be important topics to be studied.

106

Characterization of a *cdf* gene, *ttm-1* in zinc metabolism

ttm-1 (toxin-regulated target of p38MAPK) is a *cdf* gene which is the most

similar to *C. elegans cdf-2* and human ZnT-2. *ttm-1* was originally identified as one of

downstream targets of p38 kinase in the response to bacterial toxins (Huffman et al.,

2004). *ttm-1* expression is increased in response to pore-forming bacterial toxins via the

p38 MAPK signaling pathway, and RNAi of *ttm-1* causes hypersensitivity to the the

same toxins. *ttm-1* is also involved in cadmium toxicity (Cui et al., 2007a); *ttm-1*

expression is induced by cadmium, and it is important for cadmium tolerance. However,

the function of *ttm-1* has not yet been studied.

The work presented in Chapter 3 describes the functional role of *ttm-1* in zinc

metabolism in *C. elegans*. Unlike the *C. elegans cdf* genes previously characterized, *ttm-

1* encodes two isoforms, *ttm-1a* and *ttm-1b*, suggesting that *ttm-1* may have multiple

functions. First, TTM-1 may function in providing zinc into intracellular compartments

via the action of TTM-1A. Since TTM-1A is localized to intracellular compartments and

ttm-1a expression is not affected by zinc levels, it appears that TTM-1A mediates

constant influx of zinc into the intracellular compartments where it is needed for the

synthesis or activity of zinc-dependent proteins. Second, TTM-1 functions in the

excretion of zinc via action of TTM-1B. TTM-1B expression is strongly induced by high

levels of zinc and TTM-1B is localized on the apical membrane of intestinal cells where

it appears to move cytoplasmic zinc out to the lumen. It is important to note that no CDF

protein that mediates zinc efflux on the plasma membrane has been identified in the yeast.

In humans, ZnT-5 is reported to be localized on the apical membrane of small intestinal

cells. However, it is not clear whether it promotes uptake or excretion of zinc (Cragg et al., 2002; Cragg et al., 2005). Therefore, these findings demonstrate the first evidence that there is a direct flow of zinc from intestinal cells into the lumen to regulate zinc levels in animals and suggest that mammals may have similar mechanisms to control zinc homeostasis.

Interestingly, *ttm-1* functionally interacts with *cdf-2*. Although zinc excretion by *ttm-1* is not required for efficient zinc detoxification, it becomes critical in the absence of *cdf-2*, suggesting that *cdf-2* may suppress *ttm-1* activity and thereby that zinc storage process has priority over excretion process. This regulatory mechanism is important for the efficient use of dietary zinc. Once zinc is transported into intestinal cells at the cost of energy, it should be utilized by animals. Thus, *ttm-1* may be fully activated only when zinc excretion is necessary. For example, when zinc storage is saturated or defective due to mutations, zinc excretion by *ttm-1* can be an effective way to detoxify excess zinc. These findings suggest that interactions between zinc transporters can be a key mechanism to achieve the efficient control of zinc metabolism. The molecular mechanism by which *cdf-2* suppresses *ttm-1* activity will be an interesting question to be addressed in the future research. It is possible that CDF-2 has a significantly higher affinity for zinc than TTM-1B so it has the biochemical priority to zinc. This possibility can be tested by comparing zinc transporter activity of CDF-2 and TTM-1. Another possible mechanism is that the unique histidine- and glycine-rich motif at its N-terminus of TTM-1B may receive a signal from CDF-2 and regulate its activity. This possibility can be tested by analyzing engineered TTM-1B protein that has deletions or mutations in the motif.

Action of multiple CDF proteins in the intestine

Previous studies and this work have identified and characterized four *C. elegans cdf* genes, *cdf-1, cdf-2, sur-7 and ttm-1,* all of which contribute to the control of zinc metabolism (Bruinsma et al., 2002; Davis et al., 2009; Yoder et al., 2004). The intestine is the major site for the regulation of zinc metabolism in *C. elegans,* where the CDF proteins act at multiple locations (Figure 4.1). CDF-1 moves zinc through the basolateral membrane into the body cavity, and it functions in the distribution of zinc from the intestine to other tissues of the body and the indirect excretion of zinc perhaps via the excretory cell. SUR-7 moves zinc into the ER/Golgi complex, and it is probably involved in the distribution of zinc via secretory vesicles. Since *cdf-1* and *sur-7* expressions are not affected by dietary zinc levels, they appear to play an important role in the constant flow of zinc throughout the body. CDF-2 moves zinc into gut granules for storage, and its expression is strongly induced by high levels of dietary zinc. Zinc storage in the intestine mediated by CDF-2 is critical to survive in the wild where zinc levels fluctuate by functioning in detoxification and mobilization. TTM-1 moves zinc across the apical membrane to the intestinal lumen, and its expression is also induced by zinc similar to CDF-2. However, TTM-1 activity appears to be partially suppressed by CDF-2 for the efficient use of zinc via unknown mechanisms. In the condition when CDF-2 is not functional, TTM-1 promotes direct excretion of zinc out of the body to deal with zinc toxicity. Therefore, this network of CDF proteins plays a key role in zinc metabolism from the distribution of zinc to the response to unfavorable zinc conditions. There may be other zinc transporters acting in the intestine that have not been identified yet. For

example, ZIP proteins acting on the apical membrane like mammalian ZIP-4 have not been identified. Identification and characterization of these zinc transporters should be an important research topic in the *C. elegans* zinc biology.

Analysis of other zinc transporters

To expand our knowledge of zinc transporters, the work described in Appendix B conducted the initial studies of unknown 8 *zip* genes and 1 *cdf* gene. While many zinc transporters displayed similar expression patterns to their mammalian counterparts, others displayed differences, suggesting that *C. elegans* zinc transporters have conserved functions, but some of them may be specific to *C. elegans* or other nematodes. In the analysis of mutant animals, it is not surprising that many mutant animals had no phenotype, because there are a large number of zinc transporters and some of them may be functionally redundant with one another. In addition, the assays used in this study were limited to identify complicated phenotypes. Thus, the analysis of genetic interactions between multiple zinc transporters and the development of various types of assays are necessary in the study of zinc transporters. In this regard, the zinc transporters, *F55F8.9* and *F28F3.3* are interesting to follow up for further studies. *F55F8.9* and *F28F3.3* mutant animals displayed the vulva positioning defect phenotype and the sperm-related sterility phenotype, respectively. Further analysis of these mutant animals may reveal novel functions of zinc and/or zinc transporters in biological processes.

Identification of novel proteins in zinc metabolism: Future studies

All the studies presented here are based on the reverse genetic approaches and have been successful to characterize *C. elegans* zinc transporters. However, in our effort to expand the knowledge of zinc metabolism, this type of reverse genetic approach has limitations; it is impossible to identify novel proteins involved in zinc metabolism. Therefore, different approaches should be considered for further studies.

Identification of zinc-responsive transcription factors

Regulation of gene expression in response to the changes in zinc levels is an important mechanism to control zinc metabolism. The yeast Zap1 and the mammalian MTF-1 proteins play a key role in this process by acting as a zinc-responsive transcription factor. However, in *C. elegans*, zinc-responsive transcription factors have not yet been identified. There is no candidate protein that is homologous to Zap1 or MTF-1. Therefore, reverse genetic approaches are not feasible here, and other unbiased methods are needed.

To identify zinc-responsive transcription factors, we can use traditional forward genetic screens. To set up the screens, we generated a zinc-responsive reporter system which is a transgenic animal containing an integrated array that expresses GFP under the control of the *cdf-2* promoter. As *cdf-2* expression is responsive to zinc, GFP expression was induced by high levels of zinc (Figure 4.2A). Using the transgenic animals, we can perform forward genetic screens for mutations that cause defects in the gene expression induction in response to high zinc levels. These screens may identify zinc-responsive transcription factors which directly control gene expression similar to Zap1 and MTF-1. It is also possible that other proteins which respond to zinc and transmit the signals to the

gene expression machinery would be identified from the screens. These studies may contribute to dissecting of the molecular processes that regulate the gene expression in zinc metabolism.

For the identification of zinc-responsive transcription factors, we can take another approach using the zinc-responsive gene promoters. We first analyzed the promoter sequences of the four known zinc-responsive genes, *mtl-1/2, cdf-2* and *ttm-1*. Using computational analysis, we identified a DNA element that is found in the promoter of all the four genes (Figure 4.2B). DNA mutagenesis analysis demonstrated that this element is necessary for the induction of *mtl-1/2* (Deshmukh and Dimitrov, unpublished observation). We can identify candidate zinc-responsive transcription factors that bind to the element using the yeast-one-hybrid system or protein pull-down assays using biotin-labeled DNA element.

Identification of novel proteins involved in zinc metabolism

In addition to forward genetic screens, microarray experiments can be a useful and unbiased approach to identify novel proteins that play a role in zinc metabolism. We previously conducted microarray experiments to compare gene expression profiles across different zinc conditions. We identified numerous genes whose expression is induced in response to high levels of zinc (Deshmukh and Kornfeld, unpublished observation). In the list of the genes, there were the genes previously known to be induced by zinc, such as *mtl-1/2* and *cdf-2* (data not shown), suggesting that the microarray results are reliable. There were many other genes that have not been implicated in zinc or metal metabolism. Studies of these genes, therefore, may identify novel genes important for zinc

112

metabolism. For example, we found that RNAi of one of the genes, *B0218/clec-52*, which encodes a C-type lectin, resulted in mild zinc hypersensitivity, suggesting that this gene may be involved in the zinc detoxification. These studies will broaden our knowledge of the mechanism that controls zinc metabolism.

Final Thoughts

Zinc was first recognized as a mineral essential for the growth of a fungus more than a hundred years ago, and it has since been demonstrated that zinc is also an essential micronutrient for humans. However, it is just over the past few decades that we have started to understand the molecular aspects of zinc metabolism and its implication in human diseases. We have just begun to appreciate the complexity of zinc metabolism and its significance in human health. There are much more important biological functions of zinc metabolism that remain to be uncovered.

A major obstacle to the studies of zinc metabolism has been its complexity that involves numerous proteins across multiple tissues. In this work, our approach using *C. elegans* was useful to overcome this problem. We have established the functional networks of CDF proteins in the intestine to control the whole body zinc metabolism and proposed possible physiological functions of zinc or zinc transporters. Therefore, I believe that as *C. elegans* has been powerful in a variety of fields of biology, it will advance our understanding of zinc, zinc transporters and/or zinc metabolism. Furtheremore, studies of zinc metabolism using *C. elegans* may lead to new medical and pharmaceutical approaches for dieases implicated in abnormal zinc metabolism.

FIGURE LEGENDS

Figure 4.1. Action of multiple CDF proteins in the intestine. CDF-1 (blue) is localized on the basolateral membrane and transports zinc into the body cavity. CDF-2 (red) is localized on the membrane of gut granules and transports zinc into the lumen of gut granules. SUR-7 (green) is localized in the ER and transports zinc into the lumen of the ER. TTM-1 (yellow) is localized on the apical membrane and transport zinc out to the intestinal lumen.

Figure 4.2. Future studies to identify of zinc-responsive transcription factors. (A) Fluorescence microscope images of live transgenic animals containing an integrated array, *amIs4*, which expresses GFP under the control of the *cdf-2* promoter [*Pcdf-2::GFP*]. Whole animals at the adult stage are displayed with the pharynx to the bottom left and the tail to the upper right. GFP expression is highly increased in 200μM supplemental zinc. (B) DNA element present in the known zinc-responsive genes: *mtl-1, mtl-2*, *cdf-2* and *ttm-1b*. The bottom panel displays its location and sequence of the promoter region of each gene. This element was identified using the MEME module (Bailey and Elkan, 1994).

Figure 4.1

Figure 4.2

A

Supplemental Zn (µM)

| 0 | 200 |

amIs10[Pcdf-2::GFP]
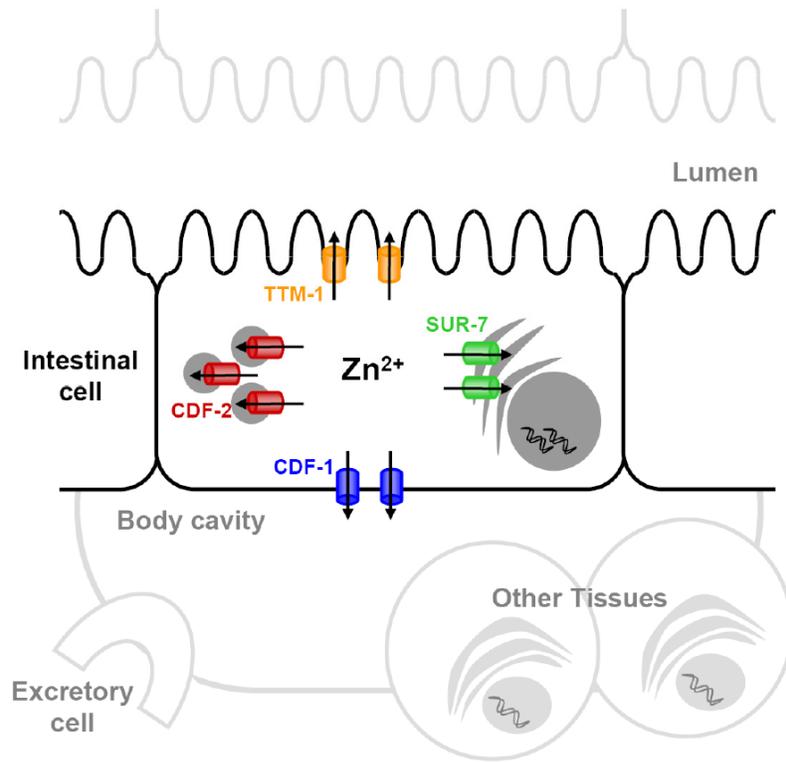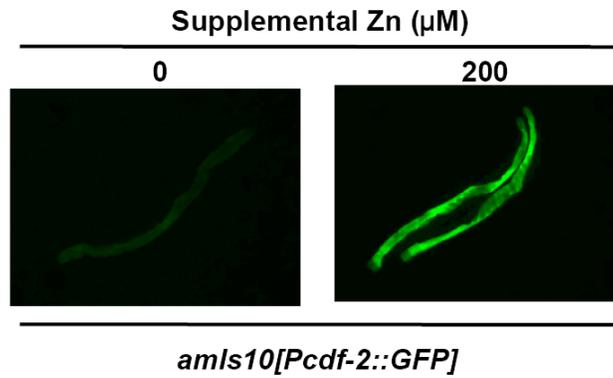
B
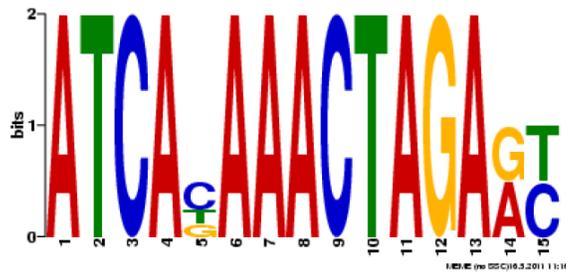
Name	Strand	Start	*p*-value	Sites
mtl-2	+	300	5.47e-09	AAAGGCCTCT ATCACAAACTAGAGT TGTGACGGAA
mtl-1	+	652	6.60e-09	AACTGATAAA ATCAGAAACTAGAGC TGTGACTGAA
ttm-1b	+	3437	1.08e-08	ACGAAACTGT ATCACAAACTAGAAT GACGTCTCCC
cdf-2	-	1177	2.98e-08	TGTGTTATCA ATCATAAACTAGAAC ATGTCTCGAG

116

APPENDIX A

The cation diffusion facilitator gene *cdf-2* mediates zinc metabolism in *Caenorhabditis elegans*

ABSTRACT

Zinc is essential for many cellular processes. To use *C. elegans* to study zinc metabolism, we developed culture conditions allowing full control of dietary zinc and methods to measure zinc content of animals. Dietary zinc dramatically effected growth and zinc content; wild-type worms survived from 7 μM to 1.3 mM dietary zinc, and zinc content varied 27 fold. We investigated *cdf-2*, which encodes a predicted zinc transporter in the cation diffusion facilitator family. *cdf-2* mRNA levels were increased by high dietary zinc, suggesting *cdf-2* promotes zinc homeostasis. CDF-2 protein was expressed in intestinal cells and localized to cytosolic vesicles. A *cdf-2* loss-of-function mutant displayed impaired growth and reduced zinc content, indicating that CDF-2 stores zinc by transport into the lumen of vesicles. The relationships between three *cdf* genes, *cdf-1*, *cdf-2*, and *sur-7,* were analyzed in double and triple mutant animals. A *cdf-1* mutant displayed increased zinc content, whereas a *cdf-1 cdf-2* double mutant had intermediate zinc content, suggesting *cdf-1* and *cdf-2* have antagonistic functions. These studies advance *C. elegans* as a model of zinc metabolism and identify *cdf-2* as a new gene that has a critical role in zinc storage.

INTRODUCTION

Zinc plays many roles in biological systems, including binding to proteins and promoting specific conformations, such as the zinc finger, and contributing to the active site of enzymes (Vallee and Falchuk, 1993). Reflecting its multiple uses, organisms that do not obtain adequate dietary zinc display a wide range of defects (Chowanadisai et al., 2005; Cole et al., 1999; Dufner-Beattie et al., 2007; Herbig et al., 2005; Kambe et al., 2004). For example, humans that are zinc deficient have abnormalities of multiple systems including the skin and immune system (Chowanadisai et al., 2006; Hambidge and Krebs, 2007; Hambidge, 2000; Maverakis et al., 2007). Excess dietary zinc can also cause defects as a result of zinc toxicity (Koh et al., 1996; Nies, 2007). The mechanisms underlying zinc toxicity have not been clearly defined but may involve the substitution of zinc for other metals such as copper (Zhao and Eide, 1997). Animals have evolved sophisticated mechanisms to regulate zinc metabolism to ensure an adequate supply of zinc but avoid zinc toxicity. Zinc metabolism involves uptake of zinc from dietary sources into intestinal cells, distribution of zinc throughout the body to supply non-intestinal cells, insertion of zinc into zinc-requiring proteins and excretion of excess zinc from cells and the animal. An essential aspect of zinc metabolism is adapting to changing levels of dietary zinc. Homeostasis is likely to involve sensors that monitor available zinc and effector mechanisms that adjust intake, storage, and excretion of zinc (Tapiero and Tew, 2003). These important processes are not well characterized.

Zinc in biological systems is the Zn^{2+} ion, and Zn^{2+} does not diffuse across lipid bilayers (Stryer, 1995). In metazoans, two families of transmembrane proteins play

critical roles in transporting zinc, the cation diffusion facilitator (CDF/SLC30) family (Palmiter and Huang, 2004) and the Zrt-, Irt- like protein (ZIP/SLC39) family (Eide, 2004; Eng et al., 1998; Guerinot, 2000). The CDF family evolved in prokaryotes and has been conserved in fungi, plants, and animals. Yeast contain multiple CDF proteins, which are localized to specific membrane compartments (Eide, 2006). Vertebrates contain 10 predicted CDF proteins (Liuzzi and Cousins, 2004; Palmiter and Huang, 2004; Seve et al., 2004). Mutations in human ZnT-2 are implicated in diseases characterized by inadequate zinc in breast milk, suggesting that CDF proteins play essential roles in zinc metabolism in humans (Chowanadisai et al., 2006). Most CDF proteins are predicted to contain six transmembrane regions, and the N- and C- termini are predicted to be cytoplasmic. Recent crystallographic data suggest that the *E. coli* CDF protein YiiP functions as a dimer (Lu and Fu, 2007), consistent with the results of cell biology studies in yeast (Ellis et al., 2005). The energy source for CDF proteins appears to be ion gradients, such as H^+ and K^+ (Chao and Fu, 2004; Guffanti et al., 2002).

Given that animals contain multiple CDF proteins, a critical question is how do these proteins function in a coordinated manner to mediate zinc metabolism throughout the animal? One mechanism is cell-type specific expression. For example, vertebrate ZnT-3 is expressed primarily in neuronal cells, where it promotes zinc accumulation in synaptic vesicles (Cole et al., 1999; Palmiter et al., 1996b). A second mechanism is localization to specific membrane compartments. For example, vertebrate ZnT-8 is localized to insulin granules (Chimienti et al., 2004), whereas vertebrate ZnT-1 is localized to the plasma membrane (Palmiter and Findley, 1995). A third mechanism is intrinsic differences in activity, which might include differences in affinity for zinc (K_m),

differences in the rate of zinc transport (V_{max}), and differences in metal specificity. A fourth mechanism is differences in regulation that adjust protein abundance and activity in response to fluctuating dietary zinc, which might include transcriptional, post-transcriptional, and post-translational regulation. These mechanisms are not mutually exclusive, and additional mechanisms may also be utilized. An understanding of how multiple CDF proteins function coordinately in an animal will require a genetically tractable model system that can be used to dissect the complementary, redundant, and antagonistic activities of multiple CDF proteins.

The nematode *Caenorhabditis elegans* has been a powerful model system to study many biological processes, but studies of nutrient biology have been limited. The use of *C. elegans* to study metal biology has included analyses of heme, magnesium, zinc, and cadmium (Bruinsma et al., 2002; Bruinsma et al., 2008; Dong et al., 2008a; Kemp et al., 2009; Rajagopal et al., 2008). The fully sequenced *C. elegans* genome contains 14 predicted genes that encode CDF proteins (Kambe et al., 2004, K. Deshmukh and K. Kornfeld unpublished observation). Two of these genes have been analyzed genetically, *cdf-1* and *sur-7* (Bruinsma et al., 2002; Yoder et al., 2004). Loss-of-function mutations of *cdf-1* and *sur-7* were identified in forward genetic screens for modifiers of abnormal vulval cell fates caused by constitutively activated Ras. In addition to promoting Ras-mediated signal transduction, *cdf-1* and *sur-7* promote survival in high dietary zinc, since loss-of-function mutations of these genes cause sensitivity to high dietary zinc (Bruinsma et al., 2002; Yoder et al., 2004). *cdf-1* is expressed in intestinal cells and vulval cells, and CDF-1 protein is localized to the plasma membrane (Bruinsma et al., 2002). *sur-7* is expressed in non-intestinal cells, and SUR-7 protein is diffusely localized to the cytosol,

suggesting it is localized to an internal membrane (Yoder et al., 2004). The functions of the remaining predicted *cdf* genes in *C. elegans* have not been determined.

To use *C. elegans* as a model system to study zinc metabolism and CDF protein function, we developed culture conditions that allow full control of dietary zinc. Here we show that worms are sensitive to both low and high dietary zinc and that sensitivity to dietary zinc can be used to assay zinc metabolism. We developed methods to measure the zinc content of *C. elegans* and demonstrated that dietary zinc strongly influences zinc content of wild-type animals. These methods advance the utility of *C. elegans* as a model system to study zinc metabolism. We investigated the function of a new predicted *cdf* gene, which we named *cdf-2*. CDF-2 is most similar to vertebrate ZnT-2, which is localized to vesicles and implicated in human diseases of zinc deficiency (Chowanadisai et al., 2006). The *cdf-2* transcript abundance was increased at high levels of dietary zinc, suggesting that *cdf-2* is involved in zinc homeostasis. CDF-2 protein was expressed in intestinal cells and localized to cytosolic vesicles. A strong loss-of-function mutation of *cdf-2* was characterized; mutant animals displayed growth defects and reduced zinc content compared to wild-type animals, indicating that *cdf-2* functions in zinc storage. To explore the relationship between the functions of multiple *cdf* genes, we analyzed double and triple mutant animals with mutations in *cdf-1*, *cdf-2*, and *sur-7*. The results indicate that *cdf-1* and *cdf-2* have antagonistic functions in mediating zinc content and *cdf-2* plays an important role in zinc storage by sequestering zinc in the lumen of cytosolic vesicles.

MATERIALS AND METHODS

122

General methods and strains: *C. elegans* were cultured at 20º on nematode growth medium (NGM) dishes with live *E. coli* as described by Brenner (1974) or in *C. elegans* maintenance medium (CeMM, described below) (Szewczyk et al., 2003). The wild-type strain and parent of all mutant strains was Bristol N2. The following mutations were used. *unc-119(ed3 R113Stop)* is a loss-of-function mutation that causes a strong uncoordinated phenotype and an inability to form dauer larvae (Maduro and Pilgrim, 1995). *let-60(n1046 G13E)* is a semi-dominant, gain-of-function allele of the Ras gene (Beitel et al., 1990). *cdf-1(n2527 Q156Stop)* is a strong loss-of-function allele caused by a nonsense change in exon four (Bruinsma et al., 2002). *sur-7(ku119)* is a partial loss-of-function allele caused by a single nucleotide change near the splice donor of exon three (Yoder et al., 2004). *cdf-2(tm788)* has an 804 bp deletion with a 68 bp insertion that removes the first 34 codons and is likely to cause a strong loss-of-function (described here). *cdf-1*, *cdf-2*, and *sur-7* are located on chromosome X, and we generated *cdf-1 cdf-2*, *cdf-1 sur-7*, and *cdf-2 sur-7* double mutant animals using standard techniques and confirmed the genotypes by PCR and gel electrophoresis (*cdf-2*) and DNA Pyrosequencing (*cdf-1* and *sur-7*; PSQ 96 MA, Biotage, Charlottesville, VA). A *cdf-1 cdf-2 sur-7* triple mutant was generated from *cdf-1 cdf-2* and *cdf-2 sur-7* double mutant animals using standard techniques.

Preparation of CeMM and culturing worms in CeMM: 2x CeMM was prepared as described by Szewczyk *et al.* (2003) with minor modifications. Briefly, we prepared five solutions (amino acids, nucleic acids, water-soluble growth factors and vitamins,

triethanolamine-soluble growth factors and vitamins, and trace metal salts without zinc chloride), combined these to yield 2x CeMM with no added zinc, adjusted the pH to 5.9 with 10% (w/v) NaOH, filtered the medium through a 0.22 µm cellulose acetate filter (Corning Inc. Life Sciences, Lowell, MA), and stored the medium in the dark at 4º for up to 8 months. To use the CeMM, we diluted with water from a Milli-Q Synthesis A10 machine (Millipore, Billerica, MA) to yield 1x CeMM. To achieve the final zinc concentration of 1x CeMM, we added the appropriate volume of 1 mm, 10 mm, 100 mm, or 1 m zinc chloride (Z0152, Sigma-Aldrich, St. Louis, MO) diluted in 40 mm HCl. To equalize the amount of HCl diluent added to each medium sample, we added the appropriate volume of 40 mm HCl with no added zinc. The 1x CeMM with added zinc was used promptly and not stored.

To introduce worms that were growing on NGM with live *E. coli* into CeMM, we collected adults and treated the animals with NaOH and bleach to generate eggs free of bacterial contamination (Wood, 1988). Subsequent procedures were performed in a tissue culture hood using sterile technique. Eggs were transferred to 25 cm^2 T-flasks (TPP, Trasadingen, Switzerland) containing 5 mL M9 buffer (85 mm NaCl, 22 mm KH_2PO_4, 42 mm Na_2HPO_4, 1 mm $MgSO_4$) and 10 µL/mL Antibiotic-Antimycotic solution (10,000 units penicillin, 10 mg streptomycin, and 25 µg amphotericin B per milliliter, Sigma-Aldrich). Eggs were cultured at 20º for 2-3 days to allow the hatching and developmental arrest of L1 larvae. Larvae were washed 2x in M9 buffer, transferred to a 25 cm^2 T-flask in 5 mL CeMM containing 30 µm zinc chloride, and cultured at 20º with no agitation for 3-4 weeks until visual inspection revealed significant growth of the population. Worms were collected using Pasteur pipets, pelleted by centrifugation at 1,000 rpm for 5 min at

124

15º, washed 2x in M9 buffer, resuspended in 15 mL CeMM containing 30 μm zinc chloride and transferred to 75 cm^2 T-flasks (TPP).

Maturity Analysis: Worms were grown on NGM with live *E. coli* and treated with NaOH and bleach to collect eggs. For experiments scored with a dissecting microscope, eggs were diluted in CeMM (19 zinc concentrations), seeded in 24-well plates (TPP) at a concentration of 100 eggs in 500 μL, and incubated at 20º in a box containing moist paper towels to increase humidity. After nine days, animals were collected, examined using a dissecting microscope, and scored as larval (less than 1 mm and larval morphology) or adult (greater than 1 mm and adult morphology). For experiments using the COPAS BIOSORT (Union Biometrica, Holliston, MA), eggs were added to 5 mL M9 buffer containing 10 μL/mL Antibiotic-Antimycotic solution (Sigma-Aldrich) and incubated for 2-3 days at 20º. Resulting L1 larvae were diluted in CeMM (18 zinc concentrations), seeded in 24-well plates at a concentration of 100 L1 larvae in 500 μL, and incubated at 20º in a box containing moist paper towels. After 12 days, animals were transferred to 96-well plates and analyzed using the REFLEX option of a COPAS BIOSORT.

Population growth rate analysis: To prepare 15-16 cultures for a comparative analysis, we generated a large population of worms growing in CeMM containing 30-75 μm zinc chloride. We counted an aliquot to determine the number of worms in the sample, collected the worms by centrifugation, washed 2x in M9 buffer, and resuspended at 10,000 worms/mL in CeMM with no added zinc. For cultures scored using a dissecting

125

microscope, 2.5 mL of worms were transferred to a 25 cm^2 T-flask containing 2.5 mL of

CeMM with added zinc to generate final zinc concentrations that ranged from 0 to 2 mm.

For cultures scored using the COPAS BIOSORT, 7.5 mL of worms were transferred to a

75 cm^2 T-flask containing 7.5 mL of CeMM with added zinc to generate final zinc

concentrations that ranged from 0 to 2.5 mm. In both cases, the initial worm

concentration was 5,000 worms/mL. The cultures were incubated at 20º for up to 22 days.

To determine the number of worms in the sample using a dissecting microscope, we

removed 100 µL of the culture, diluted the sample with M9 buffer containing 0.01%

Triton X-100 to yield an approximate worm concentration of 1 worm/µL, spotted 100 µL

onto an NGM dish, and counted the number of larvae and adults. Each sample was

scored three times. To determine the number of worms in the sample using the COPAS

BIOSORT, we employed 45 µm fluorescent beads (Fluoresbrite beads, Poly Sciences,

Inc., Warrington, PA) as a counting standard. Beads were diluted to a concentration of

approximately 20 beads/µL. We combined a known number of beads with a sample of

worms in ~8 mL M9 buffer with 0.01% Triton X-100, used the COPAS BIOSORT to

count the number of beads and the number of worms, calculated the ratio of worms to

beads, and then calculated the concentration of worms in the initial culture. The use of

the fluorescent beads allowed us to determine the total number of worms in an aliquot

even though not all of the aliquot flowed past the detector. To determine the population

growth rate, we plotted the number of worms per milliliter versus the number of days in

culture and performed a linear regression analysis using Microsoft Excel (Microsoft Co.,

Redmond, WA). The linear portion of the plot was from day 7 to day 17 (Figure A.2B

and data not shown), and we defined this slope as the population growth rate. To

determine the population growth rates that were half the maximal population growth rate (EC_{50} and IC_{50}), we analyzed the 16 population growth rates determined during a single growth trial using GraphPad Prism 5.0 (GraphPad Software, Inc., La Jolla, CA). The EC_{50} and IC_{50} were determined from the population growth rates at dietary zinc concentrations from 1 µm to 120 µm and 60 µm to 2.5 mm, respectively, by fitting these data to a dose-response curve with the bottom constrained to zero and a variable Hill slope. Two to three independent EC_{50} and IC_{50} values were determined for each strain, and the average, standard deviation, and p-values were calculated using Microsoft Excel (Microsoft Co.).

Determination of zinc content of *C. elegans* using radioactive ^{65}Zn: ^{65}ZnCl$_2$ was purchased from Perkin Elmer (Waltham, MA), and the initial specific activity varied from ~1 to 3 µCi/µg. To culture worms with ^{65}Zn, we determined the concentration of worms in a large starting culture, pelleted the worms, washed the worms 2x in M9 buffer, resuspended the worms in CeMM with no added zinc, dispensed 30,000 worms in 300 µL into 24-well plates, and added 300 µL of CeMM with added zinc to yield final zinc concentrations of 6 µm, 10 µm, 30 µm, 75 µm, 350 µm, 1 mm, and 2 mm. To generate CeMM with zinc concentrations of 6 µm, 10 µm, and 30 µm, we used undiluted ^{65}ZnCl$_2$ with a specific activity of ~1µCi/µg. To generate CeMM with zinc concentrations of 75 µm, 350 µm, 1 mm, and 2 mm, we combined ^{65}ZnCl$_2$ (~1µCi/µg) with non-radioactive ZnCl$_2$ to yield samples where the specific activity of the ^{65}Zn was reduced by the dilution factors 2.5, 11, 33, and 67, respectively. Samples were incubated at 20º for 12-15 days. To minimize evaporative loss, we placed samples in plastic bags with moist paper towels.

127

Worms were collected in a 0.2 μm Nanosep MF filtration device (Pall Scientific, East Hills, NY) by centrifugation and washed 2x in M9 with 100 mm EDTA to chelate unincorporated zinc. To eliminate ^{65}Zn in the intestinal lumen, we incubated the worms for 30 min in CeMM with the corresponding unlabeled zinc concentration and 1 mm serotonin (Sigma-Aldrich) to stimulate pharyngeal pumping and defecation (Horvitz et al., 1982). Thirty minutes was sufficient time for worms to expel ^{65}Zn from the intestinal lumen (data not shown). Worms were collected in a 0.2 μm Nanosep filtration device by centrifugation and washed 2x in M9 with 100 mm EDTA. Serial dilutions of ^{65}ZnCl$_2$ were measured with a Beckman gamma 4000 (Beckman Coulter Inc., Fullerton, CA) to generate a standard curve that was used to determine the amount of ^{65}Zn in each worm sample. The samples were stored at -80º. To determine the amount of protein in each worm sample, we added 100 mm NaCl containing Complete Mini Protease Inhibitor Cocktail tablets (Roche, Basel, Switzerland) to each sample, sonicated to disrupt the cuticle using a Digital Sonifer 450-D (Branson Ultrasonics Corporation, Danbury, CT), and determined the amount of protein using the Micro BCA Protein Assay Reagent Kit (Pierce, Rockford, IL) according to the manufacturer's instructions. The zinc content of worms (ng zinc/μg protein) was calculated using the formula: [^{65}Zn (μCi)/sample ÷ specific activity (μCi/μg) x 1000 ng/μg] ÷ [protein (μg)/volume x volume/sample].

Determination of zinc content of *C. elegans* using inductively coupled plasma-mass spectrometry (ICP-MS): A large population of worms growing in CeMM containing 30 μm zinc chloride was generated to initiate seven cultures for a comparative analysis. We determined the number of worms in the sample, collected the worms by centrifugation,

and washed the worms 2x in M9 buffer. The worms were resuspended at 20,000

worms/mL in CeMM with no added zinc, and 7.5 mL of worm solution was transferred

to a 75 cm^2 T-flask containing 7.5 mL of CeMM with added zinc to yield the zinc

concentrations 6 µm, 10 µm, 30 µm, 75 µm, 350 µm, 1 mm, and 2 mm, and an initial

worm concentration of 10,000 worms/mL. Samples were cultured at 20º for 16-18 days.

Worms were collected by centrifugation and washed 2x in M9 buffer. To eliminate zinc

in the intestinal lumen, we incubated the worms for 30 min in M9 buffer with 1 mm

serotonin. Worms were washed 2x in M9 buffer, transferred to pre-cleaned and pre-

weighed 15 mL polypropylene tubes (Stockwell Scientific, Scottsdale, AZ) and frozen at

-80º. The metal content of the sample was determined using ICP-MS as described by

Dong *et al.* (2008b). Briefly, the sample was desiccated, weighed, digested with

concentrated nitric acid and hydrogen peroxide solution (HNO$_3$, Fisher OPTIMA Grade,

Thermo Fisher Scientific, Wilmington, DE; 30% H$_2$O$_2$, Fluka *Trace*SELECT Ultra,

Sigma-Aldrich) in an ultrasonic bath at 60º for 1 hour, diluted with ultra-pure 18.2

MΩ·cm deionized water, re-weighed, mixed by repeated inversion, and diluted with 2%

HNO$_3$ in H$_2$O. Empty tubes were processed identically to the samples as a control. An

internal standard was added to each sample and control to correct for matrix effects in the

instrument. Weights were recorded at each step so that exact gravimetric dilution factors

could be calculated for all samples and controls. The copper, iron, manganese, and zinc

content of each sample and control was determined using a VG Axiom high-resolution

ICP-MS (Thermo Fisher Scientific). Instrument calibration standards were prepared by

diluting ICP-MS Multielement calibration standards (High-Purity Standards, Charleston,

SC), which are manufactured following National Institute of Standards and Technology

Standard Reference Materials procedures. The instrument limit of detection (LOD) was calculated as three times the standard deviation of the concentration of a given analyte measured in ten runs of a zero point standard (2% HNO_3 solution with internal standard). The sample LOD was calculated by multiplying the instrument LOD by the total sample dilution factor. The metal content of the worms was calculated using the following formula: [zinc/sample ÷ sample weight].

One consideration with using CeMM is the possibility that worm metabolism during the culture period significantly changes the medium composition. Szewczyk *et al*. (2003) monitored pH during a two week incubation and demonstrated that the starting pH of 6 gradually increases to about 7. We confirmed these results and observed that after ~25 days in culture the pH begins to increase significantly; therefore, worms were not cultured for longer than 22 days. To monitor changes in media zinc concentrations, we used radioactive ^{65}Zn to determine the fraction of total zinc incorporated into worms in 109 independent samples with zinc concentrations ranging from 6 μm to 2mm and initial worm concentrations of 50 worms/μL. The fraction of total zinc incorporated into worms that were cultured for 12-15 days varied from 0.02% to 2.4%. There was a trend towards lower fractional zinc incorporation as the dietary zinc concentration increased. These results indicate that worm metabolism has a minimal effect on the concentration of dietary zinc in the medium during the course of these experiments.

Analysis of *cdf-2* transcripts: RNA was isolated from wild-type animals cultured on NGM dishes with live *E. coli*. Mixed-staged animals were collected, washed in M9 buffer, and solubilized in TRIzol (Invitrogen, Carlsbad, CA). The RNA concentration and

quality was determined using a NanoDrop 100 (Thermo Fisher Scientific). cDNA was generated using the SuperScript III First-Strand Synthesis System for RT-PCR (Invitrogen) using either an oligo(dT) primer or random hexamer oligonucleotide primers. PCR and DNA sequencing were performed according to standard methods. Primers annealing in exon 1 and exon 8 amplified the expected 959 bp product and did not amplify any shorter products, suggesting that any alternatively spliced transcripts are of low abundance. A primer annealing in exon 7 and an oligo(dT) primer amplified an ~425 bp product. DNA sequencing demonstrated a ~30 bp adenosine tract immediately following the sequence ACAGC, indicating the addition of a poly-adenosine tail 120 bp downstream of the stop codon.

Quantitative, real-time PCR analysis: To generate cultures for a comparative analysis, we began by generating a large population of worms growing in CeMM containing 30 μm zinc chloride. Worms were collected by centrifugation, washed 2x in M9 buffer, resuspended in CeMM with 2 μm, 10 μm, 30 μm, 250 μm, 500 μm, 1 mm, or 2 mm zinc chloride, transferred to 25 cm^2 T-flasks, and incubated at 20º for six days. To collect a synchronous population of adult worms, we diluted the culture in 50 mm Tris HCl, pH 6.4 containing 2 μm, 10 μm, 30 μm, 250 μm, 500 μm, 1 mm, or 2 mm zinc chloride, respectively, and used the COPAS BIOSORT to select 1,000 adults from a mixed-stage population. RNA was purified using TRIzol, resuspended at a concentration of ~250 ng/μL, and treated with DNase I (Turbo DNA Free Kit, Applied Biosystems, Foster, CA). cDNA was synthesized using the High-capacity cDNA Reverse Transcription Kit from Applied Biosystems according to the manufacturer's instruction using random hexamer

oligonucleotide primers. Quantitative, real-time PCR was performed using a BioRad

MyiQ Single Color Real-Time PCR Detection System thermocycler and iQ SYBR Green

Supermix (BioRad Laboratories, Hercules, CA). Forward and reverse amplification

primers were: *ama-1*, atcggagcagccaggaactt and ggactgtatgatggtgaagctgg; *cdf-1*,

gcattaaaatcgctactcgcc and ccgtacacataaagattccgttg; *cdf-2*, atagcaatcggagagcaacg and

tgtgacaattgcgagtgagc; *rps-23*, aaggctcacattggaactcg and aggctgcttagcttcgacac; *sur-7*,

ctttatcgaaccgctggaac and cgagtgggtcgctgaattg. The amplified products were confirmed

by DNA sequencing. The efficiency (*E*) of each primer pair was determined using cDNA

from mixed-stage worms as template. The average primer pair efficiency was calculated

from three independent experiments and ranged from 87% and 109%. To calculate the

change in transcript abundance between two conditions, we used the approach of Pfaffl

(2001) by calculating the relative expression ratio (*R*) using the formula, $R=$

$[E_{target}^{\wedge}(\Delta CP_{target})] \div [E_{reference}^{\wedge}(\Delta CP_{reference})]$, where $\Delta CP = Ct_{control} - Ct_{sample}$. The $Ct_{control}$

was the Ct value at 2 µm dietary zinc, and the Ct_{sample} was the Ct value at 2 µm to 2 mm

dietary zinc. The relative expression ratio was determined independently for two

reference genes, and the average of these values is represented as Fold Change (Figure

A.5) according to Vandesompele *et al.* (2002).

Analysis of CDF-2::GFP: To determine the expression pattern of cdf-2, we generated

the plasmid pDG222 as follows: Beginning with pBluescript SK+ (Stratagene, Santa

Clara, CA), we inserted the ~3.4 kb genomic region containing *cdf-2* from 1,371 bases

upstream to 2,006 bp downstream of the ATG (eliminating the stop codon) in frame to

the coding region for green fluorescent protein (GFP) and the *unc-54* 3′ UTR, both

amplified from pPD95.77, a gift from A. Fire (Stanford University, Palo Alto, CA).

Transgenic animals were generated by co-injecting pDG222 and the dominant

transformation marker pRF4 (Mello et al., 1991) into wild-type animals, selecting F1 Rol

progeny, and selecting three independently-derived strains that transmitted the Rol

phenotype. For each of these strains, the Rol phenotype was transmitted to only a subset

of self-progeny, indicating that these three transgenes are extra-chromosomal, and we

designated these arrays *amEx1032*, *amEx1033*, and *amEx1201*. To generate plasmid

pDP15 for biolistic transformation, we modified the plasmid pMM016, a gift from J.

Austin (Praitis et al., 2001), that contains *unc-119(+)* by digesting it with *Acc*651 and

*Hin*cII and inserting a ~4.8 kb *Eag*I/*Acc*651 fragment of pDG222 containing the *cdf-2*

promoter and coding region, *gfp*, and the *unc-54* 3′ UTR. Biolistic transformation was

used to introduce pDP15 into *unc-119(ed3)* mutant animals (Praitis et al., 2001). Three

independently-derived transgenic animals that were non-Unc and segregated only non-

Unc progeny were isolated. Since the *unc-119* transgenes were transmitted to all the

progeny of these three strains, the transgenes are likely to be integrated in the genome

and were designated *amIs2*, *amIs4*, and *amIs5*.

To analyze the distribution of GFP using an anti-GFP antibody, we followed the

protocol described by Duerr (2006). Briefly, we cultured animals on NGM with live *E.*

coli, collected mixed-stage animals, washed in M9 buffer, fixed in methanol and acetone,

rehydrated through 90%, 60%, 30% and 10% acetone, blocked in 5% bovine serum

albumin in phosphate-buffered saline with 0.5% Triton X-100, stained with 1:100

dilution of Molecular Probes rabbit anti-GFP primary antibody (A11122, Invitrogen) and

1:200 dilution of Molecular Probes Alexa Fluor 488 goat anti-rabbit secondary antibody

(A11008, Invitrogen), and visualized the fluorescence using a Zeiss Axio Imager Z1 (Oberkochen, Germany). GFP localization in live animals was analyzed using the same culture conditions by directly visualizing GFP fluorescence.

Analysis of *cdf-2*(*tm788*): *cdf-2*(*tm788)* was a gift of the Mitani laboratory (National Bioresource Project, Tokyo Women's Medical University, Japan). *cdf-2*(*tm788)* was backcrossed to wild type four times. To eliminate potential mutations linked in *cis* to *cdf-2*(*tm788)* on chromosome X, we created a triple mutant of *cdf-1(n2527) cdf-2(tm788) sur-7(ku119),* crossed the strain to wild type and selected *cdf-1(+) cdf-2(tm788) sur-7(+)* animals. The *cdf-2(tm788)* molecular lesion was analyzed by determining the DNA sequence of the PCR amplified *cdf-2* locus.

RESULTS

The use of completely-defined, axenic medium to manipulate dietary zinc: The most commonly used culture medium for *C. elegans* is nematode growth medium (NGM) that is dispensed in a Petri dish and seeded with a bacterial lawn of *E. coli* (Brenner, 1974). NGM provides nutrients for *E. coli* growth, and the worms obtain nutrients by eating the *E. coli*. In these growth conditions, worms develop from egg to adult in approximately 3.5 days at 20º and generate about 300 self-progeny in the first five days of adulthood (Riddle et al., 1997). In our initial attempts to manipulate dietary zinc, we supplemented NGM with zinc sulfate and seeded this medium with *E. coli* (Bruinsma et al., 2002). *cdf-*

134

1(n2527) mutant animals displayed dose-dependent impairment of growth, indicating these medium conditions resulted in increased dietary zinc. However, zinc was not highly soluble in NGM, limiting the utility of this approach. To address the limitation of zinc solubility, we developed a culture medium that allowed effective supplementation with zinc sulfate, which we named noble agar minimal media (NAMM) (Bruinsma et al., 2008). Culture conditions involving NGM and NAMM have two significant limitations. First, the worms consume *E. coli*, which is a food source with a level of zinc that is undefined and difficult to manipulate. Second, while these cultures can be supplemented with zinc, these conditions do not permit depletion of dietary zinc. To overcome these limitations, we used *C. elegans* maintenance medium (CeMM), a completely-defined, axenic, liquid medium (Szewczyk et al., 2003). CeMM is formulated from purified vitamins, growth factors, amino acids, nucleic acids, heme, β-sitosterol, sugar, salts, and trace metals. CeMM provides adequate nutrition for indefinite propagation of *C. elegans* cultures (Szewczyk *et al.* 2003). Compared to worms cultured on NGM with live *E. coli*, worms cultured in CeMM display phenotypes suggestive of mild nutrient deprivation, such as delayed development, an extended life-span, diminished self-fertile brood sizes, and a thin adult body morphology. However, the proportion of the life cycle spent in each larval stage is similar in both media conditions (Szewczyk et al., 2003; Szewczyk et al., 2006).

Standard CeMM contains 75 µm zinc chloride (Szewczyk et al., 2003). To use this medium to manipulate dietary zinc, we prepared CeMM with no added zinc chloride (See Materials and Methods). To determine the level of zinc contamination in the medium components, we used inductively coupled plasma-mass spectrometry (ICP-MS)

to measure zinc. Medium that was formulated with no added zinc contained approximately 30 ± 18 parts per billion by weight zinc (mean of seven independent medium preparations). This corresponds to approximately 0.25 µm zinc, indicating that there is minimal zinc contamination in the medium components.

Maturation and population growth of wild-type worms required a minimal level of dietary zinc and were inhibited by high dietary zinc: To determine how dietary zinc affects the development and maturation of worms, we cultured worms on NGM dishes with live *E. coli* and transferred eggs to CeMM with 18-19 different concentrations of zinc, ranging from no added zinc to 2 mm zinc (Figure A.1A). Development was monitored after 80% of wild-type animals matured to adulthood with optimal concentrations of zinc, which required nine to twelve days in culture (Figure A.1B). Initially, maturation was monitored using a dissecting microscope, and animals were scored as larvae or adults. To automate the analysis, we employed a COPAS Biosort instrument that evaluates each animal with a laser microbeam and measures time of flight (TOF) and extinction (EXT). Time of flight measures the time necessary for the animal to flow past the laser, which is an indication of the length of the animal. Extinction measures the percent of light transmission that is blocked during the time of flight, which is an indication of the width and optical density of an animal. Time of flight and extinction are highly correlated, and both measurements indicate the size and maturity of an animal, with high values indicating a larger, more mature animal (Pulak, 2006). Figures 1B and C show that maturation is strongly affected by dietary zinc. At concentrations of 0 and 1 µm zinc, worms displayed minimal maturation. At

136

concentrations from 2 μm to 15 μm zinc, worms displayed measurable but impaired maturation. Worms displayed maximal maturation in 30 μm to 200 μm zinc and did nearly as well up to ~500 μm zinc. At zinc concentrations greater than 500 μm, worms displayed concentration-dependent impairment of growth.

The maturation assay evaluates development and growth from the egg or L1 larva to the adult stage. To examine the complete life cycle, including reproductive performance, we analyzed the growth rate of a population (Figure A.2A). Worms were cultured in CeMM containing 30-75 μm zinc for multiple generations, since these concentrations are in the range for maximal growth. Worms were transferred to CeMM containing 16 different zinc concentrations ranging from no added zinc to 2.5 mm zinc. To determine the maximum growth rate for the population, we counted the number of worms in the population at several times after transfer to the new medium. Population growth was approximately linear between 7 and 17 days in culture (Figure A.2B). Overall the results were similar to the maturation assay. With no added zinc, there was no significant population growth (Figure A.2C, D). With 1 μm to 2 μm added zinc, there was measurable but severely impaired population growth. From 2 μm to 30 μm zinc, there was a dose-dependent increase in population growth. To quantify these data, we determined the effective concentration (EC_{50}) of zinc that resulted in a population growth rate that was half the maximal population growth rate. The EC_{50} for wild-type animals was 6.8 ± 1.1 μm zinc (Table A.1). From 30 μm to 1 mm zinc, there was relatively optimal population growth (Figure A.2C, D). Concentrations greater than 1 mm caused a reduction of population growth rates. We determined the inhibitory concentration (IC_{50}) of zinc, and the IC_{50} for wild-type animals was 1.3 ± 0.3 mm zinc (Table A.1). These

137

results indicate that worms require dietary zinc for efficient maturation and reproduction, thrive in a wide-range of dietary zinc concentrations from 30 μm to 1 mm, and are susceptible to zinc toxicity at concentrations above 1 mm.

Zinc content of wild-type worms is correlated with dietary zinc: To complement the analysis of how dietary zinc affects maturation and population growth, we developed two methods to measure the zinc content of animals. The first method utilized radioactive ^{65}Zn. Animals were cultured with a range of dietary zinc and a trace amount of ^{65}Zn, the amount of internalized ^{65}Zn was determined using a gamma counter, and the sample size was determined by measuring the protein concentration. The second method utilized ICP-MS, a technique that can measure the concentration of several different elements in a single sample, including zinc. Worms were cultured with a range of dietary zinc, the metal content was determined by ICP-MS, and the dry weight was determined to establish the sample size. Both methods demonstrated that the zinc content of wild-type *C. elegans* was strongly influenced by the level of dietary zinc (Figure A.3A and Supplemental Table A.1). Worms cultured in 6 μm zinc had a zinc content of ~40 parts per million (ppm), whereas worms cultured in 2 mm zinc had a zinc content of ~1,000 ppm, a 27-fold difference. By contrast, the content of three other physiologic metals, iron, copper, and manganese, was not strongly affected by dietary zinc (Figure A.3B). The iron content displayed minimal change, and copper and manganese contents declined less than 2-fold. Figure A.3C shows that when the zinc content of wild-type animals increased above ~400 ppm there was a corresponding decrease in population growth rate that was caused by high concentrations of dietary zinc.

138

While an increase in dietary zinc always resulted in an increase in total zinc content, the

quantitative relationship between the change in zinc content and the change in dietary

zinc (the slope) displayed an interesting pattern. Figure A.3D shows that at the lowest

concentrations of dietary zinc (6-10 µm), the zinc content displayed the greatest change

in response to increased dietary zinc (3.4 ppm/µm). As the dietary zinc concentration was

increased to an optimal level (75-350 µm), the rate of change of zinc content

progressively decreased to 0.6 ppm/µm. As the dietary zinc concentration was increased

to toxic levels (1-2 mm), the rate of change of zinc content was relatively stable (0.4-0.5

ppm/µm). These results indicate that worms cultured in low concentrations of zinc

undergo robust changes in zinc content when additional dietary zinc is provided, whereas

worms cultured in high concentrations of zinc are resistant to changes in zinc content

when challenged with additional dietary zinc. However, wild-type worms continued to

accumulate zinc even at toxic concentrations of dietary zinc greater than 1 mm.

C. elegans cdf-2 **encodes a member of the cation diffusion facilitator family:**

Vertebrates contain CDF proteins localized to the plasma membrane, ZnT-1, and to

vesicular membranes, ZnT-2, ZnT-3, ZnT-4, and ZnT-8 (Gaither and Eide, 2001a; Kambe

et al., 2004; Palmiter and Findley, 1995). We demonstrated previously that *C. elegans*

CDF-1 is most similar to the vertebrate ZnT-1 sub-family by sequence criteria and by the

experimental observation that ZnT-1 can functionally substitute for CDF-1 (Bruinsma et

al., 2002). To investigate a *C. elegans* cation diffusion facilitator protein that is closely

related to the   ZnT-2, ZnT-3, ZnT-4, and ZnT-8 sub-family, we initiated an analysis of

the predicted gene T18D3.3. The computer algorithm Gene Finder predicted that the

T18D3.3 gene contains 8 exons and encodes a protein of 360 amino acids, and we experimentally validated the predicted gene structure (Figure A.4A and Materials and Methods). The predicted T18D3.3 protein contains hallmarks of the CDF family including six transmembrane-spanning segments and two histidine motifs, $(HX)_3$, in the loop between the fourth and fifth transmembrane segments (Figure A.4B), and we thus named it CDF-2. Compared to vertebrate proteins, CDF-2 is most similar to ZnT-2, which is localized to intracellular vesicles and is involved in zinc secretion into breast milk (Chowanadisai et al., 2006; Palmiter et al., 1996a). While these sequence similarities indicate that CDF-2 functions as a zinc transporter, the biochemical activity of CDF-2 has not yet been demonstrated experimentally.

cdf-2 transcript levels were regulated by dietary zinc: To investigate how dietary zinc regulates the expression of *cdf-2*, we used quantitative, real-time PCR to monitor the abundance of *cdf-2* mRNA. Wild-type worms were cultured in CeMM with added zinc chloride for six days to achieve stable gene expression. Adult animals were collected, and the abundance of *cdf-2* transcripts was determined. For comparison, the abundances of *cdf-1* and *sur-7* transcripts were also determined. The abundances of transcripts from these genes were normalized to the abundance of two genes that displayed stable expression over a range of zinc concentrations, *ama-1* and *rps-23* (data not shown). At the low concentration of 2 μm zinc, *cdf-1* transcripts were most abundant, *cdf-2* transcripts were intermediate in abundance, and *sur-7* transcripts were least abundant (data not shown). As the concentration of dietary zinc was increased, the abundance of *cdf-2* transcripts increased progressively, displaying about 2-fold induction at 30 μm zinc

and 3-4 fold induction at 250 µm to 2 mm zinc (Figure A.5). By contrast, the abundances of *cdf-1* and *sur-7* transcripts were not increased. At the high concentration of 2 mm zinc, *cdf-2* transcripts were more abundant than *cdf-1* or *sur-7* transcripts. These findings suggest that *cdf-2* has an important function in the response to increased dietary zinc.

CDF-2 localized to vesicles in intestinal cells: To determine the cells that express CDF-2 and the subcellular localization of the protein, we expressed a cdf-2::gfp fusion protein under the control of the predicted *cdf-2* promoter in transgenic worms. In an attempt to include all the relevant promoter elements that might mediate cell type specific expression, we designed the reporter construct to include 1,371 bp upstream of the predicted initiation codon, the entire open reading frame, and all of the introns. To include all of the relevant protein domains that might mediate subcellular localization, we included the entire CDF-2 protein sequence. The plasmids were introduced into wild-type animals by microinjection to yield extra-chromosomal arrays (Mello et al., 1991) and into *unc-119(ed3)* mutant animals by biolistic bombardment to yield integrated arrays (Praitis et al., 2001). To determine the reproducibility of the observed expression patterns, we identified six independently derived transgenic lines. The expression pattern of CDF-2::GFP was similar in all six independently-derived transgenic lines, indicating that this pattern is not influenced by the genomic integration sites or by rearrangements that may have occurred during the formation of extrachromosomal arrays. In wild-type animals, the intestinal cells contain granules that display autofluorescence. Autofluorescence is first detected in embryos and becomes progressively more intense as animals mature. Live CDF-2::GFP transgenic worms appeared to display enhanced

141

fluorescence in embryos compared to wild-type worms. As animals matured and the

intestinal granules displayed more intense autofluorescence, we could no longer observe

enhanced fluorescence in live CDF-2::GFP transgenic worms. Because autofluorescence

of intestinal granules made it difficult to observe CDF-2::GFP, we fixed embryos and

animals, a process that eliminates autofluorescence, and visualized CDF-2::GFP using an

anti-GFP antibody. CDF-2::GFP was expressed in embryos (Figure A.6E-L), larvae

(Figure A.6M-P), and adults (Figure A.6Q-T). The CDF-2::GFP protein was expressed in

intestinal cells in a punctate pattern that appears to be the membrane of small vesicles

(Figure A.6U). To investigate the relationship between the punctate pattern of CDF-

2::GFP and the punctate pattern of autofluorescent intestinal granules, we analyzed

fluorescence in live adult worms (Figure A.6A-D). These results indicate that CDF-

2::GFP is only expressed in puncta that are autofluorescent. These data are consistent

with the possibilities that all or only some of the autofluorescent puncta contain CDF-

2::GFP, and suggest that CDF-2::GFP is not expressed outside of autofluorescent puncta.

A CDF-1::GFP fusion protein is also expressed in intestinal cells, but it is localized to the

plasma membrane (Bruinsma et al., 2002), and it is not localized to the vesicles that

contain CDF-2. Therefore, the subcellular localization of CDF-2::GFP is unlikely to be

mediated by the GFP fusion partner and appears to be specific for CDF-2. While the

CDF-2::GFP fusion protein was designed to indicate the expression pattern of

endogenous CDF-2, the function of the CDF-2::GFP fusion protein has not been

analyzed, and it is possible that endogenous CDF-2 is expressed in a broader or more

restricted pattern than the CDF-2::GFP reporter. These results indicate that CDF-2 is

localized to vesicular membrane compartments similar to the related vertebrate proteins

ZnT-2, ZnT-3, Znt-4, and ZnT-8 (Gaither and Eide, 2001a; Kambe et al., 2004).

A *cdf-2* loss-of-function mutation resulted in delayed population growth and decreased zinc content: To investigate the function of *cdf-2*, we obtained the *tm788* deletion allele from the Mitani laboratory (National Bioresource Project, Tokyo, Japan). We determined the sequence of the *cdf-2* locus and confirmed that *tm788* is an 804 base pair deletion that removes 594 base pairs upstream of the ATG, exon 1, intron 1, and 69 base pairs of exon 2 (Figure A.4A). In addition, there is a 68 base pair insertion at the site of the deletion. The deleted DNA encodes the first 34 predicted amino acids of the CDF-2 protein. The *tm788* deletion is predicted to affect the *cdf-2* transcript in two important ways. First, *tm788* is predicted to reduce the abundance of *cdf-2* transcripts by removing the 5' upstream region that might contain promoter elements and the transcription initiation site. Second, any *cdf-2* transcripts that are produced must have an abnormal structure, since exon 1 and part of exon 2 are absent. Such abnormal transcripts would definitely lack the codons for the first 34 predicted amino acids and might lack additional codons. The first methionine codon in the *cdf-2* open reading frame that remains in the *tm788* mutant is codon 65, and a protein that initiated at codon 65 would lack half of the highly conserved first transmembrane domain.

To determine how the *cdf-2(tm788)* mutation affects the abundance of the *cdf-2* transcript, we used the sensitive method of reverse transcription-PCR. The abundance of the *cdf-2* transcript was dramatically reduced by approximately 1,000-fold in the *cdf-2(tm788)* mutant compared to wild type, and the residual *cdf-2* transcript was not induced by dietary zinc (Supplemental Figure A.1). These findings indicate that the *cdf-2*(*tm788*)

143

deletion eliminates sequences that are critical for transcript initiation and/or sequences in the transcribed region that are critical for transcript stability. These results suggest that the *cdf-2(tm788)* mutation causes a strong loss-of-function.

To analyze the phenotype of the *cdf-2*(*tm788*) mutant, we first backcrossed the strain to wild-type animals to remove extraneous mutations. *cdf-2(tm788)* mutant animals appeared to have normal morphology and body movement. *cdf-2*(*tm788*) did not cause significant lethality, and *cdf-2(tm788)* hermaphrodites and males were fertile (data not shown). The *cdf-2*(*tm788*) mutation did not suppress the multi-vulval phenotype caused by constitutively activated *let-60(n1046)* Ras (data not shown), by contrast to loss-of-function mutations of *cdf-1* and *sur-7* (Bruinsma et al., 2002; Yoder et al., 2004). To carefully monitor the ability of *cdf-2(tm788)* mutant animals to grow and develop in a wide range of dietary zinc conditions, we used CeMM to conduct maturity and population growth assays. Figure A.7A shows that maturation from L1 to adult was similar for *cdf-2(tm788)* mutant and wild-type animals in a wide range of dietary zinc. By contrast, *cdf-2*(*tm788*) mutant animals displayed reduced population growth compared to wild-type animals in 30 μm to 480 μm dietary zinc (Figure A.7B). In extremely low and high dietary zinc conditions, *cdf-2(tm788)* mutant and wild-type animals displayed similar population growth, and the EC_{50} and IC_{50} values for *cdf-2(tm788)* mutant animals were 3.8 ± 1.0 μm zinc and 1900 ± 160 μm zinc, respectively (Table A.1). These findings indicate that *cdf-2* is necessary for wild-type levels of population growth when dietary zinc is in the optimal range.

To determine how *cdf-2* influences zinc content, we analyzed *cdf-2(tm788)* mutant animals using ICP-MS. Figure A.7C shows that *cdf-2(tm788)* mutant animals

144

displayed reduced zinc content at dietary zinc concentrations of 30 μm and higher

compared to wild-type animals (Supplemental Table A.1); at a dietary zinc concentration

of 75 μm, the zinc content of the *cdf-2* mutant was reduced 2-fold, and at dietary zinc

concentrations of 350 μm, 1 mm, and 2 mm the zinc content of the *cdf-2* mutant was

reduced 3-fold. In conjunction with the localization data, these results suggest that CDF-

2 functions to store zinc in vesicles of intestinal cells.

Loss-of-function mutations in *cdf-1* and *sur-7* affect sensitivity to dietary zinc and

zinc content: *cdf-1* and *sur-7* are critical for Ras-mediated signal transduction and

resistance to high levels of dietary zinc when animals are cultured with live *E. coli*

(Bruinsma et al., 2002; Yoder et al., 2004). The role of these genes in conditions of low

dietary zinc has not been determined. We used CeMM to analyze the functions of *cdf-1*

and *sur-7* in a full range of dietary zinc. The strong loss-of-function *cdf-1(n2527)*

mutation is a nonsense change that is predicted to truncate the protein at amino acid 156

of 519, resulting in the absence of three highly conserved transmembrane domains

(Bruinsma et al., 2002). The partial loss-of-function *sur-7(ku119)* mutation affects a

predicted splice site and reduces but does not eliminate *sur-7* transcripts (Yoder et al.,

2004). We cultured *cdf-1* and *sur-7* mutant animals in a wide range of dietary zinc and

measured the ability of L1 larvae to mature to adulthood. Both *cdf-1* and *sur-7* mutant

animals displayed reduced maturation at low and high concentrations of zinc, whereas

they displayed wild-type levels of maturation at intermediate zinc concentrations (Figure

A.8A, B). Both *cdf-1* and *sur-7* mutant animals displayed reduced population growth at

concentrations of dietary zinc from 10 μm to 2.5 mm (Figure A.8C, D). The EC_{50} for

population growth rate was similar for these mutant animals and wild type, whereas the

145

IC$_{50}$ was reduced for both *cdf-1* and *sur-7* mutant animals (Table A.1). These results indicate that *cdf-1* and *sur-7* are necessary for optimal maturation in low dietary zinc, a result that has not been previously reported. These genes are necessary for optimal population growth in a wide-range of dietary zinc and are essential for survival at high dietary zinc, consistent with previous reports (Bruinsma et al., 2002; Bruinsma et al., 2008; Yoder et al., 2004).

To determine the role of *cdf-1* and *sur-7* in regulating zinc content, we analyzed loss-of-function mutant animals using ICP-MS. *cdf-1* mutant animals displayed increased zinc content at dietary zinc concentrations of 30 μm and higher (Figure A.8E and Supplemental Table A.1). *sur-7* mutant animals displayed a zinc content similar to wild type (Figure A.8F and Supplemental Table A.1). The finding that *sur-7* mutant animals displayed dramatic growth defects and relatively normal zinc content suggests that the distribution of zinc is abnormal in mutant animals. This analysis shows that *cdf* genes can have strikingly different effects on zinc content; *cdf-2* promotes zinc accumulation, whereas *cdf-1* inhibits zinc accumulation.

Analysis of *cdf-1*, *cdf-2*, and *sur-7* double and triple mutant animals: To investigate the genetic interactions between these three genes, we generated the three possible double mutant strains and the triple mutant strain and measured maturation, population growth, and zinc content of each strain (Table A.1, Supplemental Tables A.1-3). The *cdf-1 cdf-2* and *cdf-1 cdf-2 sur-7* mutant animals were particularly informative (Figure A.9). Loss-of-function mutations in *cdf-1* and *cdf-2* have opposite effects on zinc content. The *cdf-1 cdf-2* double mutant displayed a zinc content that was intermediate between the

146

two single mutant strains (Figure A.9E).   The *cdf-1 cdf-2* double mutant had slightly

impaired maturation rates compared to the *cdf-1* mutant (Figure A.9A), but had slightly

improved population growth rates compared to the *cdf-1* mutant (Figure A.9C). These

results suggest that *cdf-1* and *cdf-2* have antagonistic functions with respect to zinc

content and the more normal zinc content of the *cdf-1 cdf-2* mutant may account for the

increase in the population growth rate.

The *cdf-1 cdf-2 sur-7* triple mutant was also intermediate between the *cdf-1* and

cdf-2 single mutant animals with respect to zinc content; furthermore, the *cdf-1 cdf-2 sur-7* mutant had a zinc content that was similar to wild type (Figure A.9F). Figure A.9G

compares the change in zinc content as a function of dietary zinc for single and triple

mutant animals. The *cdf-2* single mutant displayed smaller changes in zinc content

compared to wild type at all concentrations of dietary zinc. By contrast the *cdf-1* single

mutant displayed larger changes compared to wild type in most intervals. Consistent with

the interpretation that *cdf-1* and *cdf-2* have antagonistic functions, the values for the

triple mutant were usually intermediate between *cdf-1* and *cdf-2* mutant animals.

Furthermore, at the highest concentrations of dietary zinc, *cdf-1* and *cdf-1 cdf-2 sur-7*

mutant animals displayed a trend toward increasing values in contrast to wild-type

animals that displayed decreasing or stable values (Figure A.9H). These findings suggest

that *cdf* genes are necessary for animals to resist changes in zinc content when

challenged with the highest levels of dietary zinc. The *cdf-1 cdf-2 sur-7* mutant had

increased population growth rates at optimal dietary zinc concentrations compared to the

cdf-1 mutant, but triple mutant animals were very sensitive to zinc toxicity and had an

IC_{50} of 220 μm (Figure A.9D and Table A.1). The failure of the *cdf-1 cdf-2 sur-7* mutant

to control zinc content at high dietary zinc may be responsible for the increased

sensitivity to zinc toxicity.

DISCUSSION

Zinc metabolism and homeostasis in wild-type *C. elegans*: *C. elegans* is typically

cultured with *E. coli* as a food source, which limits the ability to manipulate dietary

constituents such as zinc. Chemically defined media that support long term culture of the

related nematode *C. briggsae* have been developed (Buecher et al., 1966; Hieb and

Rothstein, 1968; Hieb et al., 1970; Lu et al., 1978). These culture conditions were

adapted for the study of *C. elegans* by Lu and Goetsch (1993), and the growth

characteristics of *C. elegans* in fully defined medium were described by Szewczyk *et al.*

(2003; 2006). To develop culture conditions that allow complete control of dietary zinc,

we analyzed worms using CeMM with no added zinc and a wide range of supplemental

zinc. These experiments revealed that *C. elegans* cannot mature or reproduce in CeMM

with no added zinc (approximately 0.25 μm zinc), demonstrating that dietary zinc is

essential for *C. elegans* survival. When dietary zinc was in the range of 1 μm   to 10 μm,

C. elegans displayed impaired but measurable growth, and the EC_{50} for dietary zinc was

~7 μm. When dietary zinc was in the range of 30 μm to 1 mm, *C. elegans* displayed

optimal growth. The finding that optimal growth occurs over a 30-fold range in dietary

zinc indicates that *C. elegans* have evolved mechanisms to thrive in a relatively broad

range of dietary zinc. When dietary zinc was in the range of 1 mm to 2.5 mm, *C. elegans*

displayed dose-dependent impairment of growth, and the IC_{50} for dietary zinc was ~1.3 mm. The EC_{50} and IC_{50} for dietary zinc differ by 190-fold and define the range of zinc that permits *C. elegans* survival.

The culture conditions described here have important advantages compared to the culture conditions that have been used previously to manipulate dietary zinc (Bruinsma et al., 2002; Bruinsma et al., 2008; Dong et al., 2008a; Yoder et al., 2004). We previously supplemented NGM or NAMM with zinc; these media conditions allowed for supplemental dietary zinc but did not allow for depletion of dietary zinc, since *E. coli* is the food source. The use of CeMM allowed us to quantitatively determine for the first time the minimum, optimum, and maximum dietary zinc levels for *C. elegans*. Similar quantitative measurements of levels have not been systematically established for other animals, and these studies provide new information about the capacity of multicellular animals to metabolize zinc.

An important method for analyzing zinc metabolism is the measurement of zinc content. The zinc content of *C. elegans* has not been previously reported. We developed two independent methods to measure zinc content. One method employed radioactive ^{65}Zn as a tracer and the second method utilized physical measurements of zinc performed by ICP-MS. Our results indicate that total animal zinc content is proportional to the concentration of dietary zinc. Over the ~30-fold range of dietary zinc that promotes optimal growth (30 μm-1 mm), worms displayed an ~7-fold increase in zinc content. However, the relationship between dietary zinc and zinc content displayed an interesting pattern. At the lowest concentrations of dietary zinc, wild-type worms displayed the most responsiveness to changes in dietary zinc, measured as the change in zinc content per

change in dietary zinc. This responsiveness decreased as dietary zinc was increased to

the optimal range for population growth and then stabilized as dietary zinc increased to

high levels. These findings suggest that at low concentrations of dietary zinc, worms are

in a physiological state that promotes uptake of dietary zinc and/or minimizes zinc

excretion, so that the animals respond to an increase in dietary zinc with a robust increase

in zinc content. By contrast, at high concentrations of dietary zinc, worms are in a

physiological state that minimizes uptake of dietary zinc and/or maximizes zinc

excretion, so that animals respond to an increase in dietary zinc with a minimal increase

in zinc content. Because zinc content never appears to be independent of dietary zinc,

even at toxic levels of dietary zinc, it appears that worms do not have the capacity to

maintain a consistent zinc content when challenged with increasing dietary zinc. These

results support the model that excess zinc content is the cause of dietary zinc toxicity.

The analysis of metal content of worms indicated that there is a relationship

between zinc metabolism and the metabolism of other metals, specifically copper and

manganese. Wild-type worms displayed approximately two-fold decreases in copper and

manganese content as dietary zinc was increased. Interestingly, this effect was abrogated

in *cdf-1* mutants. In humans, excess dietary zinc can cause copper deficiency (Prasad et

al., 1978; Vallee and Falchuk, 1993). Although the mechanisms have not been well

established, one possibility is that processes that are regulated to excrete excess zinc

and/or limit zinc uptake also act on other metals such as copper, perhaps due to

overlapping specificity. Our results suggest that similar events occur in *C. elegans*, and

raise the possibility that mechanisms that promote zinc excretion or limit zinc uptake

may also act on copper and manganese.

Studies of zinc in widely divergent species have led to the proposal that these systems have similar concentrations of zinc and that there is a universal zinc quotient (Eide, 2006; Outten and O'Halloran, 2001). The results of our studies indicate that zinc content is dependent upon the concentration of dietary zinc and, therefore, highly variable. These findings suggest that animals have a measurable but limited capacity to moderate changes in zinc content in response to changing dietary zinc, and probably have also evolved mechanisms to cope with a wide range of zinc content. Our studies measured total zinc content of the animals, and it is possible that the distribution of zinc within the animal is dynamic so that some cells or compartments maintain a relatively constant zinc concentration. For example, zinc may be sequestered in specific cells or compartments under conditions of high dietary zinc. Our analysis of *cdf-2* suggests that zinc is stored in vesicles of intestinal cells. The development of methods to localize zinc will be important for elucidating how worms partition zinc to different compartments, which may be an important aspect of zinc homeostasis.

cdf-2 **encodes a predicted zinc transporter that is localized to vesicles in intestinal cells:** We investigated *cdf-2* because it is predicted to encode a highly-conserved member of the CDF family that is most similar to vertebrate ZnT-2 and is highly related to ZnT-3, ZnT-4, and ZnT-8. ZnT-2 is expressed in the small intestine, kidney, seminal vesicle, testis, and prostate and localized to the endosomal compartment (Palmiter et al., 1996a). ZnT-4 is expressed ubiquitously and localized to the *trans* golgi network and endosomal compartment (Murgia et al., 1999). ZnT-3 is expressed in neurons and localized to synaptic vesicles (Palmiter et al., 1996b), and ZnT-8 is expressed in the pancreas and

151

localized to insulin-containing vesicles (Chimienti et al., 2004; Chimienti et al., 2006).

We used a CDF-2::GFP fusion protein to demonstrate that CDF-2 is localized to vesicles

of intestinal cells. The vesicles that contain CDF-2::GFP co-localize with autofluorescent

intestinal granules. Autofluorescent intestinal granules have been characterized by

electron microscopy, leading to the conclusion that these structures are secondary

lysosomes (Clokey and Jacobson, 1986). Furthermore, autofluorescent intestinal granules

colocalize with LysoTracker Red-stained compartments and acidified, acridine orange-

stained comportments, strongly suggesting that these granules are components of

lysosome-related organelles (Hermann et al., 2005). In light of these studies, our results

indicate that CDF-2 resides on the membrane of secondary lysosomes/lysosome-related

organelles. Thus, CDF-2 resembles ZnT-3 and ZnT-8 since it is expressed in a specific

tissue and localized to specialized vesicles.

The discovery that CDF-2 is localized to lysosome-related organelles raises the

interesting question, what is the role of zinc in the lumen of this compartment? *cdf-2*

loss-of-function mutations caused impaired growth, indicating that the function of cdf-2

in lysosome-related organelles is critical for optimal zinc metabolism and growth. The

cdf-2 mRNA was significantly increased by high dietary zinc, indicating that *cdf-2* may

mediate a response to zinc stress. Taubert *et al.* (2008) analyzed the MDT-15

transcriptional coregulator and showed that the increase in *cdf-2* transcripts requires

MDT-15. In conditions of high dietary zinc, CDF-2 may function to reduce cytosolic

levels of zinc by sequestration in the lumen of lysosome-related organelles. Consistent

with this possibility, *cdf-2* mRNA is induced by high dietary zinc and *cdf-2* mutant

animals have reduced zinc content at high dietary zinc, suggestive of a storage defect.

Strikingly, the zinc content of *cdf-2* mutant animals is one-third the zinc content of wild-type animals at high dietary zinc, suggesting that two-thirds of the zinc content of wild-type animals is stored in the lumen of intestinal vesicles. Another possibility is that CDF-2 functions to provide zinc for lysosomal enzymes. There are precedents for metal transporters supplying proteins resident in vesicles, such as the recent demonstration that ATP7A supplies copper to tyrosinase by functioning within specialized organelles called melanosomes (Setty et al., 2008). The yeast CDF proteins Msc2 and Zrg17 transport zinc into the ER to supply zinc to proteins in the secretory pathway (Eide, 2006; Ellis et al., 2005), and vertebrate ZnT-3 and ZnT-8 transport zinc into synaptic vesicles and insulin-containing vesicles, respectively (Palmiter and Huang, 2004). Our studies lay the foundation for further testing these hypotheses directly by establishing a model system to study the function of a CDF protein that is localized to the vesicular membrane.

***cdf-1* and *cdf-2* function antagonistically to regulate zinc metabolism:** Animals such as *C. elegans* and vertebrates contain extensive families of CDF proteins (Eide, 2006; Kambe et al., 2004; Liuzzi and Cousins, 2004; Palmiter and Huang, 2004). It is important to determine the extent to which these proteins have independent, redundant, or antagonistic functions. In vertebrates, loss-of-function mutations have been described for ZnT-1, ZnT-3, ZnT-4 and ZnT-5 (Palmiter and Huang, 2004); only ZnT-1 is essential for survival (Andrews et al., 2004). However, mutant animals that lack the function of two or more vertebrate *cdf* genes have not been reported.

Three *C. elegans* genes encoding cation diffusion facilitator proteins have now been characterized genetically and molecularly- *cdf-1*, *cdf-2*, and *sur-7*. *cdf-1* encodes a

153

protein whose most similar vertebrate homolog is ZnT-1. CDF-1 and ZnT-1 are localized to the plasma membrane, ZnT-1 can functionally substitute for CDF-1 in *C. elegans*, and both proteins modulate Ras-mediated signaling in vertebrates and *C. elegans* (Bruinsma et al., 2002). *cdf-1* is expressed in vulval precursor cells, and it appears to act cell autonomously in these cells to affect Ras-mediated signaling. *cdf-1* is also highly expressed in intestinal cells, and *cdf-1* appears to act non-autonomously in intestinal cells to affect Ras-mediated signaling in vulval precursor cells. CDF-1 may transport zinc from intestinal cells to the body cavity or intestinal lumen and thereby influence zinc metabolism in vulval precursor cells. A *cdf-1(lf)* mutant was previously demonstrated to be hypersensitive to high dietary zinc (Bruinsma et al., 2002). Here we confirmed this result using fully defined CeMM. We determined that the maturation of a *cdf-1(lf)* mutant was normal at optimal levels of dietary zinc but sensitive to low and high dietary zinc. The population growth rate of *cdf-1(lf)* mutant animals was reduced at all concentrations of dietary zinc, but the mutant animals were extremely sensitive to high dietary zinc. *cdf-1(lf)* mutant animals displayed increased zinc content that was most pronounced at high levels of dietary zinc. These results indicate that *cdf-1* activity promotes zinc excretion and/or limits zinc uptake. One model to explain this observation is that CDF-1 transports zinc across the plasma membrane of intestinal cells and into the intestinal lumen, thus directly promoting zinc excretion. Alternatively, CDF-1 may transport zinc from intestinal cells into the body cavity, thereby indirectly promoting zinc excretion by another cell such as the excretory cell. The findings that *cdf-1* mutant animals cultured with high dietary zinc displayed increased zinc content and decreased survival suggest that the increased zinc content may cause the reduced survival.

154

sur-7 encodes a CDF protein that does not have a closely related homolog in vertebrates. Yoder *et al.* (2004) reported that a SUR-7::GFP fusion protein was expressed in non-intestinal cells in a cytosolic pattern suggestive of endoplasmic reticulum, indicating that *sur-7* may provide zinc to proteins resident in this compartment and promote excretion of zinc from cells through the secretory pathway. Here we demonstrated that *sur-7(lf)* mutant animals displayed reduced maturation and population growth rates in high dietary zinc, consistent with previous reports (Yoder et al., 2004). Maturation was also reduced at low dietary zinc, whereas mutant and wild-type animals displayed similar maturation at a narrow range of optimal dietary zinc. The zinc content of *sur-7* mutant animals was similar to wild-type animals. Because the growth defects of *sur-7* mutants are evidence for altered zinc metabolism, the finding that the overall zinc content is similar to wild type indicates that the distribution of zinc in the *sur-7(lf)* mutant animals is abnormal. The *sur-7* phenotypes may be caused by reduced zinc in the secretory pathway and/or increased zinc in another compartment.

Because CDF-1, CDF-2, and SUR-7 are all predicted to reduce the concentration of zinc in the cytoplasm, it is possible that the functions of these proteins are redundant. In this case, double or triple mutant animals might display phenotypes that are stronger than any single mutant. In general, we did not observe this pattern, since most double and triple mutant animals displayed similar phenotypes to one of the single mutants. However, for the phenotype of controlling zinc content in high dietary zinc (Figure A.9H), the triple mutant was much more impaired than any single mutant. This result suggests that CDF-1, CDF-2, and SUR-7 might function redundantly to control zinc content at high dietary zinc.

155

By contrast to the similar effects that all CDF proteins are predicted to have on the cytoplasmic zinc concentration, CDF-1 and CDF-2 are predicted to have distinct effects on zinc concentrations in the extracellular space and lumen of intracellular compartments. Whereas *cdf-1(lf)* mutant animals displayed increased zinc content in high dietary zinc, suggesting *cdf-1* is necessary to excrete zinc, *cdf-2(lf)* mutant animals displayed reduced zinc content in high dietary zinc, suggesting *cdf-2* is necessary to store zinc. The *cdf-1 cdf-2* double mutant displayed an intermediate zinc content, suggesting that *cdf-1* and *cdf-2* function antagonistically. CDF-1 and CDF-2 are both expressed in intestinal cells; CDF-1 is localized to the plasma membrane, whereas CDF-2 is localized to vesicles. As shown in Figure A.10, we propose that CDF-1 and CDF-2 compete for cytosolic zinc. If CDF-1 transports zinc across the plasma membrane, then the zinc content of the animal is directly or indirectly decreased. If CDF-2 transports zinc into the vesicle lumen, then the zinc content of the animal is increased. This model accounts for the changes observed in the *cdf-1* and *cdf-2* mutant animals and explains why the *cdf-1 cdf-2* double mutant animals have an intermediate phenotype. These findings demonstrate the power of the *C. elegans* model system to dissect the relationships between CDF family members.

ACKNOWLEDGEMENTS

FIGURE LEGENDS

Figure A.1. The maturation of wild-type worms is affected by dietary zinc. A. To monitor maturation, we cultured adults on NGM with live *E. coli*, transferred eggs or L1 larvae to CeMM (18-19 different zinc concentrations) in 24 well plates, cultured for 9-12 days, and evaluated maturation using a dissecting microscope (B) or a COPAS Biosort (C). B. Wild-type worms were cultured in CeMM with added zinc, displayed on a logarithmic scale. To calculate the percent of eggs that matured to an adult, we counted immature and mature animals and calculated the percent mature. C. Maturation was monitored using the COPAS Biosort to measure time of flight (TOF). TOF is a measure of the time that the animal blocks light transmission and is shown in arbitrary units. The TOF value of animals at the beginning of the experiment was approximately 80 units. Values are the average (± standard deviation, SD) of four biological replicates.

Figure A.2. The population growth rate of wild-type worms is affected by dietary zinc. A. To monitor the growth rate of the population, we cultured worms in CeMM with 30-75 μm zinc for multiple generations, transferred worms to flasks of CeMM (15-16 different zinc concentrations), and counted the number of worms per mL of culture medium at multiple times. Counting was performed using a dissecting microscope (B, C) or a COPAS BIOSORT (D). B. Wild-type worms were cultured in CeMM with different concentrations of added zinc shown in μm and indicated by colored lines. The numbers of worms per mL were determined at culture days 1, 4, 7, 10, 14, 17, and 22. The increase in population was maximal and approximately linear between days 7 and 17. C.

The slopes of the lines defined by the linear range shown in panel B were used to calculate population growth rates in worms/mL/day. The concentration of added zinc is displayed on a logarithmic scale. The colors of the data points correspond to the colors of the lines shown in panel B. Values are the average (± SD) of three independent experiments, one of which is shown in panel B. D. Population growth rate was monitored using the COPAS BIOSORT to measure the number of animals at four time points between days 9 and 17. Values are the average (± SD) of three independent experiments. The growth rates calculated from the COPAS BIOSORT data are somewhat higher than the growth rates calculated from the dissecting microscope data, probably because human observers are more stringent than the instrument in scoring objects as worms. Nonetheless, the effect of zinc on population growth rate was similar when measured using a dissecting microscope or the COPAS BIOSORT.

Figure A.3. Zinc content of mixed-stage wild-type animals. Worms were cultured in CeMM with a range of added zinc, shown on a logarithmic scale. A. The zinc content was determined by ICP-MS (parts per million, closed green circles), or radiolabeled ^{65}Zn (average ng zinc/μg protein ± SD, n=2, open green circles) in independent experiments. B. ICP-MS was used to measure the content of copper (Cu, blue triangles), iron (Fe, red squares), manganese (Mn, pink diamonds), and zinc (Zn, green circles) of each sample. The dietary concentrations of copper, iron, and manganese in CeMM were 37.5 μm, 150 μm, and 112.5 μm, respectively, in all the samples. C. Zinc content was determined by ICP-MS (green circles), and population growth rate was determined by COPAS BIOSORT (black squares) in independent experiments. D. Bars indicate the change in

zinc content (ppm) divided by the change in dietary zinc (µm) for the two dietary zinc concentrations shown below. Values are the slope of the line defined by the ICP-MS data in panel A.

Figure A.4. *cdf-2* gene structure and predicted amino acid sequence. A. The line represents genomic DNA, and boxes represent exons that are untranslated (open) or translated (black). The green line indicates the extent of the *tm788* deletion, and the green triangle denotes the *tm788* insertion. B. An alignment of the predicted CDF-2 protein with human ZnT-2 and *C. elegans* CDF-1. Identical and similar amino acids are highlighted in black and grey, respectively. Green lines indicate codons deleted in the *tm788* allele. Putative zinc binding motifs, $(HX)_n$, are red. Predicted transmembrane segments are boxed and labeled I to VI.

Figure A.5. *cdf-2* transcript abundance was regulated by dietary zinc. Wild-type animals were cultured in CeMM with added zinc, shown on a logarithmic scale. The abundance of transcripts from *cdf-1* (open circles), *cdf-2* (black diamonds), and *sur-7* (grey triangles) was measured by performing quantitative, real-time PCR. The axis represents the fold change in transcript abundance, which was calculated by comparing the transcript abundance at 2 µm, 10 µm, 30 µm, 250µm, 500 µm, 1 mm, and 2 mm dietary zinc to transcript abundance at 2µm dietary zinc. Values for transcript abundance were corrected for RNA recovery and the efficiency of primer amplification (see Materials and Methods). The fold change of each gene at 2 µm zinc was set equal to 1.0, and other values were normalized relative to 2 µm zinc. Values are the average of four independent

160

replicates (±SD). Compared to transcript abundance at 2 μm zinc, *cdf-2* transcripts were significantly higher at zinc concentrations of 250 μm to 2 mm zinc (~3-4 fold, p<0.05, Welch's *t*-Test), whereas *cdf-1* and *sur-7* transcripts were significantly decreased at 2 mm zinc (~2-fold, p<0.05, Welch's *t*-Test).

Figure A.6. CDF-2 was expressed in intestinal cells and localized to membrane-bound vesicles. Transgenic animals expressing CDF-2::GFP were cultured on NGM with live *E. coli*. Live adults were immobilized and mounted (A-D). Mixed-stage worms were fixed and stained with an anti-GFP antibody (E-U). Differential interference contrast images display organism morphology (A, E, I, M, Q), green displays CDF-2::GFP and autofluorescence (B) or only CDF-2::GFP (F, J, N, R, U), red displays autofluorescence (C, G, K, O, S), yellow displays overlap between CDF-2::GFP and autofluorescence (D), and blue displays nuclear morphology using DAPI (H, L, P, T). Red in panel C shows a punctate pattern of autofluorescence in intestinal cells, whereas red in panels G, K, O, and S shows that there is no specific localization of autofluorescence following fixation, and exposure times for red in these panels were at least 5-fold longer than for green. CDF-2::GFP was first detected during embryogenesis at the E^{16}-E^{20} stage (F), and expression persisted throughout embryogenesis (J). CDF-2::GFP was expressed in a punctate pattern in intestinal cells during all larval stages (N) and in adults (R). Puncta appear to be membrane-bound vesicles ($\rightarrow$, U).

Figure A.7. *cdf-2* mutant phenotypes. Wild-type and mutant animals were cultured in CeMM with a range of added zinc, shown on a logarithmic scale. A. Maturation of wild

type (WT, black squares) and *cdf-2*(*tm788)* (open diamonds) was monitored using the

COPAS Biosort. Values are the average (± SD) of four biological replicates and are

representative of two independent experiments. B. Population growth rate was monitored

using the COPAS BIOSORT, and values are the average (±SD) of two to three

independent experiments. C. Zinc content was measured using ICP-MS.

Figure A.8. Maturation, population growth rate, and zinc content of *cdf-1* and *sur-7*

mutant animals. Wild-type and mutant animals were cultured in CeMM with a range of

added zinc, shown on a logarithmic scale. A, B. Maturation of wild type (WT, black

squares), *cdf-1(n2527)* (open circles), and *sur-7(ku119)* (open triangles) was monitored

using the COPAS Biosort. Values are the average (± SD) of four biological replicates and

are representative of two independent experiments. C, D. Population growth rate was

monitored using the COPAS BIOSORT, and values are the average (± SD) of two to

three independent experiments. E, F. Zinc content was measured by ICP-MS.

Figure A.9. Maturation, population growth rate, and zinc content of double and triple

mutant animals. Wild-type and mutant animals were cultured in CeMM with a range of

added zinc, shown on a logarithmic scale. A, B. Maturation of wild type (black squares),

cdf-1(n2527) (open blue circles), *cdf-2(tm788)* (open red diamonds), *sur-7(ku119)* (open

green triangles), *cdf-1(n2527) cdf-2(tm788)* (grey squares), and *cdf-1(n2527) cdf-*

2(tm788) sur-7(ku119) (grey squares) was monitored using the COPAS Biosort. Values

are the average of four biological replicates. C, D. Population growth rates were

monitored using the COPAS Biosort. Values are the average of two to three independent

experiments. Values (±SD) are shown in Supplemental Table A.2 (Maturation) and

Supplemental Table A.3 (Population growth rate). E-H. Zinc content was measured by

ICP-MS. The change in zinc content as a function of change in dietary zinc is displayed

in units of ppm/μm (panel G) or normalized by setting the values for 75-350 μm equal to

1.0 (panel H).

Figure A.10. A model of zinc distribution in wild-type and *cdf* mutant animals. Each

diagram shows a polarized intestinal cell. CDF-1 (blue) localizes to the plasma

membrane, and CDF-2 (red) localizes to the membrane of an intracellular compartment.

The absence of CDF-1 and CDF-2 in mutant animals is illustrated by an X (B-D). The

size of the Zn^{2+} indicates the concentration of zinc in a compartment. We propose that

CDF-1 and CDF-2 function as zinc transporters based on sequence similarity to well-

characterized CDF proteins, and the size of the arrow indicates the amount of zinc flux.

A. In wild-type animals, CDF-1 and CDF-2 compete for cytosolic zinc, resulting in

intermediate levels of zinc in the cytosol, the extracellular space, and the vesicle lumen.

B. In *cdf-1(lf)* mutant animals, the level of cytosolic zinc increases, and CDF-2 transports

additional zinc into the vesicle lumen. C. In *cdf-2(lf)* mutant animals, the level of

cytosolic zinc increases, and CDF-1 transports additional zinc into the extracellular space.

D. In *cdf-1(lf) cdf-2(lf)* double mutant animals, zinc transport into the vesicle lumen and

extracellular space both decrease.

Supplemental Figure A.1. *cdf-2* transcript levels were decreased ~1,000-fold in *cdf-*

2(tm788) mutant animals. Mixed-stage wild-type and *cdf-2(tm788)* animals were

cultured on NAMM dishes containing *E. coli* (Bruinsma *et al.* 2008) and no

supplemental zinc (-) or 0.5 mm supplemental zinc (+) for 40 hours at 20º. Animals were

collected in M9 buffer and solubilized in TRIzol (Invitrogen). 590 ng of RNA was

reverse transcribed using random hexamer primers and the SuperScript III First-Strand

Synthesis System for RT-PCR (Invitrogen). cDNA was diluted in water and PCR

amplified using KlenTaq LA DNA Polymerase (Sigma-Aldrich). The amount of input

cDNA is indicated in arbitrary units (1, no dilution; 0.1, 10x dilution; 0.01, 100x

dilution), and the intensity of the amplified products demonstrates the semi-quantitative

nature of the assay. A 325 bp *cdf-2* product was amplified using primers that annealed to

exon 5 and to the junction of exons 7 and 8. These exons are not affected by the *tm788*

deletion. A 330 bp *cdf-1* product was amplified using primers that annealed to exons 3

and 4. As a control for contamination of individual reaction components, we substituted

water for the templates and either PCR amplified (W) or reverse transcribed and PCR

amplified (RT) the reaction mixes with each primer set. PCR products were separated on

a 2% TAE agarose gel containing ethidium bromide and visualized using UV light.

Molecular weight markers (M) are labeled (100 bp DNA ladder, New England Biolabs,

Ipswich, MA). The identities of the amplified products were verified by DNA sequencing.

In wild-type animals, *cdf-2* transcripts were readily detected and induced by

supplemental zinc. In *cdf-2(tm788)* animals, *cdf-2* transcript levels were reduced ~1,000-

fold compared to wild-type animals since they were barely detectable with 1 unit of input

cDNA. Furthermore, *cdf-2* transcripts in the mutant animals were not induced by

supplemental zinc. The *cdf-1* control demonstrates that equivalent levels of amplifiable

cDNA were present in all of the samples.

Table A.1
Quantitative analysis of zinc requirements and toxicities

Strain[a]	EC_{50}	IC_{50}
WT	6.8 ± 1.1	1300 ± 290
cdf-1	5.1 ± 0.65	550 ± 350
cdf-2	3.8 ± 0.99	1900 ± 160
sur-7	5.1 ± 1.3	640 ± 170*
cdf-1 cdf-2	5.7 ± 0.05	580 ± 170*
cdf-2 sur-7	7.0 ± 0.50	480 ± 47*
cdf-1 sur-7	7.2 ± 1.3	600 ± 290
cdf-1 cdf-2 sur-7	7.9 ± 0.30	220 ± 13*

Values are dietary zinc concentrations in micromolars (average $\pm$ SD of two to three independent experiments). Values significantly different from WT ($P < 0.05$, Welch's *t*-test) are indicated with an asterisk.

[a] Mutant alleles were *cdf-1(n2527)*, *cdf-2(tm788)*, and *sur-7(ku119)*.

165

Figure A.1

Figure A.2

A
Zinc
1. Culture worms in CeMM with 30-75 μM zinc.
2. Culture worms in a range of zinc concentrations.
3. Count worms periodically over three weeks.
3 weeks

B
$[Zn^{2+}(\mu M)]$
15-120
480
10
960
240
8
6
1920
4
2
1
0

C

D
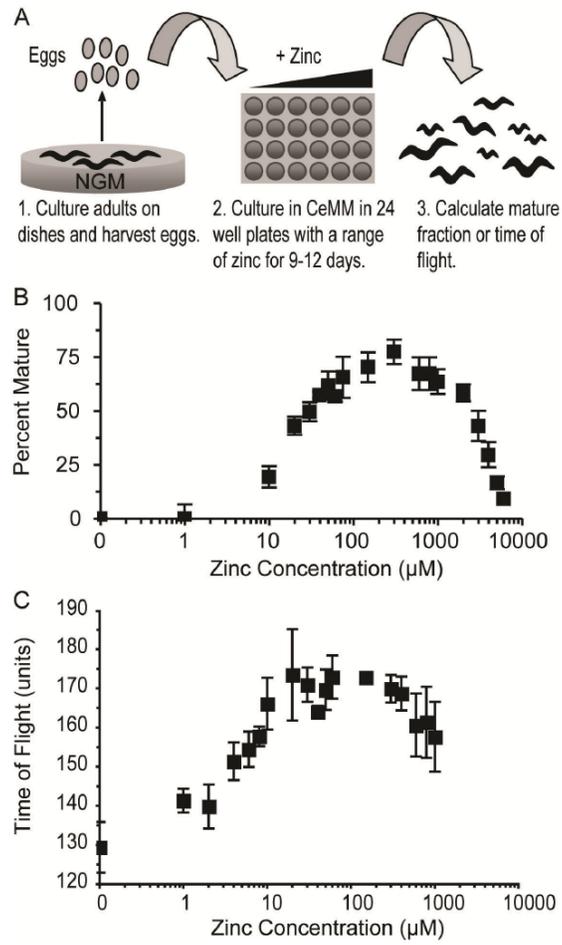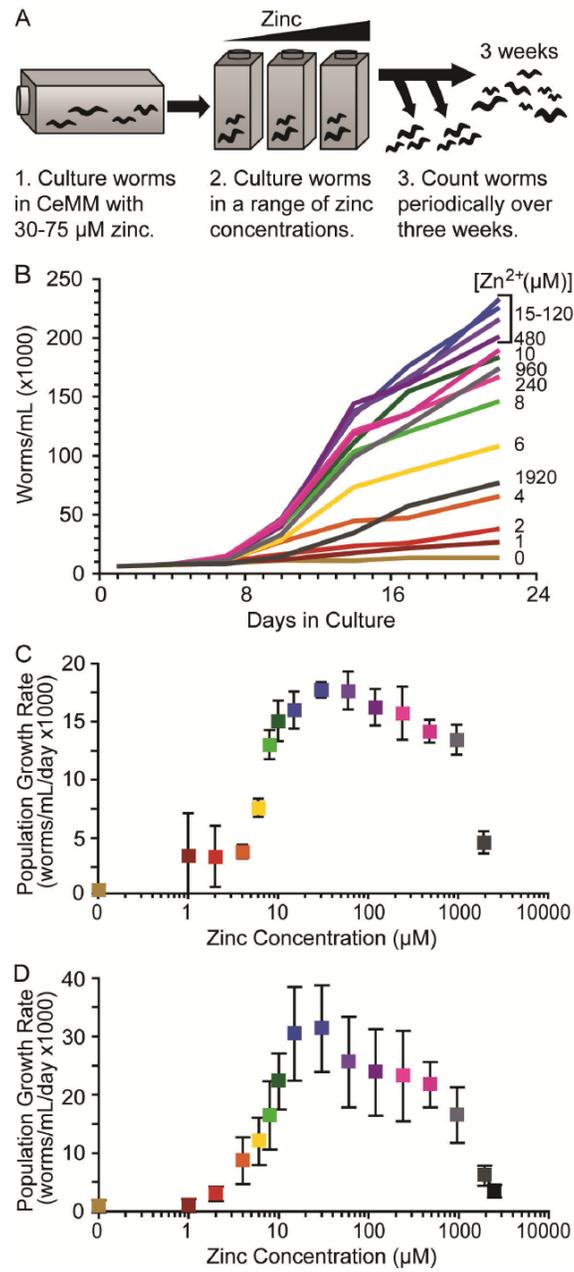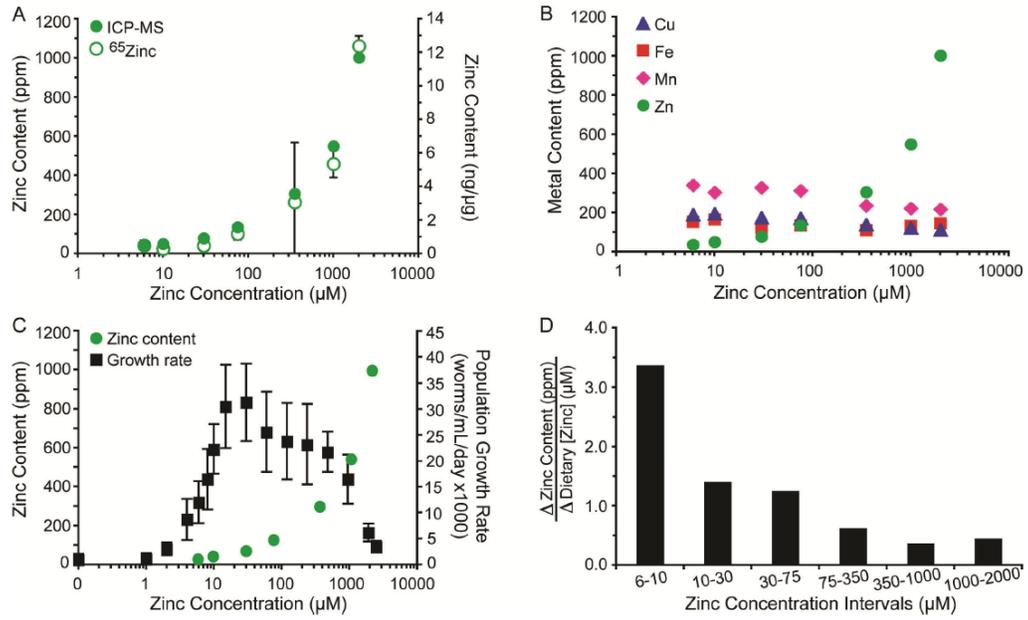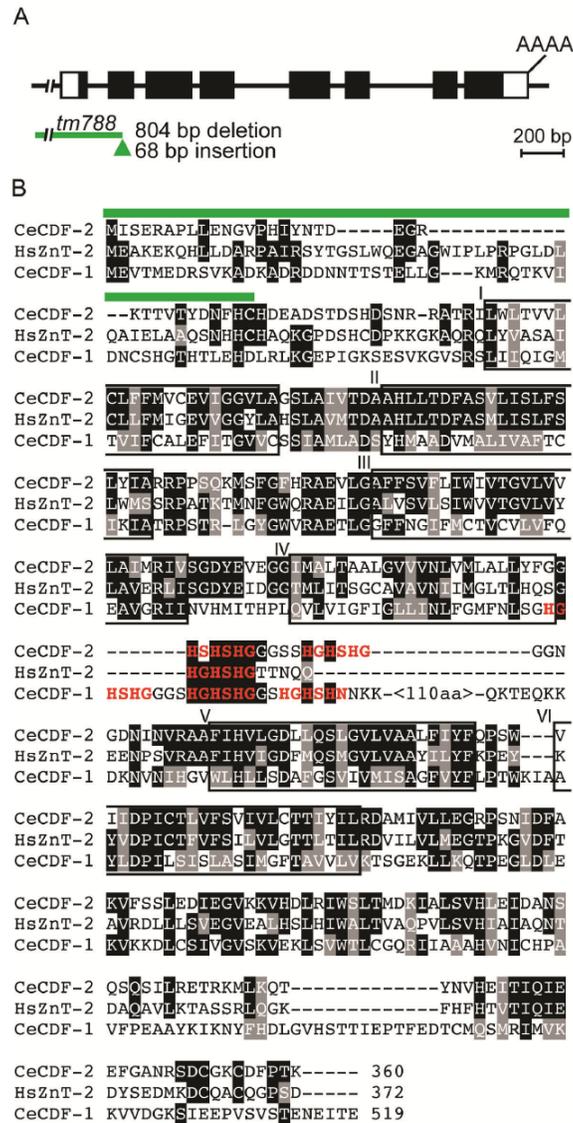
Figure A.3

Figure A.4

Figure A.5

Figure A.6

171
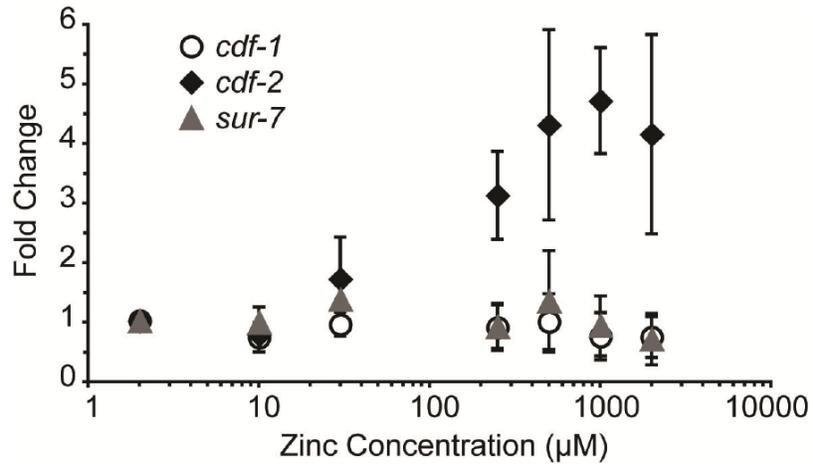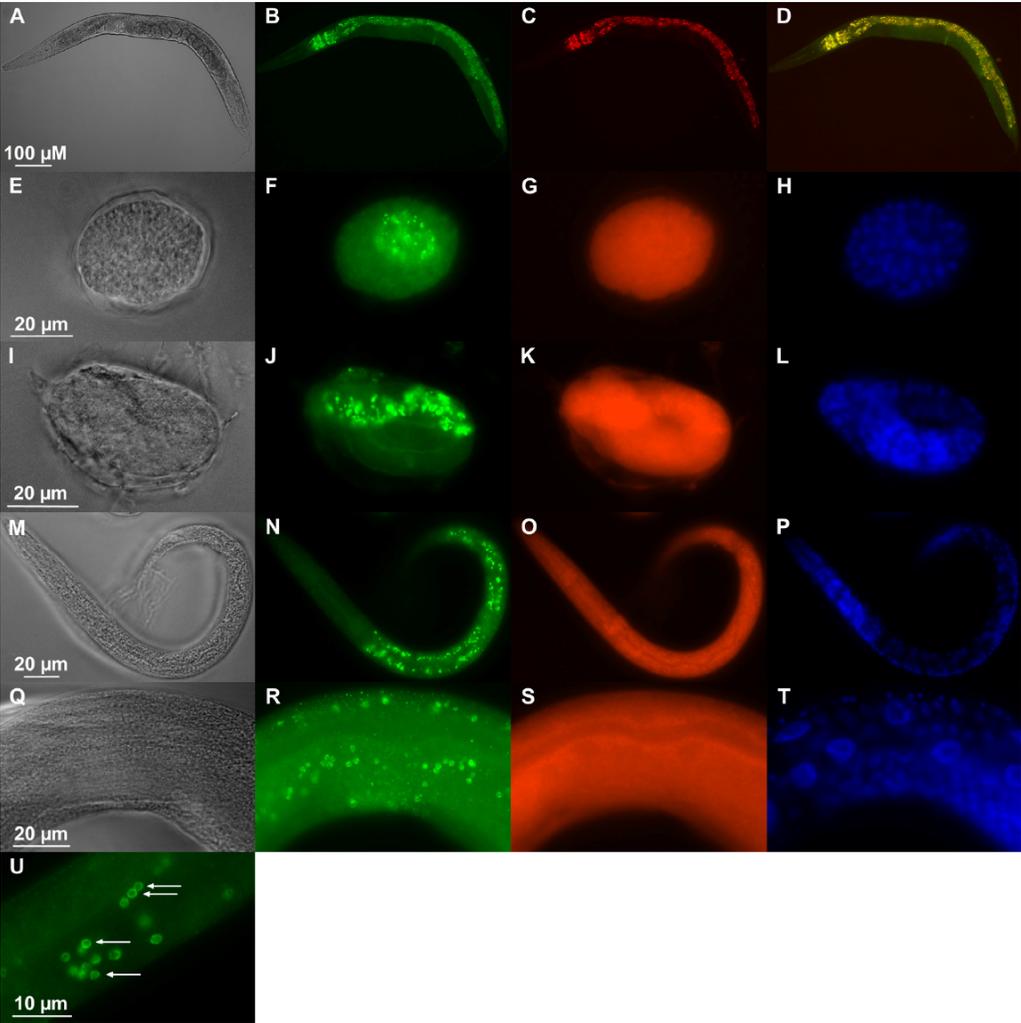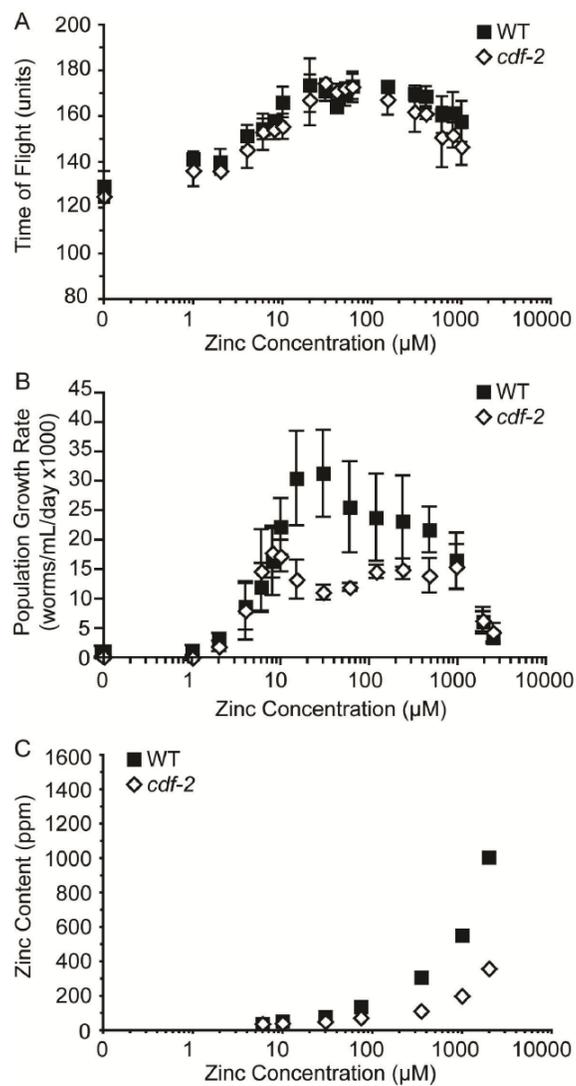
Figure A.7

Figure A.8

Figure A.9

Figure A.10

A Wild type
Zn²⁺
CDF-1
Zn²⁺
Zn²⁺
CDF-2

B *cdf-1(lf)*
Zn²⁺
CDF-1
Zn²⁺
Zn²⁺
CDF-2

C *cdf-2(lf)*
Zn²⁺
Zn²⁺
CDF-1
Zn²⁺
CDF-2

D *cdf-1(lf) cdf-2(lf)*
Zn²⁺
CDF-1
Zn²⁺
Zn²⁺
CDF-2

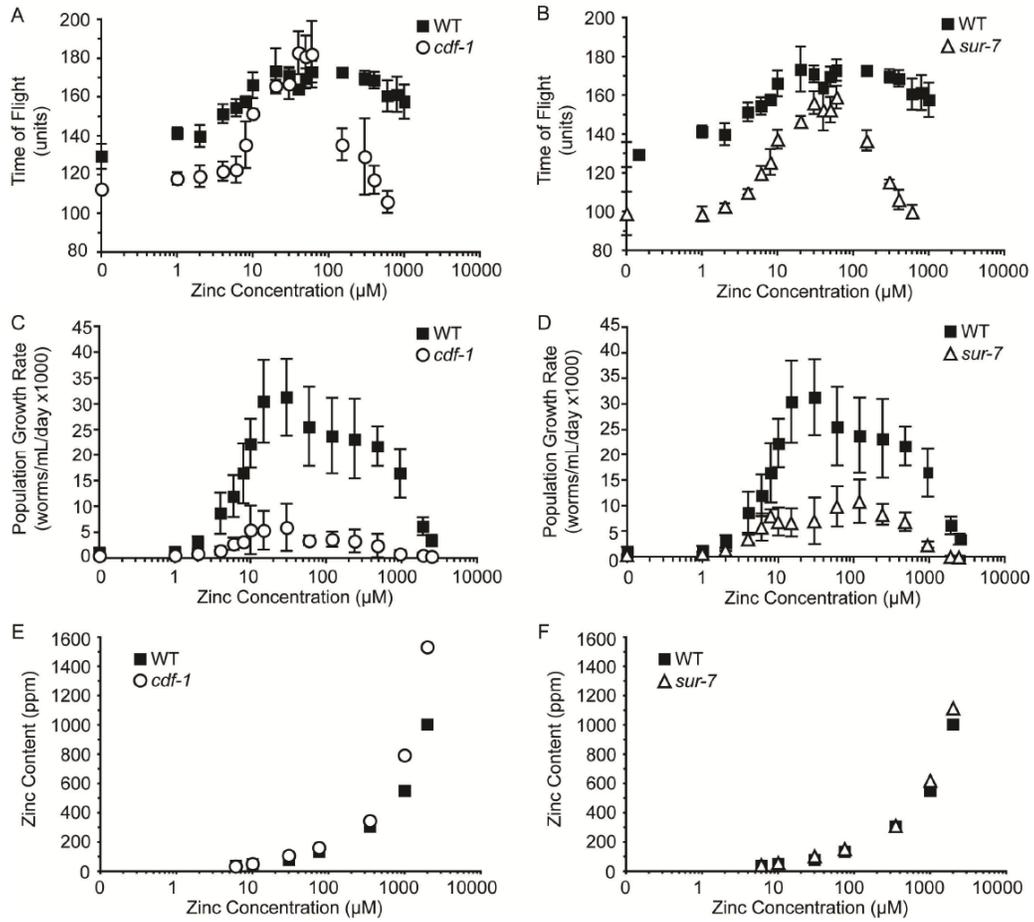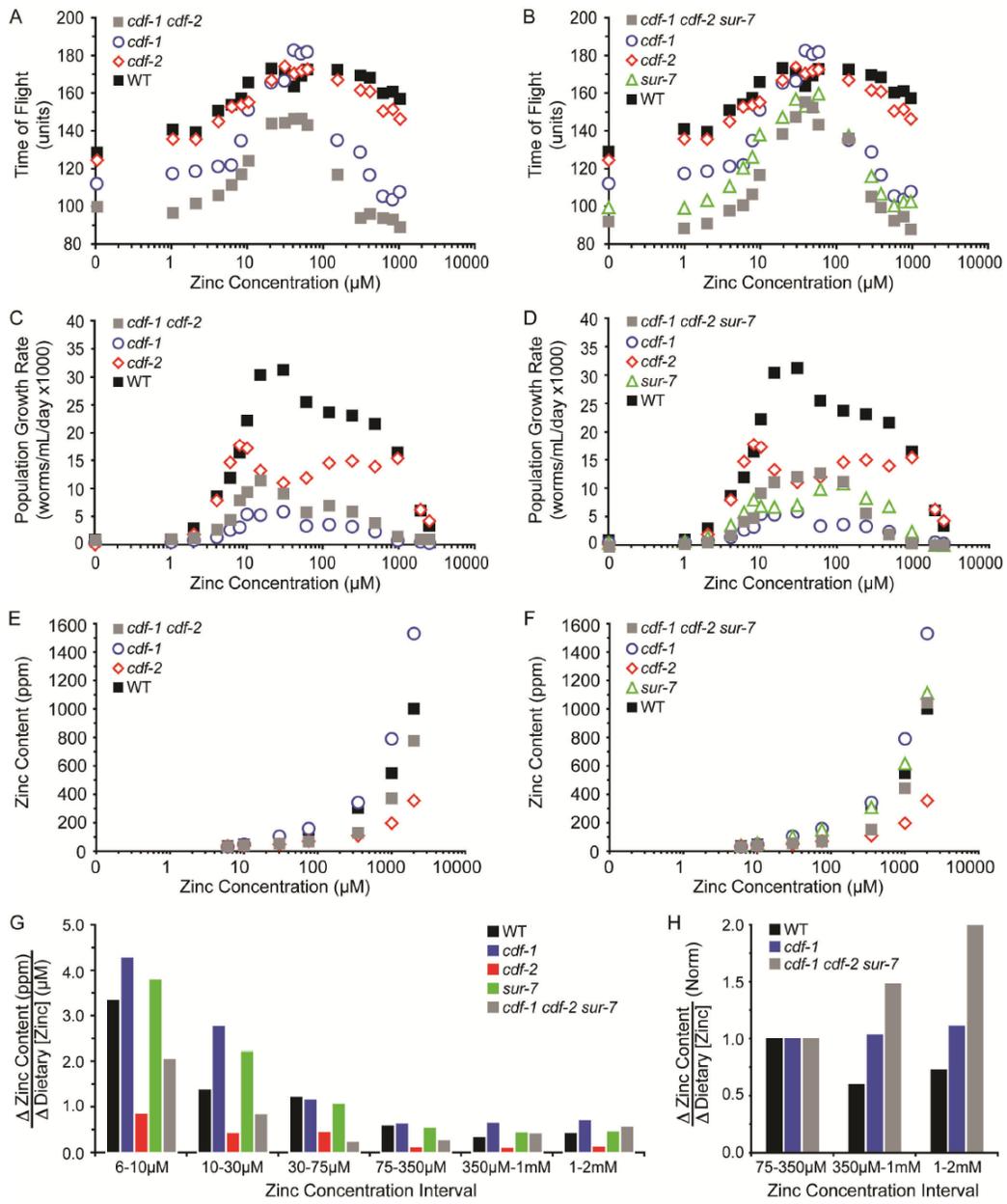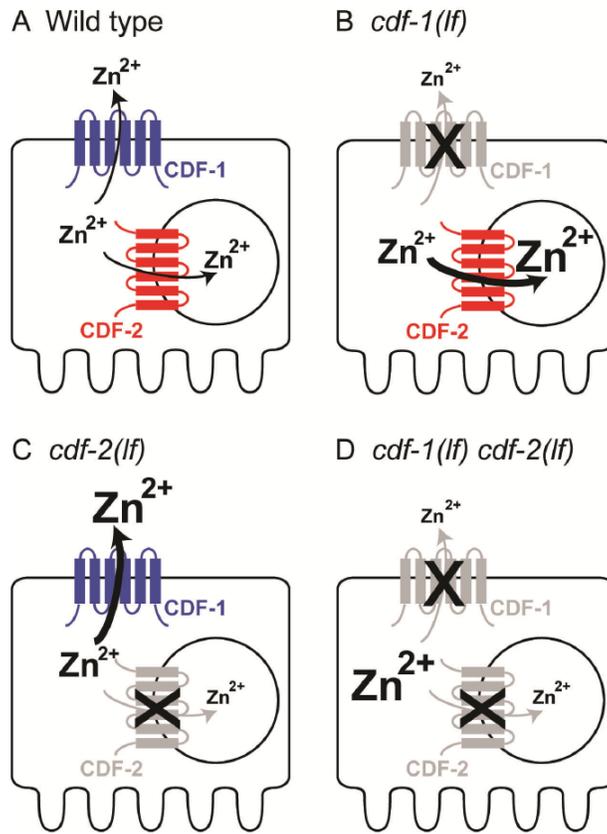**Supplemental Table A.1**
Metal content of wild-type and mutant *C. elegans* determined by ICP-MS

Metal	Genotype[a]	Dietary Zinc (µM)						
		6	10	30	75	350	1000	2000
Zinc	WT	37	50	79	135	306	550	1003
	cdf-1	33	51	107	160	344	792	1532
	cdf-2	37	41	50	72	111	199	357
	sur-7	43	59	104	153	311	619	1114
	cdf-1 cdf-2	33	43	56	70	130	374	779
	cdf-1 sur-7	34	44	87	144	345	901	1637
	cdf-1 cdf-2 sur-7	32	40	58	70	153	444	1046
Copper	WT	192	197	177	174	142	124	114
	cdf-1	167	200	195	172	127	142	176
	cdf-2	191	168	169	162	142	163	143
	sur-7	174	174	158	153	137	111	99
	cdf-1 cdf-2	166	156	142	141	138	168	177
	cdf-1 sur-7	178	157	155	155	137	144	183
	cdf-1 cdf-2 sur-7	183	171	166	138	143	179	173
Iron	WT	154	166	123	135	111	132	146
	cdf-1	187	180	173	155	151	172	239
	cdf-2	130	122	121	159	125	149	114
	sur-7	133	134	127	128	127	121	138
	cdf-1 cdf-2	170	168	152	148	152	178	219
	cdf-1 sur-7	204	178	162	173	150	186	213
	cdf-1 cdf-2 sur-7	201	205	194	159	196	219	237
Manganese	WT	341	304	329	313	237	223	218
	cdf-1	398	410	376	318	262	283	360
	cdf-2	502	459	465	348	319	397	315
	sur-7	415	399	343	315	244	249	238
	cdf-1 cdf-2	427	403	338	330	318	360	423
	cdf-1 sur-7	445	381	344	300	292	356	397
	cdf-1 cdf-2 sur-7	496	463	422	352	362	490	492

Values are the metal content in parts per million by weight.

[a] Mutant alleles were cdf-1(n2527), cdf-2(tm788), and sur-7(ku119).

Supplemental Table A.2
Maturation of *C. elegans* determined by COPAS BIOSORT

Dietary zinc (µM)	WT	cdf-1	cdf-2	sur-7	cdf-1 cdf-2	cdf-2 sur-7	cdf-1 sur-7	cdf-1 cdf-2 sur-7
				Genotype[a]				
0	129 ± 6	113 ± 2	125 ± 3	99 ± 11	101 ± 4	88 ± 2	99 ± 6	93 ± 3
1	141 ± 3	118 ± 3	136 ± 7	99 ± 4	97 ± 3	91 ± 1	103 ± 5	89 ± 3
2	140 ± 6	119 ± 6	136 ± 1	103 ± 1	102 ± 4	98 ± 7	99 ± 2	91 ± 4
4	151 ± 5	122 ± 5	145 ± 8	110 ± 2	107 ± 4	95 ± 1	102 ± 4	98 ± 6
6	154 ± 5	122 ± 7	153 ± 8	120 ± 4	112 ± 4	103 ± 3	102 ± 8	101 ± 3
8	158 ± 2	135 ± 12	154 ± 4	126 ± 7	118 ± 4	104 ± 2	109 ± 6	107 ± 8
10	166 ± 7	152 ± 2	156 ± 5	137 ± 5	125 ± 21	137 ± 7	110 ± 7	117 ± 10
20	173 ± 12	166 ± 3	167 ± 11	147 ± 3	144 ± 8	148 ± 2	111 ± 4	139 ± 10
30	171 ± 4	167 ± 8	174 ± 2	156 ± 6	145 ± 9	152 ± 7	114 ± 6	148 ± 7
40	164 ± 2	183 ± 11	171 ± 3	153 ± 11	147 ± 7	149 ± 3	120 ± 6	156 ± 16
50	170 ± 5	181 ± 11	172 ± 1	152 ± 7	147 ± 8	154 ± 7	117 ± 7	153 ± 5
60	173 ± 6	182 ± 17	173 ± 7	159 ± 6	143 ± 5	149 ± 6	110 ± 6	144 ± 10
150	173 ± 0.3	136 ± 8	167 ± 7	137 ± 5	117 ± 12	139 ± 7	112 ± 6	136 ± 6
300	170 ± 4	129 ± 20	162 ± 9	115 ± 1	95 ± 10	113 ± 6	101 ± 6	136 ± 6
400	169 ± 4	117 ± 7	161 ± 2	106 ± 5	97 ± 7	108 ± 4	99 ± 3	106 ± 4
600	161 ± 8	106 ± 6	151 ± 13	100 ± 4	95 ± 2	101 ± 3	95 ± 3	100 ± 2
800	161 ± 9	104 ± 4	152 ± 6	102 ± 3	94 ± 5	99 ± 5	96 ± 2	93 ± 3
1000	158 ± 9	108 ± 8	147 ± 8	102 ± 3	90 ± 6	94 ± 1	NA	95 ± 3

Values are the average time of flight (±SD) of four biological replicates.

[a] Mutant alleles were *cdf-1(n2527)*, *cdf-2(tm788)*, and *sur-7(ku119)*.

Supplemental Table A.3
Population growth rate of wild-type and mutant *C. elegans*

Dietary zinc (μM)	Genotype[a]							
	WT	cdf-1	cdf-2	sur-7	cdf-1 cdf-2	cdf-2 sur-7	cdf-1 sur-7	cdf-1 cdf-2 sur-7
0	1 ± 1	0.5 ± 0.3	0.1 ± 0.1	0.4 ± 0.1	0.1 ± 0.2	0.2 ± 0.2	0.7 ± 0.9	0.0 ± 0.2
1	1 ± 1	0.5 ± 0.7	-0.05 ± 0.4	0.7 ± 0.3	0.3 ± 0.4	0.51 ± 0.01	0.7 ± 0.6	0.2 ± 0.1
2	3 ± 1	0.9 ± 0.7	1.9 ± 0.9	1.4 ± 0.2	0.5 ± 0.8	0.5 ± 0.3	1 ± 1	0.44 ± 0.03
4	9 ± 4	1.4 ± 0.8	8 ± 5	3.5 ± 0.8	2 ± 2	2.0 ± 0.02	3 ± 3	2 ± 1
6	12 ± 4	3 ± 1	15 ± 7	6 ± 3	4 ± 3	3.9 ± 0.8	5 ± 2	4.1 ± 0.9
8	16 ± 6	3.2 ± 0.5	18 ± 4	8 ± 1	7 ± 7	5 ± 0	8 ± 4	5 ± 3
10	22 ± 5	5 ± 5	17 ± 3	7 ± 3	9 ± 7	7 ± 1	16 ± 1	9 ± 1
15	30 ± 8	5 ± 4	13 ± 3	7 ± 3	11 ± 10	8 ± 3	20 ± 0	11 ± 2
30	31 ± 7	6 ± 5	11 ± 1	7 ± 5	9 ± 6	9 ± 1	19 ± 1	12 ± 3
60	26 ± 8	3.4 ± 0.9	12.0 ± 0.7	10 ± 4	5 ± 3	10 ± 3	14 ± 1	13 ± 3
120	24 ± 7	4 ± 1	15 ± 1	11 ± 4	7 ± 5	11 ± 2	14 ± 1	11 ± 3
240	23 ± 8	3 ± 2	15 ± 2	8 ± 2	5 ± 3	12 ± 1	12 ± 2	6 ± 2
480	22 ± 4	2 ± 2	14 ± 3	7 ± 2	3 ± 1	5 ± 2	8 ± 5	1.9 ± 0.2
960	16 ± 5	0.8 ± 0.7	15 ± 4	2 ± 1	0.9 ± 0.6	2.0 ± 0.2	3 ± 4	0.3 ± 0.4
1920	6 ± 2	0.6 ± 0.4	6 ± 2	0.1 ± 0.1	0.3 ± 0.4	0.5 ± 0.4	0.5 ± 0.8	0.0 ± 0.2
2500	3 ± 1	0.3 ± 0.2	4 ± 2	0.0 ± 0.1	0.3 ± 0.3	0.3 ± 0.4	0.5 ± 0.2	0.0 ± 0.2

Values are the average population growth rate (±SD) of 2-3 biological replicates (worms/mL/day x 1000).

[a] Mutant alleles were *cdf-1(n2527)*, *cdf-2(tm788)*, and *sur-7(ku119)*.

Supplemental Figure A.1
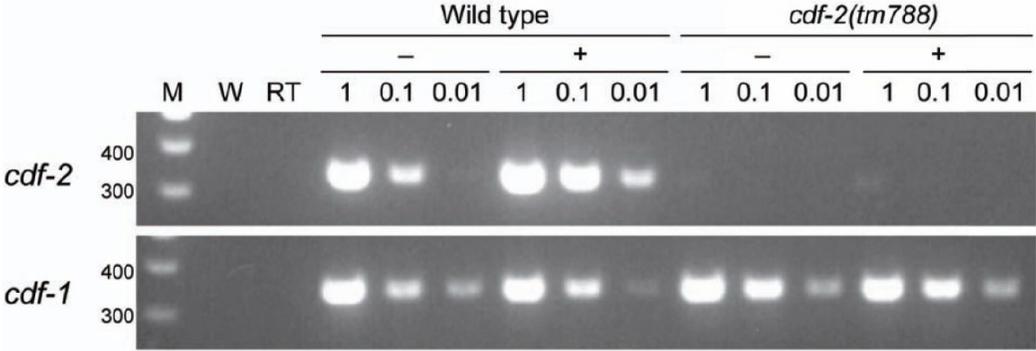
APPENDIX B

Analysis of Uncharacterized *C. elegans* Zinc Transporters

INTRODUCTION

Zinc transporters play a major role in the control of zinc metabolism. There are two families of zinc transporters, CDF and ZIP (Eide, 2006). CDF proteins move cytoplasmic zinc out of the cell or into intracellular compartments, resulting in the decrease in the cytoplasmic zinc level. In contrast, ZIP proteins uptake zinc from the outside of the cells or move zinc from intracellular compartments to the cytoplasm, leading to the increase in the cytoplasmic zinc level. Each zinc transporter family has multiple members. For example, in mammals, there are 10 members in the CDF family and 14 members in the ZIP family (Lichten and Cousins, 2009). Many zinc transporters have been studied for their expression, regulation and function. Theses studies suggested that each zinc transporter has its unique function but there are also networks of zinc transporters to control biological processes and to regulate zinc homeostasis in the body. However, due to the complexity caused by a large number of zinc transporters, understanding of the function of zinc transporters in animals is still limited.

C. elegans can be useful to study the function of zinc transporters because it has conserved multiple zinc transporters in its simple body, and thereby it can facilitate the analysis of networks of zinc transporters. In addition, the genetic power of *C. elegans* allows various and efficient approaches to study the function of zinc transporters. Genomic sequence analysis revealed that *C. elegans* has 14 putative CDF and 14 ZIP proteins (Table B.1) (Kambe et al., 2006; Krupa et al., unpublished data). Three CDF proteins have been previously characterized (Bruinsma et al., 2002; Davis et al., 2009; Yoder et al., 2004), but little is known about the other zinc transporters. Therefore, it is

important to perform the comprehensive study of *C. elegans* zinc transporter to better understand zinc metabolism and zinc-related physiological processes.

To characterize zinc transporters, we analyzed their expression patterns by generating transgenic animals and examined the phenotypes of loss-of-function mutant animals. Studying all *C. elegans* zinc transporters in this single study was practically impossible. The priority of zinc transporters was thus determined by the criteria such as the homology to human genes, implication in human heath, availability of mutant alleles and easiness of gene cloning. A subset of zinc transporters was studied (Tables B.3 and B.4). The results demonstrated that many *C. elegans* zinc transporters have similar expression patterns to their mammalian counterparts but some have differences. Genetic analysis identified new phenotypes of zinc transporter mutant animals, suggesting that those zinc transporters may be involved in specific biological processes. This study demonstrate that *C. elegans* is useful to study zinc transporter and zinc metabolism and suggest novel functions of zinc and zinc transporters.

RESULTS AND DISCUSSION

Expression Pattern Analysis

Since the tissue distribution and intracellular localization of zinc transporters are critical to understand their function in zinc metabolism, we performed expression pattern analysis. To determine the cell types expressing zinc transporters and the intracellular localization of zinc transporters, we generated transgenic animals expressing zinc

transporters fused to GFP under the control of their predicted promoter region. Of the 9 target zinc transporters, we successfully expressed four of them in transgenic animals, while one of them (C30H6.2) was made in multiple transgenic lines but its expression was not detected. H13N06.5, which is the most close to mammalian ZIP-7, was mainly expressed in the hypodermis and likely to be localized to the ER/Golgi (Figure B.1A). F55F8.9, which is similar to mammalian ZIP-2, was expressed in the hypodermis and highly in the intestine. F55F8.9 displayed cytoplasmic localization near apical membrane of intestinal cells (Figure B.1B), suggesting that it may be localized to endosomal vesicles. F59A3.4, which is *C. elegans* ortholog of mammalian ZIP-11 and close to the yeast Zrt3, was expressed in the hypodermis, intestine and spermatheca and likely localized to ER/Golgi (Figure B.1C). TOC-1, which is close to mammalian ZnT-6, was expressed in the neurons, hypodermis and intestine. As TOC-1 displayed punctate patterns in the cell, it is predicted to be localized to lysosomes (Figure B.1D). While H13N06.5 and F55F8.9 displayed the intracellular localizations which are consistent with their mammalian homologous proteins, F59A3.4 and TOC-1 displayed distinct patterns. These results suggest that *C. elegans* zinc transporters have conserved functions between species, but some of them may have *C. elegans*-specific unique functions.

Phenotype Analysis

To identify the physiological functions of zinc transporters, we analyzed mutant animals containing loss-of-function mutations. We have requested the identification of mutations in all *C. elegans* zinc transporters from the *C. elegans* knockout consortium. To date, we have obtained at least one mutant allele in 8 zinc transporter genes (Table

B.4). Of these, we tested the following strains: *Y54G9A.4 (ok2094), F55F8.9 (ok2221), C30H6.2 (ok745), T11F9.2 (ok875) and T28F3.3 (ok971).* First, we tested whether these mutant animals have phenotypes in zinc sensitivity. To determine zinc sensitivity, growth rate of animals from L1 stage with different concentrations of supplemental zinc was measured. All five strains tested displayed no significant difference from the wild animals (Table B.4 and data not shown). These results suggest that these genes may not be involved in the control of zinc toxicity or that there may be other genes functionally redundant with them.

To investigate biological processes in which zinc transporters are involved, we screened for phenotypes of mutant strains that are visibly noticeable based on growth, morphology or behaviors. *Y54G9A.4 (ok2094), C30H6.2 (ok745)* and *T11F9.2 (ok875)* displayed no phenotypes and appeared to be similar to wild type animals. *F55F8.9 (ok2221)* displayed scrawny body, slower growth rate, high larval lethality and smaller brood size compared to wild type animals (Figure B.2A and data not shown). *F55F8.9 (ok2221)* also exhibited vulva positioning defects; while the vulva of wild type animals was typically located in the middle of the body, its location in *F55F8.9 (ok2221)* was slightly shifted to the posterior side (Figure B.2B). As vulval cell patterning are controlled by the progeny of ventral hypodermal Pnp cells via the MAPK and Notch signaling pathway (Sulston and Horvitz, 1977; Sundaram, 2004), these result suggest that F55F8.9 zinc transporter may regulate those signaling pathways. In addition, a zebrafish ZIP protein ZIP-6 is involved in cell migration process during gastrulation (Yamashita et al., 2004), suggesting that F55F8.9 may function in the migration of ventral hypodermal cells.

F28F3.3 (ok971) strains were similar to wild type animals in growth rate and morphology. However, *F28F3.3 (ok971)* strains displayed sterility phenotype with a partial penetrance, and this phenotype was temperature sensitive. When eggs were cultured at 15°C, ~92% (12/13) of them were sterile. At 20°C, ~54% (7/13) were sterile, whereas none of the animals (0/12) were sterile at 25°C. While staying sterile, *F28F3.3 (ok971)* strains layed unfertilized oocytes (Figure B.3A), suggesting that the mutant strains appear to have defects in the sperm formation or mating process, not in the oocyte development. Consistently, while sterile *F28F3.3 (ok971)* strains displayed relatively normal morphology of the gonad, their uterus appeared to be empty (Figure B.3B). To examine whether *F28F3.3 (ok971)* strains have defects in the sperm formation, we mated sterile *F28F3.3 (ok971)* mutant hermaphrodites with wild type males. After mating, sterile *F28F3.3 (ok971)* hermaphrodites displayed wild type-like morphology of the uterus full of eggs and became fertile (Figure B.3C). These results suggest that the sperm development is likely to be defective in *F28F3.3 (ok971)* strains. As this sterility phenotype is more severe at lower temperatures, it is possible that mutant sperm mobility in the mutant is not as active as wild type so that increased mobility by high temperature could rescue the phenotype.

MATERIALS AND METHODS

General Methods and Strains

C. elegans strains were cultured at 20°C on nematode growth medium (NGM) seeded

with *E. coli* OP50 (Brenner, 1974). The wild-type *C. elegans* and parent of all mutant strains was Bristol N2. The following mutations were used: *Y54G9A.4 (ok2094), F55F8.9 (ok2221), C30H6.2 (ok745), T11F9.2 (ok875), H13N06.5 (ok960), T28F3.3 (ok971), T01D3.5 (ok876)*. Before analyze the phenotypes, the following mutant animals were backcrossed with N2 wild-type animals by standard methods, and the genotypes were confirmed by PCR: *Y54G9A.4 (ok2094)* five times, *F55F8.9 (ok2221)* three times, *C30H6.2 (ok745)* five times, and *T28F3.3 (ok971)* three times.

Transgenic Strain Construction

For the generation of GFP-fused zinc transporter constructs, I built plasmids with pBluescript SK+ (Stratagene, Santa Clara, CA) by inserting the genomic fragment of zinc transporter genes including promoter regions and coding sequence without the stop codon, the coding sequence of GFP and the *unc-54* 3'UTR from pPD95.77 (a gift from A. Fire). The genomic fragment of zinc transporter genes was amplified by PCR using the primers listed in Table B.2 and fosmids as templates. To make mCherry-fused constructs, the zinc transporter genomic regions were subcloned using enzyme digestion and ligation from the GFP-fused plasmids into pSC3 which contains the coding sequence for mCherry from pCJF104 (a gift from M. Nonet), and the *unc-54* 3'UTR. Transgenic animals were generated by coinjecting each plasmid construct and the coinjection marker pCJF104 (*Pmyo-3::mCherry*). All the plasmids and transgenic animals built are listed in Table B.3.

Microscopy

For differential interference contrast (DIC) and fluorescence microscopy, animals were placed into a drop of 10mM levamisole in M9 on 2% agarose pads on microscope slides. Images were captured using a Zeiss Axioplan 2 microscope equipped with a Zeiss AxioCam MRm digital camera.

Zinc Sensitivity Assays

Eggs were isolated from gravid adult hermaphrodites by treating with NaOH and bleach and were hatched in M9 overnight to obtain synchronized L1 animals. Animals were then cultured on noble agar minimum medium (NAMM) dishes supplemented with zinc sulfate ($ZnSO_4$) and seeded with concentrated OP50. After about 3 days, growth rate was determined by measuring length of animals cultured with different concentrations of zinc.

Brood Size Analysis

Ten hermaphrodite animals at L4 stages were individually cultured on NGM plates, and transferred to new plates every 1-2 days until they stops laying eggs. When progenies reached L3/L4 stage, the number of progenies was counted and the total progeny number was determined as a brood size.

Warnhoff for their assistance analyzing worm strains.

FIGURE LEGENDS

Figure B.1

Fluorescence microscope images of transgenic animals expressing GFP-fused H13N06.5 (A), F55F8.9 (B), F59A3.4 (C), and TOC-1 (D). The type of cells and intracellular organelles where each zinc transporter is localized are described on the right of the table.

Figure B.2

Phenotype analysis of *F55F8.9 (ok2221)* mutant strain. (A) Brood size analysis (B) Vulva positioning defects. The wild type animal displays the vulva (arrow) in the middle of the body (dotted line), whereas *F55F8.9 (ok2221)* strain displays the vulva (arrow) which is shifted to the right, posterior, of the middle line (dotted line).

Figure B.3

Phenotype analysis of *F28F3.3 (ok971)* mutant strain. (A) A normal fertilized egg laid by fertile *F28F3.3 (ok971)* (left, arrow head) and a string of unfertilized oocytes laid by sterile *F28F3.3 (ok971)* (right, arrow). (B) DIC images of the reproductive tissue of a sterile hermaphrodite. While the germline and the gonad appear to be normal, the uterus (parenthesis) is empty. (C) A sterile hermaphrodite was mated with wild type males and then became fertile. The uterus is full of eggs similar to wild type hermaphrodites (parenthesis).

Table B.1

CDF family		ZIP family	
C. elegans Gene	Human Ortholog	*C. elegans* Gene	Human Ortholog
cdf-1	ZnT-1, 10	Y54G9A.4	ZIP-1,2,3
cdf-2	ZnT-2,3,4,8	F55F8.9	
ttm-1		F30B5.7	
F19C6.5		C06G8.3	
Y105E8A.3	ZnT-5,7	C18A3.2	
toc-1	ZnT-6	F31C3.4	
Y71H2AM.9	ZnT-9	C30H6.2	ZIP-4,5,6,8,10,12,14
F41C6.7	None (Homologous to *A. thaliana* AtMTPc3)	T11F9.2	
ZK185.5		Y55F3BL.2	
K07G5.5		H13N06.5	ZIP-7
PDB1.1		T28F3.3	
R02F11.3		T01D3.5	ZIP-9
F56C9.3		F59A3.4	ZIP-11
sur-7	None	C14H10.1	ZIP-13

Table B.2

Gene	Forward Primer Sequence	Reverse Primer Sequence
F55F8.9	ATA GGG CCC AGT CTG GTG ACT GCT TC	TCG CCC GGG ATG TCC ATA GTC ATC AAA AG
C30H6.2	GGG GTA CCT GAA TCT CAT CGT TGC GGA	CCC CCC GGG GAT GTG AAA GCT ATA ATA
T11F9.2	CGC AAG CTT CTG TGA AAT CTT ATA C	GCG ATA TCA AAG TCC ACA GAG TTC AC
H13N06.5	GGG GTA CCT GAA CAT AGC CGC CTC GTT C	CCC CCG GGC TCA TTG CTA TTT ATG AG
T28F3.3	CGG GTA CCG CAA TTC CTA AAT ACT TAC	GAG AAT TCC TCG ACC AAA CTG ACG
T01D3.5	CCG GGT ACC GCC CTT ATA AAC TAT TC	ATC CCG GGA TGA GAG TGA CCA GAA G
F59A3.4	GGG GTA CCT TCG GTC AAA TAT TTA GC	CCG GAA TTC ACC CAA TCC AAC ATC CAT G
toc-1	ATA GGT ACC GAG AAC TAG ACG GAT ACG	CCG GAA TTC ATG ATA AAA AAC GCC GTC

191

Table B.3

Gene	Human Ortholog	GFP-fusion plasmid	mCherry-fusion plasmid	Transgenic animals
Y54G9A.4	ZIP-2	N/A	N/A	N/A
F55F8.9	ZIP-2	pSC4	pSC17	*amEx128, amEx130*
C30H6.2	ZIP-4	pSC2	pSC16	*amEx125, amEx126*
T11F9.2	ZIP-4	pSC13	pSC19	N/A
H13N06.5	ZIP-7	pSC1	pSC15	*amEx123, amEx124*
T28F3.3	ZIP-7	pSC14	pSC22	N/A
T01D3.5	ZIP-9	pSC12	pSC21	N/A
F59A3.4	ZIP-11	pSC11	pSC20	*amEx134*
toc-1	ZnT-6	pSC5	pSC18	*amEx131*

Table B.4

Gene	Human Ortholog	Mutant Alleles	Visible Phenotype	Zinc Sensitivity
Y54G9A.4	ZIP-2	*ok2094*	None	WT-like
F55F8.9	ZIP-2	*ok2221*	Slow growth, small brood size, high larval lethality, vulva positioning defects	WT-like
C30H6.2	ZIP-4	*ok745, gk254*	None	WT-like
T11F9.2	ZIP-4	*ok875, gk250, gk251*	None	WT-like
H13N06.5	ZIP-7	*ok960, gk256*	N/A	N/A
T28F3.3	ZIP-7	*ok971*	Partial sterility	WT-like
T01D3.5	ZIP-9	*ok876*	N/A	N/A
F59A3.4	ZIP-11	N/A	N/A	N/A
toc-1	ZnT-6	*tm4492*	embryonic lethal (clear body color by RNAi)	N/A

Figure B.1

	Gene	Fluorescence microscopy images		Cell type	Organelle
A	H13N06.5			Hypodermis	ER/Golgi
B	F55F8.9			Hypodermis, Intestine	Endosomal vesicles
C	F59A3.4			Hypodermis, Intestine, Spermatheca	ER/Golgi
D	TOC-1			Neuron, Hypodermis, Intestine	Lysosome
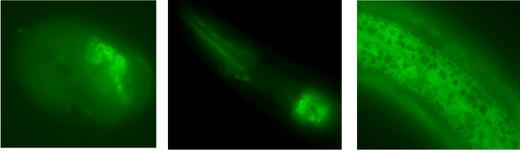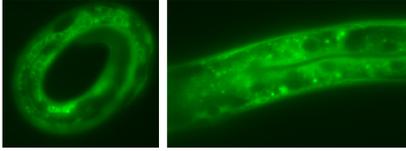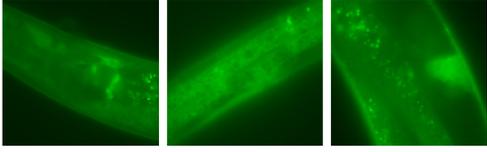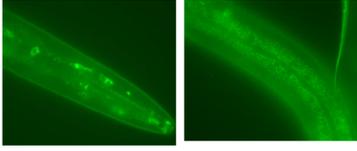
Figure B.2

A

B

WT   *F55F8.9(ok2221)*
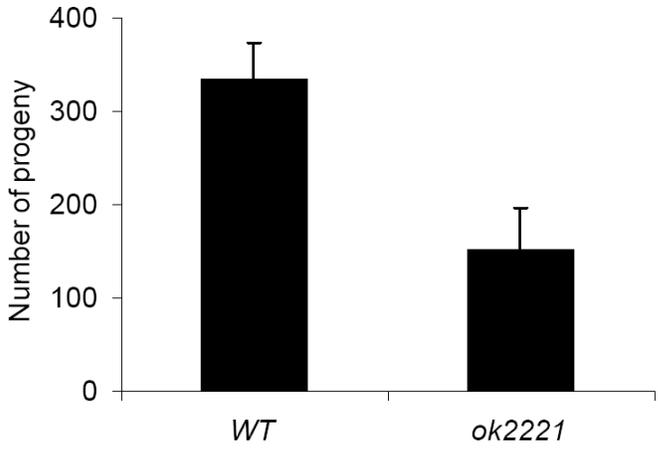
Figure B.3

REFERENCES

Adlard, P.A., Parncutt, J.M., Finkelstein, D.I., and Bush, A.I. (2010). Cognitive loss in zinc transporter-3 knock-out mice: a phenocopy for the synaptic and memory deficits of Alzheimer's disease? J Neurosci *30*, 1631-1636.
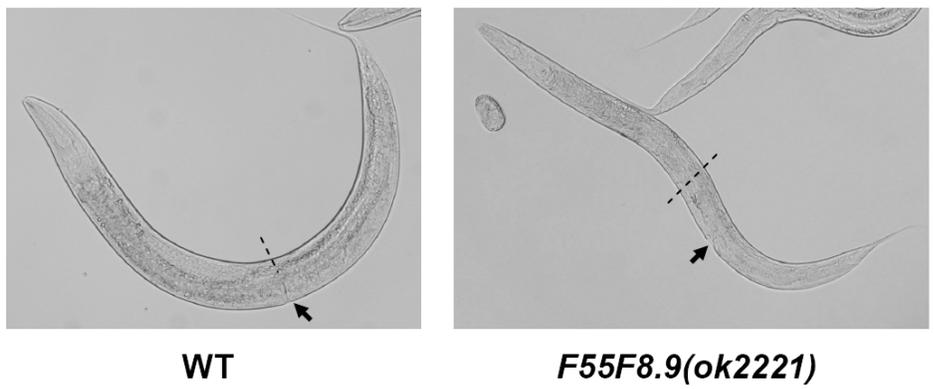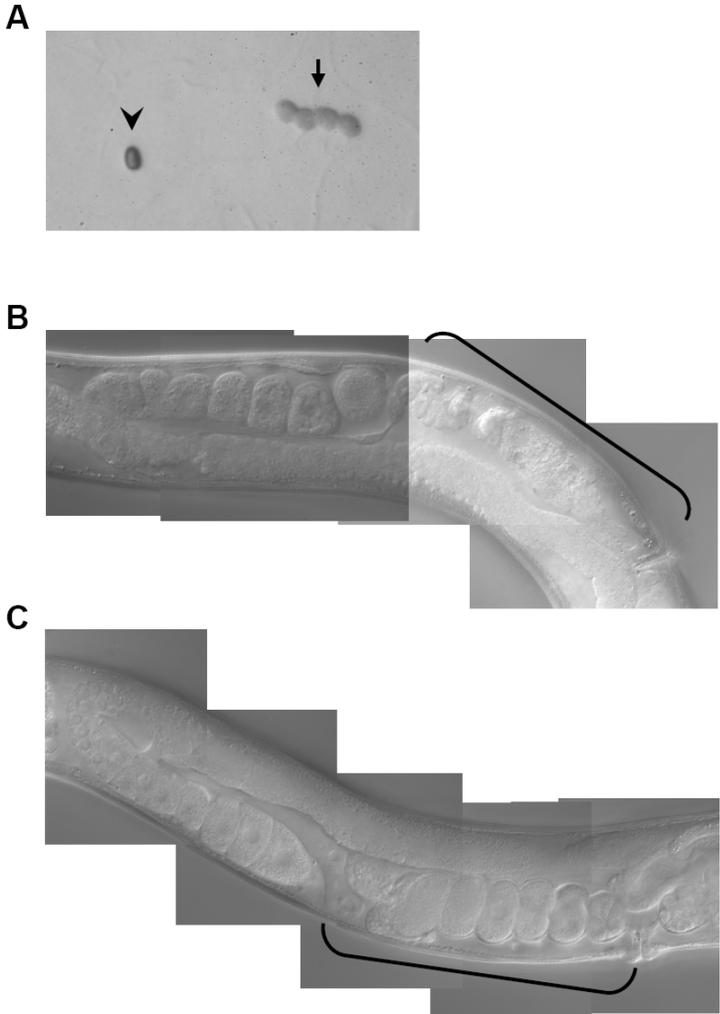
Andreini, C., Banci, L., Bertini, I., and Rosato, A. (2006). Counting the zinc-proteins encoded in the human genome. J Proteome Res *5*, 196-201.

Andrews, G.K., Wang, H., Dey, S.K., and Palmiter, R.D. (2004). Mouse zinc transporter 1 gene provides an essential function during early embryonic development. Genesis *40*, 74-81.

Aydemir, T.B., Liuzzi, J.P., McClellan, S., and Cousins, R.J. (2009). Zinc transporter ZIP8 (SLC39A8) and zinc influence IFN-gamma expression in activated human T cells. J Leukoc Biol *86*, 337-348.

Bailey, T.L., and Elkan, C. (1994). Fitting a mixture model by expectation maximization to discover motifs in biopolymers. Proc Int Conf Intell Syst Mol Biol *2*, 28-36.

Begum, N.A., Kobayashi, M., Moriwaki, Y., Matsumoto, M., Toyoshima, K., and Seya, T. (2002). Mycobacterium bovis BCG cell wall and lipopolysaccharide induce a novel gene, BIGM103, encoding a 7-TM protein: identification of a new protein family having Zn-transporter and Zn-metalloprotease signatures. Genomics *80*, 630-645.

Beighton, P., De Paepe, A., Steinmann, B., Tsipouras, P., and Wenstrup, R.J. (1998). Ehlers-Danlos syndromes: revised nosology, Villefranche, 1997. Ehlers-Danlos National Foundation (USA) and Ehlers-Danlos Support Group (UK). Am J Med Genet *77*, 31-37.

Beitel, G.J., Clark, S.G., and Horvitz, H.R. (1990). *Caenorhabditis elegans* ras gene *let-60* acts as a switch in the pathway of vulval induction. Nature *348*, 503-509.

Berg, J.M., and Shi, Y. (1996). The galvanization of biology: a growing appreciation for the roles of zinc. Science *271*, 1081-1085.

Beyersmann, D., and Haase, H. (2001). Functions of zinc in signaling, proliferation and differentiation of mammalian cells. Biometals *14*, 331-341.

Brenner, S. (1974). The genetics of *Caenorhabditis elegans*. Genetics *77*, 71-94.

Bruinsma, J.J., Jirakulaporn, T., Muslin, A.J., and Kornfeld, K. (2002). Zinc ions and cation diffusion facilitator proteins regulate Ras-mediated signaling. Dev Cell *2*, 567-578.

Bruinsma, J.J., Schneider, D.L., Davis, D.E., and Kornfeld, K. (2008). Identification of mutations in *Caenorhabditis elegans* that cause resistance to high levels of dietary zinc and analysis using a genomewide map of single nucleotide polymorphisms scored by pyrosequencing. Genetics *179*, 811-828.

Buecher, E.J., Jr., Hansen, E., and Yarwood, E.A. (1966). Ficoll activation of a protein essential for maturation of the free-living nematode *Caenorhabditis briggsae*. Proc Soc Exp Biol Med *121*, 390-393.

Chalfie, M., Tu, Y., Euskirchen, G., Ward, W.W., and Prasher, D.C. (1994). Green fluorescent protein as a marker for gene expression. Science *263*, 802-805.

Chao, Y., and Fu, D. (2004). Kinetic study of the antiport mechanism of an *Escherichia coli* zinc transporter, ZitB. J Biol Chem *279*, 12043-12050.

Chausmer, A.B. (1998). Zinc, insulin and diabetes. J Am Coll Nutr *17*, 109-115.

Chen, C.C., Schweinsberg, P.J., Vashist, S., Mareiniss, D.P., Lambie, E.J., and Grant, B.D. (2006). RAB-10 is required for endocytic recycling in the Caenorhabditis elegans intestine. Mol Biol Cell *17*, 1286-1297.

Chimienti, F., Devergnas, S., Favier, A., and Seve, M. (2004). Identification and cloning of a beta-cell-specific zinc transporter, ZnT-8, localized into insulin secretory granules. Diabetes *53*, 2330-2337.

Chimienti, F., Devergnas, S., Pattou, F., Schuit, F., Garcia-Cuenca, R., Vandewalle, B., Kerr-Conte, J., Van Lommel, L., Grunwald, D., Favier, A.*, et al.* (2006). In vivo expression and functional characterization of the zinc transporter ZnT8 in glucose-

induced insulin secretion. Journal of cell science *119*, 4199-4206.

Chowanadisai, W., Kelleher, S.L., and Lonnerdal, B. (2005). Zinc deficiency is associated with increased brain zinc import and LIV-1 expression and decreased ZnT-1 expression in neonatal rats. J Nutr *135*, 1002-1007.

Chowanadisai, W., Lonnerdal, B., and Kelleher, S.L. (2006). Identification of a mutation in SLC30A2 (ZnT-2) in women with low milk zinc concentration that results in transient neonatal zinc deficiency. J Biol Chem *281*, 39699-39707.

Clokey, G.V., and Jacobson, L.A. (1986). The autofluorescent "lipofuscin granules" in the intestinal cells of *Caenorhabditis elegans* are secondary lysosomes. Mech Ageing Dev *35*, 79-94.

Cole, T.B., Wenzel, H.J., Kafer, K.E., Schwartzkroin, P.A., and Palmiter, R.D. (1999). Elimination of zinc from synaptic vesicles in the intact mouse brain by disruption of the ZnT3 gene. Proc Natl Acad Sci U S A *96*, 1716-1721.

Costello, L.C., and Franklin, R.B. (2006). The clinical relevance of the metabolism of prostate cancer; zinc and tumor suppression: connecting the dots. Molecular cancer *5*, 17.

Coyle, P., Philcox, J.C., Carey, L.C., and Rofe, A.M. (2002). Metallothionein: the multipurpose protein. Cell Mol Life Sci *59*, 627-647.

Cragg, R.A., Christie, G.R., Phillips, S.R., Russi, R.M., Kury, S., Mathers, J.C., Taylor, P.M., and Ford, D. (2002). A novel zinc-regulated human zinc transporter, hZTL1, is localized to the enterocyte apical membrane. J Biol Chem *277*, 22789-22797.

Cragg, R.A., Phillips, S.R., Piper, J.M., Varma, J.S., Campbell, F.C., Mathers, J.C., and Ford, D. (2005). Homeostatic regulation of zinc transporters in the human small intestine by dietary zinc supplementation. Gut *54*, 469-478.

Cui, Y., McBride, S.J., Boyd, W.A., Alper, S., and Freedman, J.H. (2007a). Toxicogenomic analysis of Caenorhabditis elegans reveals novel genes and pathways involved in the resistance to cadmium toxicity. Genome Biol *8*, R122.

Cui, Y., Vogt, S., Olson, N., Glass, A.G., and Rohan, T.E. (2007b). Levels of zinc, selenium, calcium, and iron in benign breast tissue and risk of subsequent breast cancer. Cancer Epidemiol Biomarkers Prev *16*, 1682-1685.

Cummings, J.E., and Kovacic, J.P. (2009). The ubiquitous role of zinc in health and disease. J Vet Emerg Crit Care (San Antonio) *19*, 215-240.

Davis, D.E., Roh, H.C., Deshmukh, K., Bruinsma, J.J., Schneider, D.L., Guthrie, J., Robertson, J.D., and Kornfeld, K. (2009). The cation diffusion facilitator gene cdf-2 mediates zinc metabolism in Caenorhabditis elegans. Genetics *182*, 1015-1033.

Davis, S.R., and Cousins, R.J. (2000). Metallothionein expression in animals: a physiological perspective on function. J Nutr *130*, 1085-1088.

Docampo, R., de Souza, W., Miranda, K., Rohloff, P., and Moreno, S.N. (2005). Acidocalcisomes - conserved from bacteria to man. Nat Rev Microbiol *3*, 251-261.

Dong, J., Boyd, W.A., and Freedman, J.H. (2008a). Molecular characterization of two homologs of the *Caenorhabditis elegans* cadmium-responsive gene *cdr-1*: *cdr-4* and *cdr-6*. J Mol Biol *376*, 621-633.

Dong, J., Robertson, J.D., Markesbery, W.R., and Lovell, M.A. (2008b). Serum zinc in the progression of Alzheimer's disease. J Alzheimers Dis *15*, 443-450.

Duerr, J.S. (2006). Immunohistochemistry. WormBook, 1-61.

Dufner-Beattie, J., Huang, Z.L., Geiser, J., Xu, W., and Andrews, G.K. (2006). Mouse ZIP1 and ZIP3 genes together are essential for adaptation to dietary zinc deficiency during pregnancy. Genesis *44*, 239-251.

Dufner-Beattie, J., Kuo, Y.M., Gitschier, J., and Andrews, G.K. (2004). The adaptive response to dietary zinc in mice involves the differential cellular localization and zinc regulation of the zinc transporters ZIP4 and ZIP5. J Biol Chem *279*, 49082-49090.

Dufner-Beattie, J., Langmade, S.J., Wang, F., Eide, D., and Andrews, G.K. (2003). Structure, function, and regulation of a subfamily of mouse zinc transporter genes.

J Biol Chem *278*, 50142-50150.

Dufner-Beattie, J., Weaver, B.P., Geiser, J., Bilgen, M., Larson, M., Xu, W., and Andrews, G.K. (2007). The mouse acrodermatitis enteropathica gene Slc39a4 (Zip4) is essential for early development and heterozygosity causes hypersensitivity to zinc deficiency. Hum Mol Genet *16*, 1391-1399.

Eide, D.J. (2004). The SLC39 family of metal ion transporters. Pflugers Arch *447*, 796-800.

Eide, D.J. (2006). Zinc transporters and the cellular trafficking of zinc. Biochim Biophys Acta *1763*, 711-722.

Ellis, C.D., Macdiarmid, C.W., and Eide, D.J. (2005). Heteromeric protein complexes mediate zinc transport into the secretory pathway of eukaryotic cells. J Biol Chem *280*, 28811-28818.

Eng, B.H., Guerinot, M.L., Eide, D., and Saier, M.H., Jr. (1998). Sequence analyses and phylogenetic characterization of the ZIP family of metal ion transport proteins. J Membr Biol *166*, 1-7.

Feeney, G.P., Zheng, D., Kille, P., and Hogstrand, C. (2005). The phylogeny of teleost ZIP and ZnT zinc transporters and their tissue specific expression and response to zinc in zebrafish. Biochim Biophys Acta *1732*, 88-95.

Fire, A., Xu, S., Montgomery, M.K., Kostas, S.A., Driver, S.E., and Mello, C.C. (1998). Potent and specific genetic interference by double-stranded RNA in *Caenorhabditis elegans*. Nature *391*, 806-811.

Fosmire, G.J. (1990). Zinc toxicity. The American journal of clinical nutrition *51*, 225-227.

Frederickson, C.J., Koh, J.Y., and Bush, A.I. (2005). The neurobiology of zinc in health and disease. Nature reviews *6*, 449-462.

Frederickson, C.J., Maret, W., and Cuajungco, M.P. (2004). Zinc and excitotoxic brain injury: a new model. Neuroscientist *10*, 18-25.

Freedman, J.H., Slice, L.W., Dixon, D., Fire, A., and Rubin, C.S. (1993). The novel metallothionein genes of Caenorhabditis elegans. Structural organization and inducible, cell-specific expression. J Biol Chem *268*, 2554-2564.

Fukada, T., Civic, N., Furuichi, T., Shimoda, S., Mishima, K., Higashiyama, H., Idaira, Y., Asada, Y., Kitamura, H., Yamasaki, S.*, et al.* (2008). The zinc transporter SLC39A13/ZIP13 is required for connective tissue development; its involvement in BMP/TGF-beta signaling pathways. PLoS ONE *3*, e3642.

Gaither, L.A., and Eide, D.J. (2001a). Eukaryotic zinc transporters and their regulation. Biometals *14*, 251-270.

Gaither, L.A., and Eide, D.J. (2001b). The human ZIP1 transporter mediates zinc uptake in human K562 erythroleukemia cells. J Biol Chem *276*, 22258-22264.

Gee, K.R., Zhou, Z.L., Ton-That, D., Sensi, S.L., and Weiss, J.H. (2002). Measuring zinc in living cells. A new generation of sensitive and selective fluorescent probes. Cell Calcium *31*, 245-251.

Geraki, K., Farquharson, M.J., and Bradley, D.A. (2002). Concentrations of Fe, Cu and Zn in breast tissue: a synchrotron XRF study. Phys Med Biol *47*, 2327-2339.

Giblin, L.J., Chang, C.J., Bentley, A.F., Frederickson, C., Lippard, S.J., and Frederickson, C.J. (2006). Zinc-secreting Paneth cells studied by ZP fluorescence. J Histochem Cytochem *54*, 311-316.

Giunta, C., Elcioglu, N.H., Albrecht, B., Eich, G., Chambaz, C., Janecke, A.R., Yeowell, H., Weis, M., Eyre, D.R., Kraenzlin, M.*, et al.* (2008). Spondylocheiro dysplastic form of the Ehlers-Danlos syndrome--an autosomal-recessive entity caused by mutations in the zinc transporter gene SLC39A13. American journal of human genetics *82*, 1290-1305.

Gourley, B.L., Parker, S.B., Jones, B.J., Zumbrennen, K.B., and Leibold, E.A. (2003). Cytosolic aconitase and ferritin are regulated by iron in Caenorhabditis elegans. J Biol Chem *278*, 3227-3234.

Guerinot, M.L. (2000). The ZIP family of metal transporters. Biochim Biophys Acta

1465, 190-198.

Guffanti, A.A., Wei, Y., Rood, S.V., and Krulwich, T.A. (2002). An antiport mechanism for a member of the cation diffusion facilitator family: divalent cations efflux in exchange for K+ and H+. Mol Microbiol *45*, 145-153.

Gunes, C., Heuchel, R., Georgiev, O., Muller, K.H., Lichtlen, P., Bluthmann, H., Marino, S., Aguzzi, A., and Schaffner, W. (1998). Embryonic lethality and liver degeneration in mice lacking the metal-responsive transcriptional activator MTF-1. EMBO J *17*, 2846-2854.

Hambidge, K.M., and Krebs, N.F. (2007). Zinc deficiency: a special challenge. J Nutr *137*, 1101-1105.

Hambidge, M. (2000). Human zinc deficiency. J Nutr *130*, 1344S-1349S.

Hantke, K. (2001). Bacterial zinc transporters and regulators. Biometals *14*, 239-249.

Herbig, A., Bird, A.J., Swierczek, S., McCall, K., Mooney, M., Wu, C.Y., Winge, D.R., and Eide, D.J. (2005). Zap1 activation domain 1 and its role in controlling gene expression in response to cellular zinc status. Mol Microbiol *57*, 834-846.

Hermann, G.J., Schroeder, L.K., Hieb, C.A., Kershner, A.M., Rabbitts, B.M., Fonarev, P., Grant, B.D., and Priess, J.R. (2005). Genetic analysis of lysosomal trafficking in Caenorhabditis elegans. Mol Biol Cell *16*, 3273-3288.

Hieb, W.F., and Rothstein, M. (1968). Sterol requirement for reproduction of a free-living nematode. Science *160*, 778-780.

Hieb, W.F., Stokstad, E.L., and Rothstein, M. (1970). Heme requirement for reproduction of a free-living nematode. Science *168*, 143-144.

Ho, E., Quan, N., Tsai, Y.H., Lai, W., and Bray, T.M. (2001). Dietary zinc supplementation inhibits NFkappaB activation and protects against chemically induced diabetes in CD1 mice. Exp Biol Med (Maywood) *226*, 103-111.

Horvitz, H.R., Chalfie, M., Trent, C., Sulston, J.E., and Evans, P.D. (1982). Serotonin and octopamine in the nematode *Caenorhabditis elegans*. Science *216*, 1012-1014.

Huang, L., and Gitschier, J. (1997). A novel gene involved in zinc transport is deficient in the lethal milk mouse. Nat Genet *17*, 292-297.

Huang, L., Yu, Y.Y., Kirschke, C.P., Gertz, E.R., and Lloyd, K.K. (2007). Znt7 (Slc30a7)-deficient mice display reduced body zinc status and body fat accumulation. J Biol Chem *282*, 37053-37063.

Huffman, D.L., Abrami, L., Sasik, R., Corbeil, J., van der Goot, F.G., and Aroian, R.V. (2004). Mitogen-activated protein kinase pathways defend against bacterial pore-forming toxins. Proc Natl Acad Sci U S A *101*, 10995-11000.

Jackson, K.A., Helston, R.M., McKay, J.A., O'Neill, E.D., Mathers, J.C., and Ford, D. (2007). Splice variants of the human zinc transporter ZnT5 (SLC30A5) are differentially localized and regulated by zinc through transcription and mRNA stability. J Biol Chem *282*, 10423-10431.

Kamath, R.S., Fraser, A.G., Dong, Y., Poulin, G., Durbin, R., Gotta, M., Kanapin, A., Le Bot, N., Moreno, S., Sohrmann, M.*, et al.* (2003). Systematic functional analysis of the Caenorhabditis elegans genome using RNAi. Nature *421*, 231-237.

Kambe, T., Geiser, J., Lahner, B., Salt, D.E., and Andrews, G.K. (2008). Slc39a1 to 3 (subfamily II) Zip genes in mice have unique cell-specific functions during adaptation to zinc deficiency. Am J Physiol Regul Integr Comp Physiol *294*, R1474-1481.

Kambe, T., Narita, H., Yamaguchi-Iwai, Y., Hirose, J., Amano, T., Sugiura, N., Sasaki, R., Mori, K., Iwanaga, T., and Nagao, M. (2002). Cloning and characterization of a novel mammalian zinc transporter, zinc transporter 5, abundantly expressed in pancreatic beta cells. J Biol Chem *277*, 19049-19055.

Kambe, T., Suzuki, T., Nagao, M., and Yamaguchi-Iwai, Y. (2006). Sequence similarity and functional relationship among eukaryotic ZIP and CDF transporters. Genomics Proteomics Bioinformatics *4*, 1-9.

Kambe, T., Yamaguchi-Iwai, Y., Sasaki, R., and Nagao, M. (2004). Overview of mammalian zinc transporters. Cell Mol Life Sci *61*, 49-68.

Kawachi, M., Kobae, Y., Mimura, T., and Maeshima, M. (2008). Deletion of a histidine-rich loop of AtMTP1, a vacuolar Zn(2+)/H(+) antiporter of *Arabidopsis thaliana,* stimulates the transport activity. J Biol Chem *283*, 8374-8383.

Kelleher, S.L., and Lonnerdal, B. (2003). Zn transporter levels and localization change throughout lactation in rat mammary gland and are regulated by Zn in mammary cells. J Nutr *133*, 3378-3385.

Kemp, B.J., Church, D.L., Hatzold, J., Conradt, B., and Lambie, E.J. (2009). *gem-1* Encodes an SLC16 Monocarboxylate Transporter-Related Protein That Functions in Parallel to the *gon-2* TRPM Channel During Gonad Development in *Caenorhabditis elegans*. Genetics *181*, 581-591.

Kirschke, C.P., and Huang, L. (2003). ZnT7, a novel mammalian zinc transporter, accumulates zinc in the Golgi apparatus. J Biol Chem *278*, 4096-4102.

Kitamura, H., Morikawa, H., Kamon, H., Iguchi, M., Hojyo, S., Fukada, T., Yamashita, S., Kaisho, T., Akira, S., Murakami, M.*, et al.* (2006). Toll-like receptor-mediated regulation of zinc homeostasis influences dendritic cell function. Nat Immunol *7*, 971-977.

Klaassen, C.D., and Liu, J. (1998). Metallothionein transgenic and knock-out mouse models in the study of cadmium toxicity. J Toxicol Sci *23 Suppl 2*, 97-102.

Koh, J.Y., Suh, S.W., Gwag, B.J., He, Y.Y., Hsu, C.Y., and Choi, D.W. (1996). The role of zinc in selective neuronal death after transient global cerebral ischemia. Science *272*, 1013-1016.

Kostich, M., Fire, A., and Fambrough, D.M. (2000). Identification and molecular-genetic characterization of a LAMP/CD68-like protein from Caenorhabditis elegans. Journal of cell science *113 (Pt 14)*, 2595-2606.

Krebs, N.E., and Hambidge, K.M. (2001). Zinc metabolism and homeostasis: the application of tracer techniques to human zinc physiology. Biometals *14*, 397-412.

Krebs, N.F. (2000). Overview of zinc absorption and excretion in the human gastrointestinal tract. J Nutr *130*, 1374S-1377S.

Kury, S., Dreno, B., Bezieau, S., Giraudet, S., Kharfi, M., Kamoun, R., and Moisan, J.P. (2002). Identification of SLC39A4, a gene involved in acrodermatitis enteropathica. Nat Genet *31*, 239-240.

Langmade, S.J., Ravindra, R., Daniels, P.J., and Andrews, G.K. (2000). The transcription factor MTF-1 mediates metal regulation of the mouse ZnT1 gene. J Biol Chem *275*, 34803-34809.

Lemaire, K., Ravier, M.A., Schraenen, A., Creemers, J.W., Van de Plas, R., Granvik, M., Van Lommel, L., Waelkens, E., Chimienti, F., Rutter, G.A.*, et al.* (2009). Insulin crystallization depends on zinc transporter ZnT8 expression, but is not required for normal glucose homeostasis in mice. Proc Natl Acad Sci U S A *106*, 14872-14877.

Li, L., and Kaplan, J. (2001). The yeast gene MSC2, a member of the cation diffusion facilitator family, affects the cellular distribution of zinc. J Biol Chem *276*, 5036-5043.

Liang, J.Y., Liu, Y.Y., Zou, J., Franklin, R.B., Costello, L.C., and Feng, P. (1999). Inhibitory effect of zinc on human prostatic carcinoma cell growth. The Prostate *40*, 200-207.

Liao, V.H., and Freedman, J.H. (1998). Cadmium-regulated genes from the nematode Caenorhabditis elegans. Identification and cloning of new cadmium-responsive genes by differential display. J Biol Chem *273*, 31962-31970.

Lichten, L.A., and Cousins, R.J. (2009). Mammalian zinc transporters: nutritional and physiologic regulation. Annu Rev Nutr *29*, 153-176.

Lichtlen, P., and Schaffner, W. (2001). The "metal transcription factor" MTF-1: biological facts and medical implications. Swiss Med Wkly *131*, 647-652.

Liuzzi, J.P., Blanchard, R.K., and Cousins, R.J. (2001). Differential regulation of zinc transporter 1, 2, and 4 mRNA expression by dietary zinc in rats. J Nutr *131*, 46-52.

Liuzzi, J.P., and Cousins, R.J. (2004). Mammalian zinc transporters. Annu Rev Nutr *24*, 151-172.

Liuzzi, J.P., Lichten, L.A., Rivera, S., Blanchard, R.K., Aydemir, T.B., Knutson, M.D., Ganz, T., and Cousins, R.J. (2005). Interleukin-6 regulates the zinc transporter Zip14 in liver and contributes to the hypozincemia of the acute-phase response. Proc Natl Acad Sci U S A *102*, 6843-6848.

Lu, M., and Fu, D. (2007). Structure of the zinc transporter YiiP. Science *317*, 1746-1748.

Lu, N.C., and Goetsch, K.M. (1993). Carbohydrate requirement of *Caenorhabditis elegans* and the final development of a chemically defined meduim. Nematologica *39,* 303-311.

Lu, N.C., Hugenberg, G., Briggs, G.M., and Stokstad, E.L. (1978). The growth-promoting activity of several lipid-related compounds in the free-living nematode *Caenorhabditis briggsae*. Proc Soc Exp Biol Med *158*, 187-191.

MacDiarmid, C.W., Gaither, L.A., and Eide, D. (2000). Zinc transporters that regulate vacuolar zinc storage in *Saccharomyces cerevisiae*. Embo J *19*, 2845-2855.

MacDiarmid, C.W., Milanick, M.A., and Eide, D.J. (2002). Biochemical properties of vacuolar zinc transport systems of Saccharomyces cerevisiae. J Biol Chem *277*, 39187-39194.

Maduro, M., and Pilgrim, D. (1995). Identification and cloning of *unc-119,* a gene expressed in the *Caenorhabditis elegans* nervous system. Genetics *141*, 977-988.

Manning, D.L., Daly, R.J., Lord, P.G., Kelly, K.F., and Green, C.D. (1988). Effects of oestrogen on the expression of a 4.4 kb mRNA in the ZR-75-1 human breast cancer cell line. Mol Cell Endocrinol *59*, 205-212.

Maverakis, E., Fung, M.A., Lynch, P.J., Draznin, M., Michael, D.J., Ruben, B., and Fazel, N. (2007). Acrodermatitis enteropathica and an overview of zinc metabolism. Journal of the American Academy of Dermatology *56*, 116-124.

McMahon, R.J., and Cousins, R.J. (1998). Regulation of the zinc transporter ZnT-1 by dietary zinc. Proc Natl Acad Sci U S A *95*, 4841-4846.

Mello, C.C., Kramer, J.M., Stinchcomb, D., and Ambros, V. (1991). Efficient gene

transfer in *C.elegans*: extrachromosomal maintenance and integration of transforming sequences. Embo J *10*, 3959-3970.

Moynahan, E.J. (1974). Letter: Acrodermatitis enteropathica: a lethal inherited human zinc-deficiency disorder. Lancet *2*, 399-400.

Munoz, M., Villar, I., and Garcia-Erce, J.A. (2009). An update on iron physiology. World J Gastroenterol *15*, 4617-4626.

Murakami, M., and Hirano, T. (2008). Intracellular zinc homeostasis and zinc signaling. Cancer Sci *99*, 1515-1522.

Murgia, C., Vespignani, I., Cerase, J., Nobili, F., and Perozzi, G. (1999). Cloning, expression, and vesicular localization of zinc transporter Dri 27/ZnT4 in intestinal tissue and cells. Am J Physiol *277*, G1231-1239.

Murphy, J.T., Bruinsma, J.J., Schneider, D.L., Collier, S., Guthrie, J., Chinwalla, A., Robertson, J.D., Mardis, E.R., and Kornfeld, K. (2011). Histidine Protects Against Zinc and Nickel Toxicity in Caenorhabditis elegans. PLoS Genet *7*, e1002013.

Nies, D.H. (2007). Biochemistry. How cells control zinc homeostasis. Science *317*, 1695-1696.

Outten, C.E., and O'Halloran, T.V. (2001). Femtomolar sensitivity of metalloregulatory proteins controlling zinc homeostasis. Science *292*, 2488-2492.

Palmiter, R.D., Cole, T.B., and Findley, S.D. (1996a). ZnT-2, a mammalian protein that confers resistance to zinc by facilitating vesicular sequestration. Embo J *15*, 1784-1791.

Palmiter, R.D., Cole, T.B., Quaife, C.J., and Findley, S.D. (1996b). ZnT-3, a putative transporter of zinc into synaptic vesicles. Proc Natl Acad Sci U S A *93*, 14934-14939.

Palmiter, R.D., and Findley, S.D. (1995). Cloning and functional characterization of a mammalian zinc transporter that confers resistance to zinc. Embo J *14*, 639-649.

Palmiter, R.D., and Huang, L. (2004). Efflux and compartmentalization of zinc by

members of the SLC30 family of solute carriers. Pflugers Arch *447*, 744-751.

Peters, J.L., Dufner-Beattie, J., Xu, W., Geiser, J., Lahner, B., Salt, D.E., and Andrews, G.K. (2007). Targeting of the mouse Slc39a2 (Zip2) gene reveals highly cell-specific patterns of expression, and unique functions in zinc, iron, and calcium homeostasis. Genesis *45*, 339-352.

Pfaffl, M.W. (2001). A new mathematical model for relative quantification in real-time RT-PCR. Nucleic Acids Res *29*, e45.

Praitis, V., Casey, E., Collar, D., and Austin, J. (2001). Creation of low-copy integrated transgenic lines in *Caenorhabditis elegans*. Genetics *157*, 1217-1226.

Prasad, A.S., Brewer, G.J., Schoomaker, E.B., and Rabbani, P. (1978). Hypocupremia induced by zinc therapy in adults. JAMA *240*, 2166-2168.

Pulak, R. (2006). Techniques for analysis, sorting, and dispensing of *C. elegans* on the COPAS flow-sorting system. Methods Mol Biol *351*, 275-286.

Rabbitts, B.M., Ciotti, M.K., Miller, N.E., Kramer, M., Lawrenson, A.L., Levitte, S., Kremer, S., Kwan, E., Weis, A.M., and Hermann, G.J. (2008). glo-3, a novel Caenorhabditis elegans gene, is required for lysosome-related organelle biogenesis. Genetics *180*, 857-871.

Radtke, F., Heuchel, R., Georgiev, O., Hergersberg, M., Gariglio, M., Dembic, Z., and Schaffner, W. (1993). Cloned transcription factor MTF-1 activates the mouse metallothionein I promoter. Embo J *12*, 1355-1362.

Rajagopal, A., Rao, A.U., Amigo, J., Tian, M., Upadhyay, S.K., Hall, C., Uhm, S., Mathew, M.K., Fleming, M.D., Paw, B.H.*, et al.* (2008). Haem homeostasis is regulated by the conserved and concerted functions of HRG-1 proteins. Nature *453*, 1127-1131.

Riddle, D.L., Blumental, T., Meyer, B.J., and Preiss, J.R. (1997). *C. elegans* II (Cold Spring Harbor, NY, Cold Spring Harbor Laboratory Press).

Rutter, G.A. (2010). Think zinc: New roles for zinc in the control of insulin secretion.

Islets *2*, 49-50.

Schneider, J., Ruschhaupt, M., Buness, A., Asslaber, M., Regitnig, P., Zatloukal, K., Schippinger, W., Ploner, F., Poustka, A., and Sultmann, H. (2006). Identification and meta-analysis of a small gene expression signature for the diagnosis of estrogen receptor status in invasive ductal breast cancer. Int J Cancer *119*, 2974-2979.

Schroeder, L.K., Kremer, S., Kramer, M.J., Currie, E., Kwan, E., Watts, J.L., Lawrenson, A.L., and Hermann, G.J. (2007). Function of the Caenorhabditis elegans ABC transporter PGP-2 in the biogenesis of a lysosome-related fat storage organelle. Mol Biol Cell *18*, 995-1008.

Setty, S.R., Tenza, D., Sviderskaya, E.V., Bennett, D.C., Raposo, G., and Marks, M.S. (2008). Cell-specific ATP7A transport sustains copper-dependent tyrosinase activity in melanosomes. Nature *454*, 1142-1146.

Seve, M., Chimienti, F., Devergnas, S., and Favier, A. (2004). In silico identification and expression of SLC30 family genes: an expressed sequence tag data mining strategy for the characterization of zinc transporters' tissue expression. BMC Genomics *5*, 32.

Sindreu, C., Palmiter, R.D., and Storm, D.R. (2011). Zinc transporter ZnT-3 regulates presynaptic Erk1/2 signaling and hippocampus-dependent memory. Proc Natl Acad Sci U S A *108*, 3366-3370.

Sladek, R., Rocheleau, G., Rung, J., Dina, C., Shen, L., Serre, D., Boutin, P., Vincent, D., Belisle, A., Hadjadj, S.*, et al.* (2007). A genome-wide association study identifies novel risk loci for type 2 diabetes. Nature *445*, 881-885.

Smirnova, I.V., Bittel, D.C., Ravindra, R., Jiang, H., and Andrews, G.K. (2000). Zinc and cadmium can promote rapid nuclear translocation of metal response element-binding transcription factor-1. J Biol Chem *275*, 9377-9384.

Stryer, L. (1995). Biochemistry, 4 edn (New York, W. H. Freeman and Company).

Sulston, J.E., and Horvitz, H.R. (1977). Post-embryonic cell lineages of the nematode,

Caenorhabditis elegans. Developmental biology *56*, 110-156.

Sundaram, M.V. (2004). Vulval development: the battle between Ras and Notch. Curr Biol *14*, R311-313.

Szewczyk, N.J., Kozak, E., and Conley, C.A. (2003). Chemically defined medium and *Caenorhabditis elegans*. BMC Biotechnol *3*, 19.

Szewczyk, N.J., Udranszky, I.A., Kozak, E., Sunga, J., Kim, S.K., Jacobson, L.A., and Conley, C.A. (2006). Delayed development and lifespan extension as features of metabolic lifestyle alteration in *C. elegans* under dietary restriction. J Exp Biol *209*, 4129-4139.

Tapiero, H., and Tew, K.D. (2003). Trace elements in human physiology and pathology: zinc and metallothioneins. Biomed Pharmacother *57*, 399-411.

Taubert, S., Hansen, M., Van Gilst, M.R., Cooper, S.B., and Yamamoto, K.R. (2008). The Mediator subunit MDT-15 confers metabolic adaptation to ingested material. PLoS Genet *4*, e1000021.

Taylor, K.M., Morgan, H.E., Smart, K., Zahari, N.M., Pumford, S., Ellis, I.O., Robertson, J.F., and Nicholson, R.I. (2007). The emerging role of the LIV-1 subfamily of zinc transporters in breast cancer. Mol Med *13*, 396-406.

Taylor, K.M., Vichova, P., Jordan, N., Hiscox, S., Hendley, R., and Nicholson, R.I. (2008). ZIP7-mediated intracellular zinc transport contributes to aberrant growth factor signaling in antihormone-resistant breast cancer Cells. Endocrinology *149*, 4912-4920.

Terres-Martos, C., Navarro-Alarcon, M., Martin-Lagos, F., Lopez, G.d.l.S.H., Perez-Valero, V., and Lopez-Martinez, M.C. (1998). Serum zinc and copper concentrations and Cu/Zn ratios in patients with hepatopathies or diabetes. J Trace Elem Med Biol *12*, 44-49.

Treusch, S., Knuth, S., Slaugenhaupt, S.A., Goldin, E., Grant, B.D., and Fares, H. (2004). Caenorhabditis elegans functional orthologue of human protein h-mucolipin-1 is required for lysosome biogenesis. Proc Natl Acad Sci U S A *101*, 4483-4488.

Vallee, B.L., and Falchuk, K.H. (1993). The biochemical basis of zinc physiology. Physiol Rev *73*, 79-118.

Vandesompele, J., De Preter, K., Pattyn, F., Poppe, B., Van Roy, N., De Paepe, A., and Speleman, F. (2002). Accurate normalization of real-time quantitative RT-PCR data by geometric averaging of multiple internal control genes. Genome Biol *3*, RESEARCH0034.

Vatamaniuk, O.K., Bucher, E.A., Ward, J.T., and Rea, P.A. (2001). A new pathway for heavy metal detoxification in animals. Phytochelatin synthase is required for cadmium tolerance in Caenorhabditis elegans. J Biol Chem *276*, 20817-20820.

Wang, F., Dufner-Beattie, J., Kim, B.E., Petris, M.J., Andrews, G., and Eide, D.J. (2004). Zinc-stimulated endocytosis controls activity of the mouse ZIP1 and ZIP3 zinc uptake transporters. J Biol Chem *279*, 24631-24639.

Wang, K., Zhou, B., Kuo, Y.M., Zemansky, J., and Gitschier, J. (2002). A novel member of a zinc transporter family is defective in acrodermatitis enteropathica. American journal of human genetics *71*, 66-73.

Wenzlau, J.M., Juhl, K., Yu, L., Moua, O., Sarkar, S.A., Gottlieb, P., Rewers, M., Eisenbarth, G.S., Jensen, J., Davidson, H.W.*, et al.* (2007). The cation efflux transporter ZnT8 (Slc30A8) is a major autoantigen in human type 1 diabetes. Proc Natl Acad Sci U S A *104*, 17040-17045.

Wimmer, U., Wang, Y., Georgiev, O., and Schaffner, W. (2005). Two major branches of anti-cadmium defense in the mouse: MTF-1/metallothioneins and glutathione. Nucleic Acids Res *33*, 5715-5727.

Wood, W.B. (1988). The Nematode *Caenorhabditis elegans* (Cold Spring Harbor, New York, Cold Spring Harbor Laboratory Press).

Yamashita, S., Miyagi, C., Fukada, T., Kagara, N., Che, Y.S., and Hirano, T. (2004). Zinc transporter LIVI controls epithelial-mesenchymal transition in zebrafish gastrula organizer. Nature *429*, 298-302.

Yoder, J.H., Chong, H., Guan, K.L., and Han, M. (2004). Modulation of KSR activity in

Caenorhabditis elegans by Zn ions, PAR-1 kinase and PP2A phosphatase. Embo J *23*, 111-119.

Zerial, M., and McBride, H. (2001). Rab proteins as membrane organizers. Nat Rev Mol Cell Biol *2*, 107-117.

Zhang, Y., Li, X., Grassme, H., Doring, G., and Gulbins, E. (2010). Alterations in ceramide concentration and pH determine the release of reactive oxygen species by Cftr-deficient macrophages on infection. J Immunol *184*, 5104-5111.

Zhao, H., and Eide, D. (1996a). The yeast ZRT1 gene encodes the zinc transporter protein of a high-affinity uptake system induced by zinc limitation. Proc Natl Acad Sci U S A *93*, 2454-2458.

Zhao, H., and Eide, D. (1996b). The ZRT2 gene encodes the low affinity zinc transporter in *Saccharomyces cerevisiae*. J Biol Chem *271*, 23203-23210.

Zhao, H., and Eide, D.J. (1997). Zap1p, a metalloregulatory protein involved in zinc-responsive transcriptional regulation in *Saccharomyces cerevisiae*. Mol Cell Biol *17*, 5044-5052.